

SEPARATION OF CARBON DIOXIDE FROM FUEL GAS ("PRE-COMBUSTION CAPTURE") VIA HYDRATE CRYSTALLIZATION

by

Rajnish Kumar

Bachelor of Engineering (Chem. Eng.), Pt. R.S. University, India, 2001

Master of Science (Chem. Eng.), Indian Institute of Science, India, 2003

A THESIS SUBMITTED IN PARTIAL FULFILLMENT OF THE
REQUIREMENTS FOR THE DEGREE OF

DOCTOR OF PHILOSOPHY

in

THE FACULTY OF GRADUATE STUDIES

(Chemical and Biological Engineering)

THE UNIVERSITY OF BRITISH COLUMBIA
(Vancouver)

July 2009

© Rajnish Kumar, 2009

ABSTRACT

Conventional coal-fired power plants that rely on the combustion of the coal are the largest anthropogenic point sources of atmospheric carbon dioxide (CO_2). An alternative approach of producing electricity with CO_2 capture is pre-combustion decarbonisation whereby the coal is used to produce an intermediate hydrogen-rich gas (CO_2/H_2 mixture). This route is known as integrated gasification combined cycle (IGCC). The CO_2/H_2 mixture is called *fuel gas* and is separated into a CO_2 -rich and a H_2 -rich stream. The H_2 may be burnt to produce electricity or used in fuel cells. The assumption is that the CO_2 can possibly be stored safely in a suitable geological formation. It is noted that other fossil fuels may be used in a similar manner as coal. This thesis examines the prospect of employing a novel method for the separation of carbon dioxide (CO_2) from CO_2/H_2 mixture (fuel gas mixture) via clathrate hydrate crystal formation. Experiments and theory are employed at the engineering (macroscopic) and molecular level to achieve the objectives. The focus is on the study of the thermodynamic and kinetic properties of CO_2/H_2 and $\text{CO}_2/\text{H}_2/\text{C}_3\text{H}_8$ hydrates. The basis for separation of the CO_2 is the fact that when a CO_2/H_2 or $\text{CO}_2/\text{H}_2/\text{C}_3\text{H}_8$ mixture is allowed to form hydrate, CO_2 preferentially gets incorporated into the hydrate phase. The addition of 2.5 mol % C_3H_8 in the fuel gas mixture was found to reduce the hydrate formation pressure and thus improve the process economics. Based on the data obtained a conceptual separation process was developed. It involves two hydrate stages coupled with a membrane-based gas separation stage. The two hydrate stages operate at ~ 3.5 MPa and 273.7 K. The power penalty for a 500 MW power plant is estimated to be about 2.5% of the power output. Crystal structures and cage occupancies for the CO_2/H_2 and the $\text{CO}_2/\text{H}_2/\text{C}_3\text{H}_8$ hydrate were determined using several spectroscopic techniques. This enabled an understanding of the separation efficiency values obtained for the process.

TABLE OF CONTENTS

ABSTRACT.....	ii
TABLE OF CONTENTS.....	iii
LIST OF TABLES.....	vii
LIST OF FIGURES.....	viii
NOMENCLATURE.....	xii
ACKNOWLEDGEMENT.....	xiv
DEDICATION.....	xv
CO-AUTHORSHIP STATEMENT.....	xvi
1. LITERATURE REVIEW	1
1.1. CARBON DIOXIDE CAPTURE AND STORAGE (CCS).....	1
1.2. BACKGROUND ON GAS HYDRATES.....	7
1.2.1. Gas hydrates, structure and properties	7
1.2.2. Hydrates of CO ₂ & H ₂	15
1.3. RESEARCH OBJECTIVES	17
1.4. THESIS ORGANIZATION.....	18
1.5. REFERENCES	21
2. INCIPIENT HYDRATE PHASE EQUILIBRIUM FOR GAS MIXTURES CONTAINING HYDROGEN, CARBON DIOXIDE & PROPANE.....	28
2.1. INTRODUCTION.....	28
2.2. EXPERIMENTAL APPARATUS AND PROCEDURE	31
2.2.1. Apparatus and materials.....	31
2.2.2. Procedure	32

2.3. RESULTS AND DISCUSSION	34
2.3.1. Incipient phase equilibrium data.....	34
2.3.2. Structural analysis from phase equilibrium data.....	37
2.3.2.1. CO ₂ /H ₂ /H ₂ O system.....	37
2.3.2.2. CO ₂ /H ₂ /C ₃ H ₈ /H ₂ O system.....	40
2.4. CONCLUSIONS	41
2.5. REFERENCES	42
3. KINETICS OF GAS HYDRATE FORMATION FROM CO₂/H₂ MIXTURES AND SEPARATION EFFICIENCY OF HYDRATE BASED PROCESS	44
3.1. INTRODUCTION	44
3.2. EXPERIMENTAL SECTION	46
3.2.1. Materials	46
3.2.2. Apparatus and procedure	46
3.2.3. Calculation of the amount of gas consumed.....	48
3.2.4. Gas phase analysis	50
3.3. HYDRATE CRYSTAL/ GAS SEPARATION	50
3.3.1. CO ₂ recovery and separation factor	52
3.4. RESULTS AND DISCUSSION.....	53
3.4.1. Gas separation efficiency	60
3.4.2. Hydrate-membrane process for CO ₂ recovery from fuel gas.....	61
3.5. CONCLUSIONS	64
3.6. REFERENCES	65

4. KINETICS OF GAS HYDRATE FORMATION FROM CO₂/H₂/C₃H₈ MIXTURES AND SEPARATION EFFICIENCY OF THE HYDRATE BASED PROCESS.....	68
4.1. INTRODUCTION.....	68
4.2. EXPERIMENTAL SECTION	69
4.2.1. CO ₂ recovery and efficiency	71
4.3. RESULTS AND DISCUSSION.....	72
4.3.1. Membrane separation unit.....	84
4.4. CONCLUSIONS	85
4.5. REFERENCES	86
5. STRUCTURAL AND COMPOSITIONAL CHARACTERIZATION OF HYDRATES FORMED FROM CO₂/H₂ AND CO₂/H₂/C₃H₈ GAS MIXTURES	88
5.1. INTRODUCTION.....	88
5.2. EXPERIMENTAL SECTION	90
5.3. RESULTS AND DISCUSSION.....	93
5.3.1. Determination of cage occupancy.....	112
5.4. CONCLUSIONS	115
5.5. REFERENCES	117
6. APPLICATION OF THE ATR-IR SPECTROSCOPIC TECHNIQUE FOR THE CHARACTERIZATION OF HYDRATES FORMED BY CO₂, CO₂/H₂ AND CO₂/H₂/C₃H₈.....	120
6.1. INTRODUCTION.....	120
6.2. MATERIALS AND EXPERIMENTAL SETUP.....	123

6.3. RESULTS AND DISCUSSION	124
6.3.1. Quantitative determination of the cage occupancy from FTIR results	132
6.4. CONCLUSIONS	137
6.5. REFERENCES	138
7. SUMMARY OF CONCLUSIONS, CONTRIBUTION TO KNOWLEDGE, AND RECOMMENDATIONS FOR FUTURE WORK.....	140
7.1. SUMMARY OF CONCLUSIONS.....	140
7.2. CONTRIBUTION TO THE KNOWLEDGE	143
7.3. RECOMMENDATIONS FOR FUTURE WORK	144
7.4. REFERENCES	147
8. APPENDIX A	148
9. APPENDIX B	152
10. APPENDIX C	154

LIST OF TABLES

Table 1-1: Estimated world sink capabilities of CO ₂ disposal options.....	6
Table 1-2: Structural properties of hydrates (adapted from Sloan, 1998)	10
Table 1-3: Size ratio for CO ₂ and H ₂ (adapted from Sloan, 1998)	12
Table 2-1: Incipient hydrate formation conditions from a CO ₂ - H ₂ gas mixture	35
Table 2-2: Incipient hydrate formation conditions from a CO ₂ - H ₂ - C ₃ H ₈ gas mixture	36
Table 3-1: Experimental conditions along with measured induction times and hydrate formation rates for CO ₂ /H ₂ /H ₂ O system at 273.7 K.	54
Table 3-2: Vapor phase composition during hydrate formation from CO ₂ /H ₂ mixture. ..	58
Table 3-3: Split fraction and separation factors for the two stages for CO ₂ /H ₂ separation	63
Table 4-1: List of experimental conditions along with measured induction times and hydrate formation rates at temperature T = 273.7 K.....	71
Table 4-2: Gas phase analysis during hydrate formation at T = 273.7 K	76
Table 4-3: Split fraction and separation factor for the two CO ₂ recovery stages	81
Table 5-1: Phase composition at the start and end of the experiment as analyzed by gas chromatography	96
Table 5-2: Estimate of cage occupancy values obtained by combination of results from gas chromatography and NMR. θ_s' represents hydrogen doublet in small cages	115
Table 6-1: Estimate of cage occupancy values obtained by combination of results from Infrared spectroscopy and Gas chromatography.....	134

LIST OF FIGURES

Figure 1-1: Schematic of IGCC plant (adapted from Joshi & Lee, 1996).....	3
Figure 1-2: Gas hydrate cavity structures (Ripmeester et al., 1994)	9
Figure 1-3: Equilibrium hydrate formation conditions for pure carbon dioxide hydrate.	16
Figure 2-1: Experimental apparatus to study incipient equilibrium hydrate formation condition (adapted from Lee et al., 2005b).....	32
Figure 2-2: A Clausius-Clapeyron plot showing the hydrate's guest mixtures with HLV phases, with lines of same reference slope.	38
Figure 2-3: A Clausius-Clapeyron plot showing the hydrate's guest mixtures with HLV phases with line of same reference slope.....	40
Figure 3-1: Kinetic Apparatus. (Adapted from Englezos & Ngan, 1994)	46
Figure 3-2: Simplified schematic of hydrate based gas separation process.....	51
Figure 3-3: Block diagram of the experimental methods for the hydrate formation kinetic and separation experiments.....	51
Figure 3-4: A typical gas uptake measurement curve together with the temperature profile in the aqueous phase. This is experiment 4 (table 3-1).....	55
Figure 3-5: Gas uptake curves for CO ₂ /H ₂ at 8.5 MPa (experiment 1, table 3-1), and 7.5 MPa (experiment 3, table 3-1) with the corresponding induction point.	57
Figure 3-6: Mole consumption and molar ratio for the CO ₂ /H ₂ /H ₂ O system at 8.5 MPa.	59
Figure 3-7: Mole consumption and molar ratio for the CO ₂ /H ₂ /H ₂ O system at 7.5 MPa.	60
Figure 3-8: Hydrate based separation for CO ₂ (39.2 mol %) – H ₂ (60.8 mol %) gas mixture, Temperature = 273.7 K.....	62
Figure 3-9: A hybrid hydrate-membrane process for CO ₂ recovery from fuel gas	63

Figure 4-1: Gas uptake measurement curves for hydrate formation from fresh water and from memory water at $P_{\text{exp}}=4.8$ MPa and 273.7 K. The equilibrium hydrate formation pressure P_{eq} is equal to 2.1 MPa.....	73
Figure 4-2: Gas uptake measurement curves for hydrate formation from fresh water and from memory water at $P_{\text{exp}}=3.8$ MPa and 273.7 K. The equilibrium hydrate formation pressure P_{eq} is equal to 2.1 MPa.....	74
Figure 4-3: Comparison of gas uptake curves for the system with 2.5% propane and the system without propane (Chapter 3).	75
Figure 4-4: Mole consumption for the $\text{CO}_2/\text{H}_2/\text{C}_3\text{H}_8/\text{H}_2\text{O}$ system at 4.8 MPa and 273.7 K. (experiment 1). The induction time was 14.1 min.	77
Figure 4-5: Mole consumption for the $\text{CO}_2/\text{H}_2/\text{C}_3\text{H}_8/\text{H}_2\text{O}$ system at 3.8 MPa and 273.7 K (experiment 6). The induction time was 28.3 min.	78
Figure 4-6: CO_2 content in the gas phase (initial composition), hydrate phase and residual gas phase (final composition) for two stages. The first stage operates at 3.8 MPa and the second at 3.5 MPa.....	79
Figure 4-7: Gas uptake curve for hydrate formation for second stage CO_2 (80%) / H_2 (18.8%) / C_3H_8 (1.2%)- H_2O system at 273.7 K and 3.5 MPa (experiment 9). The induction time was 11.0 min. The equilibrium hydrate formation pressure P_{eq} is equal to 1.6 MPa.....	80
Figure 4-8: Block flow diagram for a hybrid hydrate-membrane process for CO_2 recovery from fuel gas in presence of propane. Hydrate stage 1 operates at 3.8 MPa and the second at 3.5 MPa. Both operate at 273.7 K.....	82

Figure 5-1: Gas uptake profile during hydrate formation from ice powder and the CO ₂ /H ₂ mixture synthesized at 8 MPa.	94
Figure 5-2: The X-ray diffraction pattern of the (40/60 mol%) CO ₂ /H ₂ hydrate. The X-ray powder diffraction data were collected at –110 °C and atmospheric pressure. CO ₂ /H ₂ forms sI hydrate whereas the CO ₂ /H ₂ /C ₃ H ₈ mixture forms hydrate of sI & sII at 5.0 MPa (a) and only sII hydrate at 3.8 MPa (b). The composition of the CO ₂ /H ₂ /C ₃ H ₈ gas mixture is given in Table 5-1.	95
Figure 5-3: Temperature dependent PXRD profile for (40/60 mol%) CO ₂ /H ₂ hydrate from –110°C to 5 °C. Inset shows intensity ratio of hydrate peak as a function of temperature during transformation of CO ₂ /H ₂ hydrate (8 MPa & -20°C) and CO ₂ /H ₂ /C ₃ H ₈ hydrate (3.8 MPa & -20°C) into ice.	99
Figure 5-4: Mass of decomposed gas coming out of (40/60 mol%) CO ₂ /H ₂ hydrate with respect to time.	100
Figure 5-5: Mass of decomposed gas coming out of (40/60 mol%) CO ₂ /H ₂ hydrate with respect to time. Mass number 2 is for hydrogen leaving the hydrate lattice on decomposition, mass 1 is shown as a reference.	101
Figure 5-6: Raman spectrum for the Fermi diad of CO ₂ incorporated into hydrate phase from the CO ₂ /H ₂ /C ₃ H ₈ gas mixture. Note the rotational modes for H ₂ occupying the hydrate cages and several C-C stretching modes of C ₃ H ₈ . The figure in the inset suggests the broadening and red shift of CO ₂ incorporated in hydrate phase (a) compared to CO ₂ in gas phase (b).	103
Figure 5-7: Raman spectra of the vibron region for H ₂ gas and H ₂ incorporated into hydrates of CO ₂ /H ₂ and CO ₂ /H ₂ /C ₃ H ₈ . H-H stretching of H ₂ gas was recorded	

at room temperature whereas H-H stretching of H ₂ in hydrate phase was recorded at liquid nitrogen temperature. It is noted that the CO ₂ /H ₂ mixture forms structure I hydrate where as CO ₂ /H ₂ /C ₃ H ₈ mixture forms structure II hydrate.....	105
Figure 5-8: ¹³ C CP MAS NMR spectra for CO ₂ /H ₂ /C ₃ H ₈ . Upper inset shows the expanded signal of C ₃ H ₈ in large cages of resultant sII hydrate. T=173K, spinning speed of 2500 Hz.....	108
Figure 5-9: ¹ H MAS (T=173K, 3000 Hz) of CO ₂ /H ₂ hydrate prepared in D ₂ O. The inset shows expanded central region of the spectrum without spinning sidebands. The peak at 6.59 ppm is due to the proton impurity in D ₂ O.	110
Figure 5-10: ¹ H MAS (T=173K, 3000 Hz) of CO ₂ /H ₂ /C ₃ H ₈ hydrate in D ₂ O. Expanded signals for propane are shown on the right inset along with a weak signal from H ₂ on the left inset.	112
Figure 6-1: Schematic of ATR-IR Experiment.....	122
Figure 6-2: ¹³ C NMR spectra for CO ₂ /H ₂ (sI) and CO ₂ /H ₂ /C ₃ H ₈ (sII) hydrate obtained at atmospheric pressure and 173 K, spinning speed of 2500 Hz. Inset shows the close-up view of the peak at 125 ppm.	125
Figure 6-3: Raman Spectra showing Fermi diad of CO ₂ in the hydrate phase for CO ₂ /H ₂ (sI) and CO ₂ /H ₂ /C ₃ H ₈ (sII) hydrate.....	127
Figure 6-4: ATR-IR spectra of CO ₂ showing unique peaks under different conditions.	128
Figure 6-5: ATR-IR spectra showing CO ₂ in the small and large cages of hydrate phase for (a) simple CO ₂ hydrate (b) CO ₂ /C ₃ H ₈ (sII), (c) CO ₂ /H ₂ (sI) and (d) CO ₂ /H ₂ /C ₃ H ₈ (sII) hydrate.	129

NOMENCLATURE

Abbreviation	Full Form
n_T	total number of moles
CR	crystallizer
SV	supply vessel
n_H	moles of the gas in Hydrate + Water phase of CR
n_G	moles of gas in gas phase of CR
n_{SV}	moles of gas in SV
Δn_H^i	mole consumption for i component in hydrate + liquid phase
t_{ind}	induction time (min)
V_G	volume of gas phase in CR
V_{SV}	volume of supply vessel
y_i	mole fraction in gas phase
$n_{CO_2}^{Feed}$	number of moles of CO ₂ in feed gas
$n_{CO_2}^H$	number of moles of CO ₂ in hydrate phase
$n_{H_2}^H$	number of moles of H ₂ in the hydrate phase
$n_{CO_2}^{gas}$	number of moles of CO ₂ in the gas phase at the end of the kinetic experiment
$n_{H_2}^{gas}$	number of moles of H ₂ in the gas phase at the end of kinetic experiment
z	compressibility factor
THF	tetrahydrofuran
TDF	Deutrated tetrahydrofuran
D ₂ O	Deutrated water
P	pressure
T	temperature
R	gas constant
IGCC	Integrated Gasification Combined Cycle
sI	Structure I

sII	Structure II
PXRD	Powder x-Ray Diffraction
NMR	Nuclear Magnetic Resonance
MAS	Magic Angle Spinning
CSA	Chemical Shift Anisotropy
FTIR	Fourier Transformed Infrared Spectroscopy
ATR	Attenuated Total Reflection
MS	Mass Spectrometer
GC	Gas Chromatography
CCD	Charge Coupled Device
θ_{L-i}	Large cage occupancy of i th gas
θ_{S-i}	Small cage occupancy of i th gas
$\Delta\mu_w^o$	Chemical potential of water in gas hydrate
ΔH_d	Heat of hydrate dissociation

ACKNOWLEDGEMENTS

The work contained in this thesis would not have been possible without the contributions and support of following people:

To my family, thank you for your support and encouragement through out the years, and for providing the basic foundations which have enabled my success. I am truly indebted.

To my supervisor Professor Peter Englezos, for not only giving me the opportunity and freedom to work on gas hydrate but also for his great efforts to explain things clearly and simply whenever there was a need. Thank you for all the guidance, encouragement and support at academic and personal level.

To Dr. John Ripmeester for his supervision, advice, and guidance. His passion toward science and his truly scientist intuition has made him as a constant oasis of ideas, which exceptionally inspired and enriched my growth as a student, and as a researcher.

Many thanks go to everyone at Material Structure and Function (MSF) group at NRC Chris, Gary, Graham, Hailong, Hiroshi, Igor, Jeff, Kostia, Olga, Robin, Satoshi, Sergey, Steve, and others for their valuable advice in science discussion through group meetings and personal discussions.

I am indebted to many present and past colleagues at UBC: Praveen, Shiva, Judong, Dr. Song, Huijie, Nayef, Adebola, Cef, Nagu and Jeffry for providing a stimulating and fun environment in which to learn and grow. I am especially grateful to my lab mate and my friend Praveen Linga, he was always there to help me out whatever be the need.

I would also like to thank Natural Science and Engineering Research Council of Canada (NSERC), Canada Foundation for Innovation (CFI) and Natural Resources Canada (NRCan) for providing funding for this project.

*Dedicated to my parents
and
My wife Smita*

CO-AUTHORSHIP STATEMENT

The work of this thesis consists of six different manuscripts which correspond to chapter two to six. The authors include Kumar R., Linga P., Huijie, W., Moudrakovski, I.L., Lang, S., Ripmeester, J.A., Englezos P. Professor Peter Englezos is my research supervisor. Dr. John Ripmeester oversees my work at SIMS, National Research Council, Ottawa. Dr. Igor Moudrakovski is research officer at SIMS, National Research Council Ottawa. Dr. Stephan Lang is technical officer at SIMS, National Research Council Ottawa and Linga P. (Ph.D.), Huijie W., (M.Sc) are fellow researchers in our lab at UBC.

The literature review, experimental design, performing experiments and data analysis were done extensively by me under supervision of Professor P. Englezos and Dr. John Ripmeester. Moudrakovski IL, provided assistance with NMR measurement Lang S, provided assistance with the experimental facility in general. Finally, I did the final preparation for each manuscript after careful revision and approval of my research supervisor.

1. LITERATURE REVIEW

1.1. CARBON DIOXIDE CAPTURE AND STORAGE (CCS)

CO₂, CH₄, N₂O, SF₆, CFC'S (chloro-fluorocarbons), and HFC'S (hydro-fluorocarbons) have climate change potential according to the IPCC (Intergovernmental Panel on Climate Change). While CO₂ has the lowest Global Warming Potential (IPCC, 1996; IPCC, 2001); it has the largest impact on climate change because of the quantity emitted (Olsen et al., 2002)

The world will continue to rely on fossil fuels as the source of energy in the next 25 years (WEO, 2000). Thus, there is a need to reduce CO₂ emissions. A major source of CO₂ is the combustion of fossil fuels in power plants, transportation, industrial processes like cement manufacture and residential and commercial buildings (IPCC, 2005). According to Freund (Freund, 1997) four options are typically considered for reducing carbon dioxide emissions: (a) improving energy efficiency in power generation and end use; (b) switching to fuels containing less carbon; (c) providing electricity from carbon free sources; and (d) implementing carbon capture and storage (CCS). In practice it is likely that a combination of these options would be employed. According to the IPCC report on climate change, CCS will play an important role as a mitigation strategy (IPCC, 2005). It should also be noted that CO₂ emissions in the residential, commercial and transportation sectors are individually small and often mobile, and therefore are not suitable for CCS.

Broadly, three different capture approaches exist:

- (a) In **post-combustion**, CO₂ is removed after combustion of the fossil fuel. This approach is relevant to conventional power plants. Here, CO₂ is captured from the flue gas mixture. Current post-combustion capture systems typically employ an organic solvent such as monoethanolamine (MEA) to chemically absorb the CO₂. However, this technology has a high energy cost associated with the regeneration of the solvent.
- (b) In **Oxy-fuel combustion** the fuel is burned in oxygen instead of air in order to limit the flame temperature to a level achieved in conventional combustion, flue gas is re-circulated into the combustion chamber. The resulting concentrated CO₂ stream can be transported to a storage site. The approach is promising; however, the air separation process is energy intensive.
- (c) **Pre-combustion** carbon capture, involves the removal of carbon before the fuel (coal; natural gas or oil) is used (NETL, 2004; Audus *et al.*, 1998). Hydrocarbons react with steam to produce carbon monoxide (CO) and hydrogen (H₂). Carbon monoxide is then reacted with steam in a catalytic shift converter to produce CO₂ and more H₂. The fuel gas produced contains a high concentration of CO₂ (typically 40 %) at a pressure between 2 and 7 MPa (IPCC, 2005). The separation (capture) of CO₂ leaves H₂ which can then be used in gas turbines or fuel cells. Audus *et al.*, (1998) reported that there are no technical barriers for the integrated process of coal gasification for power generation with carbon capture. However, there is a need to demonstrate it at commercial scale. It is noted that much of the coal gasification technology is currently available (NETL, 2004).

There are three main reasons that make a pre-combustion approach more attractive than post-combustion or oxy-fuel combustion for green field projects:

- (a) It is based on industrial H_2 production processes e.g. natural gas reforming.
- (b) Fuel gas has higher concentration of CO_2 compared to conventional flue gases and exists at higher pressure.
- (c) H_2 is produced.

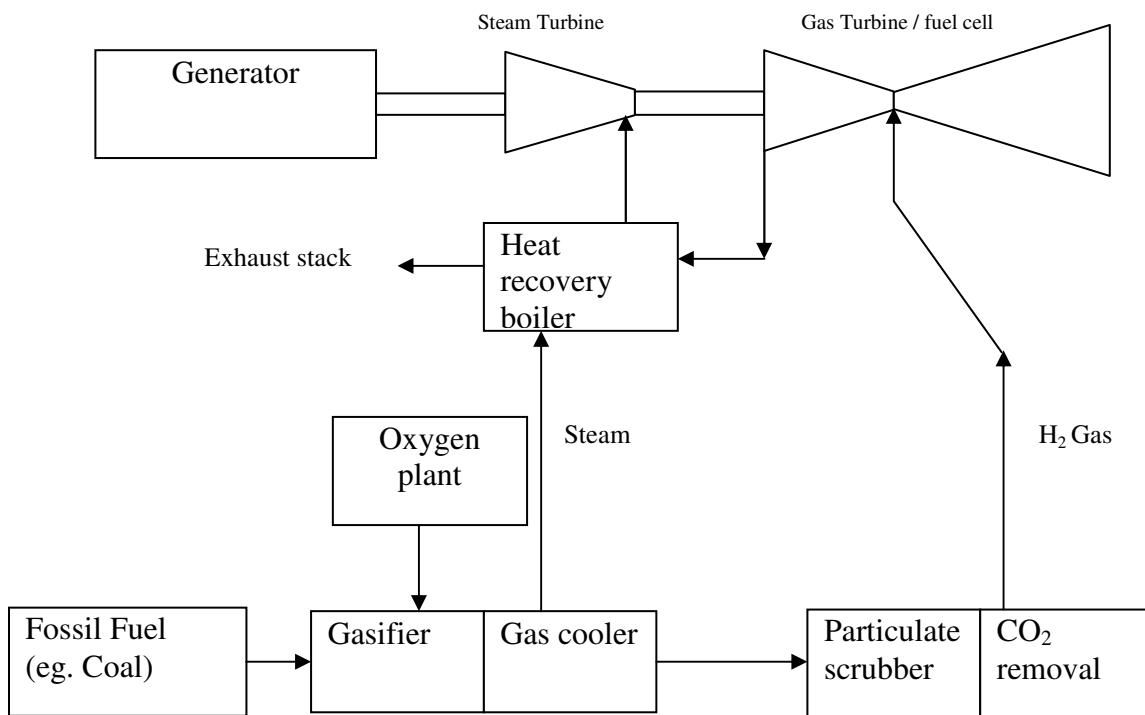


Figure 1-1: Schematic of IGCC plant (adapted from Joshi & Lee, 1996)

An integrated gasification combined cycle (IGCC) power plant with CO_2 removal is shown in Figure 1-1. The gasifier receives coal from coal handling and preparation equipment and oxidant from an air treatment plant and gasifies the coal by a partial oxidation / reduction process involving coal, oxygen and steam. The fuel gas from the gasifier emerges at 1000-2600°F (Joshi & Lee, 1996). It is treated for the removal of

particulate matter, hydrogen sulfide and carbon monoxide (Joshi & Lee, 1996). The steam produced is utilized by a steam turbine to produce electricity. The H_2 can be sent to a gas turbine or to a fuel cell (Audus *et al.*, 1998).

Cryogenic separation of CO_2 from CO_2/N_2 (post combustion capture) is highly energy intensive for flue gas from conventional power plants mainly due to a lean CO_2 mixture in the flue gas (Aaron and Tsouris, 2005; Barchas and Davis, 1992; Kikkinides *et al.*, 1993). Physical or chemical absorption by a solvent which has affinity toward CO_2 , or adsorption in zeolite are other approaches for capturing CO_2 (Riemer, 1996). The solvent or the zeolite can be regenerated by heating/depressurizing it and driving off the CO_2 .

Amine based processes have been used commercially for the removal of acid gas impurities (CO_2 and H_2S) from natural gas. Mono-ethanol amine (MEA) possesses the highest theoretical absorption capacity for carbon dioxide (Herzog *et al.*, 1997). Corrosion is a serious issue in amine processes (Barchas & Davis, 1992; GPSA, 1998; Mariz, 1998). In physical absorption, CO_2 is physically absorbed in a solvent at high partial pressures of CO_2 and low temperatures. This process requires relatively little energy, but the CO_2 must be at high partial pressure. Hence, it is suitable for recovering CO_2 from systems where the exhaust CO_2 would leave the gasifier at elevated pressures (Pre-combustion system). Typical solvents are Selexol (dimethylether of polyethylene glycol) (Sweny & Valentine, 1970) and Rectisol (cold methanol) (Helmut & Griesheim, 1968; Scholz, & Linde, 1970).

There are several novel ideas in research and development stage for CO_2 separation from flue gas (post combustion) and fuel gas (pre combustion). Membrane separation and hydrate-based gas separation are such promising approaches (Yang *et al.*,

2008). The commercial membranes for CO₂ separation are mainly prepared from cellulose acetate, polysulfone, and polyimide (Moritaka & Norio, 1989). Compared to absorption separation, the advantages of the membrane process are as follows: (a) it does not require a separating agent, thus no regeneration is required; and (b) it has low maintenance requirements because there are no moving parts in the membrane unit. However, further development may be required for economically capturing CO₂ from flue/fuel gas on a large scale (Yang et al., 2008). A new process for the separation of gas mixture by hydrate formation has been proposed (Englezos and Lee 2005; Kang and Lee, 2000; Klara and Srivastava, 2002; Spencer, 1998; Spencer & Tam, 1999). Clathrate or gas hydrates are crystals formed by water and substances such as CO₂, N₂, O₂, H₂, and natural gas components (Davidson, 1973, Englezos, 1993; Ripmeester, 2000; Sloan, 1998). When gas hydrate crystals are formed from a mixture of gases, the concentration of these gases in the hydrate crystals is different than that in the original gas mixture. This is the basis for the utilization of clathrate hydrate formation/decomposition as a separation process (Makogon, 1981; Englezos, 1993). Similar to physical absorption, hydrate based technology needs to be operated at lower temperature and higher pressure, which makes it more suitable for pre-combustion capture where a CO₂ rich mixture (~40:60 mixture of CO₂/H₂) is obtained at 2-7 MPa (IPCC, 2005).

Captured CO₂ must be transported to a suitable storage site. This can be done by pipelines. Various approaches are considered for permanent storage of CO₂. Table 1-1 summarizes the estimated capacities of the earth's major potential storage options.

Table 1-1: Estimated world sink capabilities of CO₂ disposal options

Sequestration option	worldwide capacity (Gt CO ₂)
Ocean	10002 to uncertain
Deep saline formation	1000 – possibly 10 ⁴
Depleted oil and gas reservoirs	675-900
Coal seams (ECBM)	3–200 GtC

Thus, technologies and processes exist at different stages of development that can prevent emissions from the production and use of fossil fuels from reaching the atmosphere. They are discussed in detail in a Technology Status Report from the International Energy Agency (McKee, 2002) and recently in an IPCC report (IPCC, 2005). These reports conclude that these technologies have not been optimized. Thus, it is recommended that *R&D* is continued and the focus should be directed towards reducing costs. Recently, in July 2008 at a summit in Hokkaido (Japan), the G8 (Britain, Canada, France, Germany, Italy, Japan, Russia and United States) nations agreed in principle to build at least 20 fully integrated industrial scale sites (larger than 1 Mt per year), with the idea that the expertise gained from these sites could be used for cost reduction, and broad deployment of CCS by 2020 (CSLF, 2008).

As discussed above, gas hydrate formation is one of the novel approaches of CO₂ separation where the working fluid is water, which is non-toxic, non-volatile and inexpensive, compared to other solvents. Also, disposal of CO₂ in the ocean or in deep saline aquifers in the form of CO₂ hydrate (Takahashi et al., 2000; Yamasaki, 2000) requires a thorough understanding of phase equilibria and kinetics of hydrate conversion. *The goal of this thesis is to examine the formation of hydrates from fuel gas mixtures at macro and molecular levels in order to obtain thermodynamic and kinetic data relevant to the hydrate-based process for CO₂ capture from a fuel gas mixture.*

Next, the thesis presents essential background information. A basic description of gas hydrates structure and properties are presented and are followed by a short discussion on work already done on CO₂ and H₂ hydrate. Later in the chapter the objectives of the thesis are presented followed by the organization of the thesis.

1.2. BACKGROUND ON GAS HYDRATES

1.2.1. Gas hydrates, structure and properties

Gas hydrates (or *clathrates*) were first documented in 1810 by Sir Humphrey Davy. They are crystalline water based solids physically resembling ice, in which small gaseous molecules (CH₄, C₃H₈, CO₂, H₂) are trapped inside "cages" of hydrogen bonded water molecules. The guest molecule must not interfere with the hydrogen bonding of the lattice. Clathrate hydrates are not chemical compounds; inside the cage guest molecules interact with water molecules by van der Waals forces (Davidson, 1973; Englezos, 1993; Ripmeester, 2000; Sloan, 1998). Therefore, the formation and decomposition of clathrate hydrates are first order phase transitions, not chemical reactions. Most low molecular weight gases, as well as some higher hydrocarbons and freons form hydrates at suitable temperatures and pressures. Gas hydrates from a single guest are described by the general formula M-nH₂O, where *M* is a molecule of hydrate-forming gas, and *n* is the ratio that indicate the quantity of water molecules associated with 1 molecule of gas (*n* varies from 5.75 to 17).

Different, polyhedral cavity structures can be formed depending on the size and chemical properties of guest molecules. In nature, gas hydrates usually form two crystallographic cubic structures – structure (type) I (sI) and structure (type) II (sII) of

space groups $Pm\bar{3}n$ and $Fd\bar{3}m$, respectively. However, a third hexagonal structure of space group $P6/mmm$ may be observed (Type H) (Ripmeester et al., 1987, Udachin & Ripmeester 1999; Lu et al., 2007).

Structure I hydrates consist of two different types of cavities. The first cavity is formed when water molecules hydrogen bond in such a way that they form a structure with 12 pentagonal faces called a pentagonal dodecahedron (5^{12}). This cavity or cage is present in all three gas hydrate structures mentioned above. When the pentagonal dodecahedra link together by their vertices they create a second type of cavity, a polyhedron with 12 pentagonal and 2 hexagonal faces ($5^{12}6^2$) called a tetrakaidecahedron, which is larger than the dodecahedron. A unit cell of structure I hydrate consists of six large $5^{12}6^2$ cavities, and two small 5^{12} cavities created by 46 water molecules. Structure I is formed with molecules smaller than 6 Å, such as methane, ethane, carbon dioxide, and hydrogen sulfide. Nitrogen and other small molecules ($d < 4.2$ Å) are exceptions and form structure II as single guests or multiple guests in each cage. When the pentagonal dodecahedra link together through face sharing, not by the vertices as in structure I, then the structure formed is known as structure II. By linking together through face sharing, they create a hexakaidecahedron, a polyhedron with 12 pentagonal and 4 hexagonal faces. Because of bending in the hydrogen bonding the cavity is larger than the large cavity in structure I, while the small cavity in structure II is slightly smaller than the small cavity in structure I. Structure II hydrate consists of 16 small and 8 large cavities made up by 136 water molecules. Molecules forming structure II have diameters less than 4.2 Å or greater than 6 Å up to 7 Å. Hydrogen, nitrogen and propane are some of the structure II forming gases.

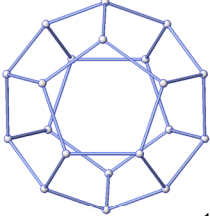
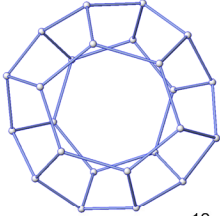
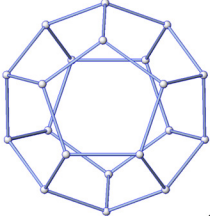
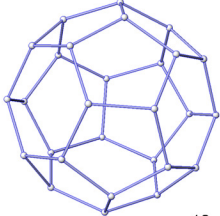
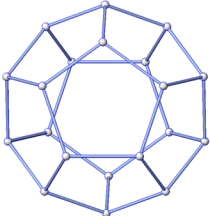
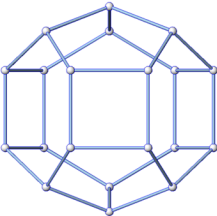
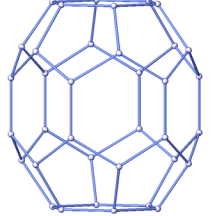
Small (S)	Medium (M)	Large (L)	Structure (Formula)
 5^{12}		 $5^{12}6^2$	Structure I (sI) 2S.6L.46H ₂ O
 5^{12}		 $5^{12}6^4$	Structure II (sII) 16S.8L.136H ₂ O
 5^{12}	 $4^3 5^6 6^3$	 $5^{12}6^8$	Structure H (sH) 3S.2M.1L.34H ₂ O

Figure 1-2: Gas hydrate structures

Structure H was discovered in 1987 at National Research Council in Canada (Ripmeester et al., 1987). It consists of three different kinds of crystal cavities, two of which are small and of comparable sizes, and one large non-spherical cavity. Like structure I and structure II, structure H has the basic 5^{12} cage. However, it is unique compared to the two previous structures because it requires molecules of at least two different sizes to stabilize the crystal. The two other cavities consist of a $4^3 5^6 6^3$ cage which has three fairly strained square faces, six pentagonal and three hexagonal faces and

a large $5^{12}6^8$ cage made up of twelve pentagonal and eight hexagonal faces. The latter cavity is the largest hydrate cavity of any of the structures and is estimated to fit guests up to 9 Å in diameter (Ripmeester et al., 1994). Small molecules, known as help guests, such as methane, xenon or hydrogen sulfide, can occupy the two small cages in structure H, while intermediate sized hydrocarbons such as adamantane, cycloheptane or 2,2-dimethylbutane, also known as neohexane, can fill the large cavity of structure H. The shapes of all the cavities formed in structure I, Structure II and structure H are shown in Figure 1-2.

Table 1-2: Structural properties of hydrates (adapted from Sloan, 1998)

	Structure I	Structure II	Structure H
Cavity Description	Small (S), large (L)	Small (S), large (L)	Small (S), medium (M), large (L)
	$5^{12}, 5^{12}6^2$	$5^{12}, 5^{12}6^4$	$5^{12}, 4^35^66^3, 5^{12}6^8$
Radius (Å)	3.91, 4.33	3.90, 4.73	3.91, 4.06, 5.71
Unit cell	2S.6L.46H ₂ O	16S.8L.136 H ₂ O	3S.2M.1L.34H ₂ O
Crystal type	Cubic	Cubic	hexagonal

Table 1-2 compares the structural properties of structures I, II and H. Depending upon the guest size, shape and hydrate forming pressure different hydrate structure forms. However, there is a considerable complexity in the relationship between the structure and size of the hydrate former once more than a single species is present in the gas phase. The earlier measurements of von Stackelberg (von Stackelberg, 1949) showed that some single guest molecules that are structure I formers will form structure II in binary guest mixtures, a somewhat counter-intuitive notion. The structure of hydrate that is formed is primarily a function of the gas(es) used to form the hydrate. In certain cases, such as

when hydrates are formed from mixtures of two different gases one of which forms structure I hydrate and other forms structure II hydrate, there is a structural transition that is a function of the feed gas composition. For example methane and ethane mixtures form pure structure I hydrate, a mixture of structure I and structure II hydrate as well as pure structure II hydrate depending on initial gas composition (Hendriks et al., 1996; Subramanian et al., 2000). This emphasizes the need to obtain structural information together with thermodynamic and kinetic measurements, especially in multi-component systems.

Sloan (1998) proposed that the size ratio of the guest molecule to the cavity determines whether the guest can form a stable hydrate structure. In order to obtain a stable hydrate structure the ratio needs to be approximately 0.9. If the ratio is significantly less or above unity, stable hydrates structures will not be formed. The molecular diameters to cavity diameter ratios of gases relevant for this work like hydrogen, carbon dioxide and propane are shown in Table 1-3. Based on the above explanation, it was a general perception that hydrogen molecules are too small to fit into the hydrate cages, and no stable clathrate hydrate structure can be formed. Recently, hydrogen clathrate with the type II structure was synthesized and characterized (Mao et al., 2002). More surprisingly, the hydrogen clathrate was found to have an unusually high H_2/H_2O ratio (1:2) by high-pressure x-ray diffraction, Raman, and infrared spectroscopy (Mao et al., 2002). The chemical composition of these clathrates could only be accounted for if multiple occupancies of the clathrate cages are assumed, which was significant departure from the observation made so far, where it was suggested that each cavity could occupy only single guest molecule. This emphasizes the need to characterize the

solid hydrate phase so that exact cage occupancy in the hydrate cages could be monitored directly.

Table 1-3: Size ratio for CO₂ and H₂ (adapted from Sloan, 1998)

		Structure I		Structure II	
	Cavity type =>	5 ¹²	5 ¹² 6 ²	5 ¹²	5 ¹² 6 ⁴
Molecule	Guest diameter (Å)	(Guest diameter)/(Cavity Diameter)			
Carbon dioxide	5.12	1.0	0.834	1.02	0.769
Hydrogen	2.72	0.533	0.464	0.542	0.408
Propane	6.28	1.23	1.07	1.25	.943

The phase equilibria of gas hydrates are the most important set of properties which differentiate it from physically similar ice crystals. The thermodynamics of gas hydrate has been studied extensively over the years. Experimental data on the thermodynamics of gas hydrate formation has been obtained for many systems and the computational methods to predict gas hydrate formation conditions are well established. Studies on hydrate equilibria are focused on gathering incipient equilibrium hydrate formation data as well as developing predictive methods for the calculation of phase equilibria. Incipient hydrate formation conditions refer to the situation in which an infinitesimal amount of the hydrates is present in equilibrium with the fluid phases. The knowledge of equilibrium hydrate forming (pressure-temperature) conditions is necessary for the rational and economic design of processes in the various chemical fields of oil and gas as well as for gas separation process via hydrate formation. The first experimental observation of gas hydrates was made by Sir Humphry Davy (1811), whereas Carson and Katz (1942) were the first to study the four phase equilibria of gas-mixtures in the presence of gas hydrates and of hydrocarbon-rich liquids. A thorough account of the

experimental work and the computational methods on hydrate equilibria is available (Davidson, 1973; Englezos, 1993; Holder et al., 1987; Makogon, 1981; Sloan, 1998).

Time dependent hydrate nucleation and growth phenomena are substantially more challenging than time independent phenomena of hydrate thermodynamics discussed in the previous paragraph. The study of hydrate kinetics deals with two fundamental questions: (1) when will hydrates begin to nucleate? (2) How rapidly do the hydrate nuclei grow? Hydrate nucleation, which has been found to be a stochastic process, refers to the process where small hydrate crystals called nuclei, grow and disperse until they attain a critical size for continued growth. Nucleation is a phenomenon and involves tens to thousands of molecules yet it is difficult to observe experimentally. If the size of the nuclei is less than the critical size (Natarajan et al., 1994), the nuclei are unstable and may continue to grow or break in the aqueous solution. If the growing nuclei reach a critical size then they become stable and continue to grow. This period, from when the hydrate nuclei are forming and dissolving in a supersaturated solution to the time when the nuclei reach the critical size is called the induction time which depends on (a) History of Water (Natarajan et al., 1994); (b) Degree of Supersaturation (Bishnoi and Natarajan, 1996); (c) Stirring Rate (Englezos et al., 1987); (d) Temperature and Pressure (Sloan, 1998); (e) Molecular diameter to cavity size ratio (Sloan, 1998); (f) surface area of contact between gas and water (Sloan, 2008)

Miller and Smythe (1970) made one of the first attempts to quantify gas hydrate crystal growth by measuring the isothermal rate of formation of carbon dioxide from ice. Vysniauskus and Bishnoi (1983a; 1983b; 1985) pioneered kinetic studies of gas hydrate formation above the ice point with isothermal and isobaric experiments in a semi-batch

stirred tank reactor. The hydrate growth rate was monitored through gas uptake measurements. It can be said that kinetics through gas uptake measurements and macroscopic techniques, in general, is in reality the “average kinetics” over the whole sample. The observation of gradual conversion in bulk samples only arises as a result of averaging over many local environments (Moudrakovski et al., 2004). In addition, intermediate steps may also exist during the phase change into hydrate, which are not stable thermodynamically. For example, a meta-stable sII hydrate might be observed in the stability region of sI hydrate as reported for methane hydrate (Schicks and Ripmeester, 2004). The occupancy of the cages may also change during the formation which further complicates the study of the kinetics (Kumar et al., 2008).

In order to get a complete picture of hydrate formation recently the focus has shifted to the analysis of solid hydrate phases. The classical method to obtain information on any crystal structure is via diffraction crystallography and over the years it has been used successfully for accurate determination of hydrate structure (Uchida et al., 2003, Sloan, 2003). Measurement of microscopic properties like hydrate phase composition, water/gas diffusion and structure identification has benefited from the development of spectroscopy tools like Nuclear Magnetic Resonance (NMR) spectroscopy (Moudrakovski et al., 2001; Susilo et al., 2006) and Raman spectroscopy (Komai et al., 2004; Sum et al., 1997) techniques. Infrared spectroscopy has been used by Bertie and co-worker (1973, 1983) and Fleyfel and Devlin (1991) for growth and analysis of solid hydrate phases when synthesized in presence of ethylene oxide. Our work in this thesis suggests that FTIR can be a very important tool in studying the hydrates of CO₂. Diffraction and spectroscopic measurement when done on solid hydrate phases can

provide several important pieces of information, like hydration numbers and relative cage occupancies which are not accessible through macroscopic measurements.

1.2.2. Hydrates of CO₂ & H₂

The equilibrium hydrate formation conditions for pure carbon dioxide have been extensively investigated and are available in the literature. These range from 151.5 K to 292.7 K and 5.35 kPa to 186.2 kPa (Deaton and Frost, 1946; Falabella, 1975; Larson, 1955; Miller and Smythe, 1970; Ng and Robinson, 1985; Robinson and Mehta, 1971; Song and Kobayashi, 1987; Unruh and Katz, 1949). The equilibrium hydrate formation conditions for carbon dioxide are shown in Figure 1-3. As it can be seen in the Figure, for example at 274.15 K, the equilibrium pressure is 1.414 MPa. Hydrate is stable above this pressure while they do not exist below this pressure at 274.15 K. The CO₂ saturation curve is also shown. It has been shown previously that CO₂ molecules occupy primarily the large cavities and very few small cages of resultant structure I hydrate (Davidson et al., 1984). However, the small cages (5¹²) are almost the exclusive sites for CO₂ in structure II hydrate (binary hydrate) when formed using a help compound, which by itself forms sII hydrate (Ripmeester and Ratcliffe, 1998; Udachin et al., 2001).

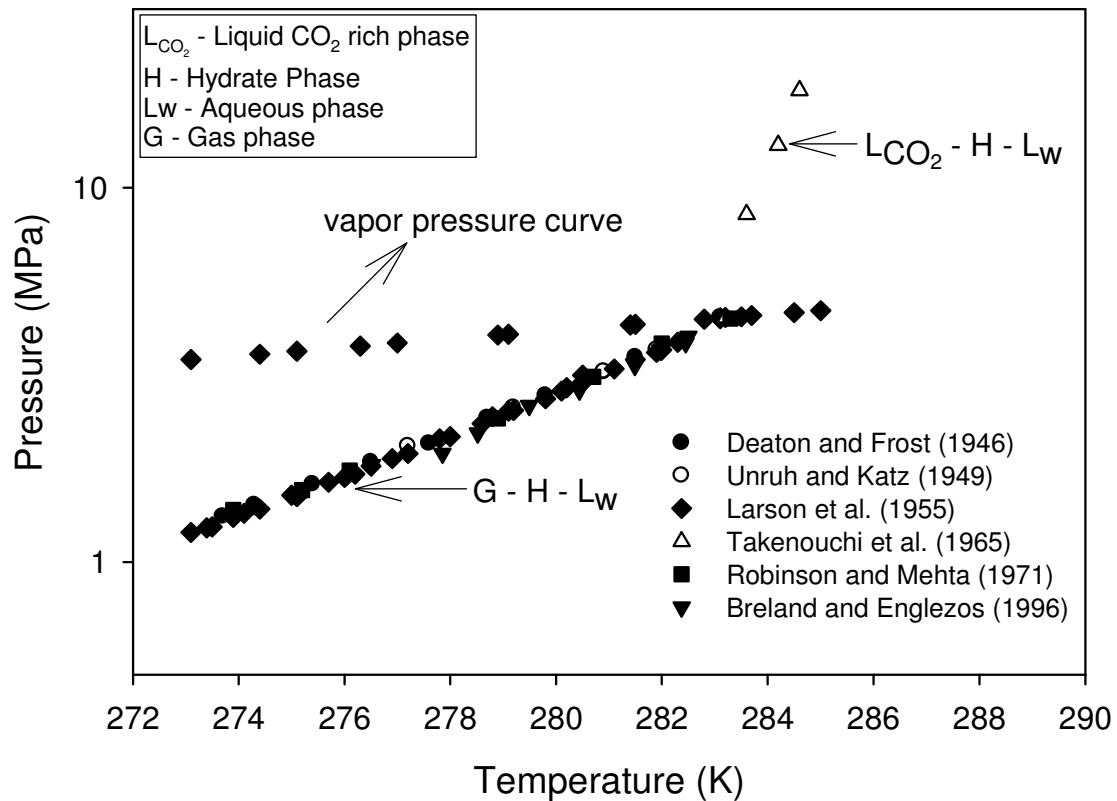


Figure 1-3: Equilibrium hydrate formation conditions for pure carbon dioxide hydrate.

It was a general perception that hydrogen molecules are too small to fit into the hydrate cages, and no stable clathrate hydrate structure can be formed. For the first time Vos et al., in 1993 reported hydrogen clathrate like structure in which hydrogen molecules were found to fill small cavities in ice II and ice Ic structure at high pressure. In 1999 Dyadin *et al.* (1999a, b) demonstrated the first simple hydrogen hydrate (H_2+H_2O). Although the hydrate structure was not confirmed through diffraction, clathrate hydrate formation was inferred from the shape of the liquid water + hydrate + vapor three phase transition curve. However, more recently hydrogen clathrate of classical sII structure was synthesized and characterized (Mao et al., 2002), surprisingly it

was found that, the hydrogen clathrate has an unusually high $\text{H}_2/\text{H}_2\text{O}$ ratio (1:2). The result was confirmed by high-pressure x-ray diffraction, Raman, and infrared spectroscopy (Mao et al., 2002) and by statistical mechanical model in conjunction with first principle quantum chemistry calculation (Patchkovskii and Tse, 2003). This unusually high ratio of hydrogen to water was attributed to the fact that hydrogen can stabilize the relatively bigger cages in sII by occupying it in clusters of 2-4 hydrogen molecules. Florusse et al (2004) synthesized binary hydrate of H_2/THF where tetrahydrofuran (THF) acts as hydrate promoter. The addition of THF was found to significantly reduce the hydrate formation pressure by a factor of 40 (from 200 to 5 MPa at 280 K) by filling the large cages and stabilizing the sII structure; the small cages can then be filled by molecular hydrogen.

Since the focus of this thesis is to use hydrate formation for the separation of CO_2 from a CO_2/H_2 mixture the thermodynamic phase equilibrium of CO_2 / H_2 hydrate need to be evaluated. Spencer et al., (1998, 1999, 2002) carried out work on CO_2/H_2 separation from synthesis gas however, the thermodynamic and kinetic behavior of CO_2/H_2 hydrate was not reported. At the time when work on this thesis started phase equilibrium measurements on CO_2/H_2 binary hydrate were not available in the literature. Relevant additional literature on CO_2/H_2 hydrate is discussed later in this thesis.

1.3. RESEARCH OBJECTIVES

The main purpose of this research is to assess how hydrate formation can be used to develop a separation process for recovering CO_2 and H_2 from fuel gas mixture obtained in an IGCC plant. The generation of a conceptual process flowsheet requires determination of the pressure/temperature operating conditions, assessment of rate of

formation/dissociation of the hydrate, and determination of the separation efficiency. Moreover, molecular level measurements need to be carried out to determine hydrate cage occupancy, which would help in increasing the separation efficiency by tuning and optimizing the amount of additives used. Thus, the purpose of this thesis is to provide the above information. The objectives are as follows

1. Provide incipient equilibrium hydrate formation data for the CO₂/H₂ hydrate.
2. Identify suitable additives that reduce the required formation pressure and provide the relevant incipient equilibrium data.
3. Determine nucleation time and rate of hydrate formation for hydrate formation from the CO₂/H₂ and CO₂/H₂/additive systems.
4. Propose a conceptual flow sheet for a hydrate-based CO₂/H₂ separation process.
5. Determine the separation efficiency of the hydrate-based separation process.
6. Characterize the relevant solid hydrate phases in terms of crystal structure and cage occupancy.

1.4. THESIS ORGANIZATION

CO₂ mitigation and technologies available are discussed in chapter 1. This chapter also gives the basic information on gas hydrates and current knowledge on gas hydrate research relevant to CO₂ capture and storage.

Chapter 2 reports the incipient hydrate phase equilibrium for a fuel gas mixture of CO₂ (39.2%) and rest H₂. A small amount of propane as an additive has been identified and added in the fuel gas mixture, thermodynamics phase boundary for hydrate formation has been determined. This study has been published.

- Kumar, R., Wu, H., Englezos, P., “Incipient hydrate phase equilibrium for gas mixtures containing hydrogen, carbon dioxide and propane”, *Fluid Phase Equilibria*, 2006, 244, 167–171

Chapter 3 reports the kinetic data on hydrate formation for a fuel gas mixture of CO₂ (39.2 mol%) and rest H₂. This chapter also reports the clathrate hydrate process for the separation of CO₂ from fuel gas mixtures in two stages coupled with a membrane process to treat the lean CO₂ stream. Two metrics defining CO₂ recovery or split fraction and Separation factor were presented to assess the separation process. The material for this chapter is published.

- Linga, P., Kumar, R., and Englezos, P., 2007. Gas hydrate formation from hydrogen/carbon dioxide and nitrogen/carbon dioxide gas mixtures. *Chemical Engineering Science* 62(16), 4268-4276.
- Linga, P., Kumar, R., and Englezos, P., 2007. The clathrate hydrate process for post and pre-combustion capture of carbon dioxide. *Journal of Hazardous Materials* 149(3), 625-629.

Chapter 4 reports kinetic data on the effect of propane on separation of CO₂ from the fuel gas mixture. It was found that use of 2.5 mol% propane significantly reduces the operating pressure without compromising the CO₂ recovery and separation factor significantly. The material for this chapter has been published.

- Kumar, R., Linga, P., Ripmeester, J. A., Englezos, P. 2009 “A two-stage clathrate hydrate/membrane process for pre-combustion capture of carbon dioxide and hydrogen” *Journal of Environmental Engineering*, 135, 411-417.

Chapter 5 employs molecular level techniques to look at the formation and decomposition of sI hydrate of CO₂/H₂ and sII hydrate of CO₂/H₂/C₃H₈. This chapter also gives a complete solid-state analysis of the hydrate phase characterized by several independent measurements. The crystal structure, cage occupancy, and hydrate phase

composition are reported using X-ray Diffraction, Nuclear Magnetic Resonance (NMR) spectroscopy, Raman Spectroscopy and gas chromatography. The material for this chapter has been published.

- Kumar, R., Moudrakovski, I., Ripmeester, J. A., Englezos, P. 2009. Structure and composition of CO_2/H_2 and $\text{CO}_2/\text{H}_2/\text{C}_3\text{H}_8$ hydrate in relation to simultaneous CO_2 capture and H_2 production. *AIChE J.* 55, 1584-1594.

Chapter 6 presents a detailed study on use of Infrared spectroscopy for studying CO_2 hydrates. The solid hydrate phase has been characterized by *in-situ* hydrate formation of CO_2 , $\text{CO}_2/\text{C}_3\text{H}_8$, CO_2/H_2 and $\text{CO}_2/\text{H}_2/\text{C}_3\text{H}_8$ hydrate. The material for this chapter has been published.

Kumar, R., Stephen, L., Englezos, P., Ripmeester, J. A. 2009. Application of the ATR-IR spectroscopic technique to the characterization of hydrates formed by CO_2 , CO_2/H_2 , $\text{CO}_2/\text{H}_2/\text{C}_3\text{H}_8$. *J. Phys. Chem. A.* 113, 6308-6313.

Finally, in Chapter 7 the conclusions are highlighted and recommendations for future work are given.

1.5. REFERENCES

- Aaron, D., and Tsouris, C. 2005. Separation of CO₂ from flue gas: A review. *Separation Science and Technology* 40, 321-348
- Audus, H., Olav, K. and Geoff, S. 1998. CO₂ capture by pre-combustion decarbonization of natural gas Proceedings of the International Conference on Greenhouse Gas Control Technologies, Interlaken, Switz., 557-562
- Barchas, R., and Davis, R., 1992. The Kerr-Mcgee Abb Lummus Crest Technology for the Recovery of CO₂ from Stack Gases. *Energy Conversion and Management* 33, 333-340
- Bertie, J. E., Othen, A. D. 1973. The Infrared Spectrum of Ethylene Oxide Clathrate Hydrate at 100K between 4000 and 360 cm⁻¹ *Can. J. Chem.*, 51, 1159-1168
- Bertie, J. E., Devlin, J. P. 1983. Infrared spectroscopic proof of the formation of the structure I hydrate of oxirane from annealed low-temperature condensate *J. Chem. Phys.*, 78, 6340-6341
- Bishnoi, P. R., and Natarajan, V. 1996. Formation and decomposition of gas hydrates. *Fluid Phase Equilibria* 117, 168-177
- Breland, E., and Englezos, P. 1996. Equilibrium Hydrate Formation Data for Carbon Dioxide in Aqueous Glycerol Solutions. *Journal of Chemical and Engineering Data* 41, 11-13
- Carson, D. B., and Katz, D. L., 1942. Natural Gas Hydrates. *Trans. A.I.M.E.* 146, 150-158
- CSLF. (2008). "Results from G8-IEA Calgary Workshop on Near-Term Opportunities for Carbon Capture and Storage." Carbon Sequestration Leadership Forum, Calgary.
- Davidson, D. W., 1973. Gas Hydrates. In *Water: A Comprehensive Treatise*, Plenum Press, New York.
- Davidson, D. W. Garg, S. K. Gough, S. R. Handa, Y. P. Ratcliffe, C. I. Tse, J. S. Ripmeester, J. A. 1984. Some structural and thermodynamic studies of clathrate hydrates *Journal of inclusion phenomena* 2, 231-238
- Davy, H. 1811. The Bakerian Lecture. On Some of the Combinations of Oxymuriatic Gas and Oxygen, and on the Chemical Relations of these Principles to Infl. *Phil Trans Roy Soc (London)* 101, 1-35
- Deaton, W. M., and Frost, E. M. 1946. Gas Hydrates and Their Relation to the Operation of Natural-Gas Pipelines. U.S. Dept. of the Interior, 1-101

- Dyadin, Y. A., Larionov, E. G., Aladko, E. Y., Manakov, A. Y., Zhurko, F. V., Mikina, T. V., Komarov, V. Y., and Grachev, E. V. 1999a. Clathrate Formation in Water-Noble Gas (Hydrogen) Systems at High Pressure. *J. Struct. Chem.*, 40, 790-791
- Dyadin, Y. A., Larionov, E. G., Manakov, A. Y., Zhurko, F. V., Aladko, E. Y., Mikina, T. V., and Vladislav, Y. K. 1999b. Clathrate hydrates of hydrogen and neon. *Mendeleev Commun.*, 5, 209-210
- Englezos, P., 1993. Clathrate Hydrates. *Industrial & Engineering Chemistry Research* 32, 1251-1274
- Englezos, P., Kalogerakis, N., Dholabhai, P. D., and Bishnoi, P. R., 1987. Kinetics of Formation of Methane and Ethane Gas Hydrates. *Chemical Engineering Science* 42, 2647-2658
- Englezos, P., and Lee, J. D. 2005. Gas hydrates: A cleaner source of energy and opportunity for innovative technologies. *Korean Journal of Chemical Engineering* 22, 671-681
- Falabella, B. J., 1975. A Study of Natural Gas Hydrates. Ph.D. Dissertation, University of Massachusetts
- Fleyfel, F., Devlin, J. P. 1991. Carbon Dioxide Clathrate Hydrate Epitaxial Growth: Spectroscopic Evidence for Formation of the Simple Type-II COP Hydrate The *Journal of Physical Chemistry*, 95, 3811-3815
- Florusse, L. J., Peters, C. J., Schoonman, J., Hester, K. C., Koh, C. A., Dec, S. F., Marsh, K. N., Sloan, E. D. 2004. Stable low pressure hydrogen clusters stored, in a binary clathrate hydrate, *Science*, 306, 469-471
- Freund, P. 1997. Waste Management. The International Symposium on Ocean Disposal of Carbon Dioxide, 343-352
- GPSA. (1998) Gas Processors Suppliers Association, Engineering Data Book, Volume II, Section 21, Tulsa, Oklahoma.
- Helmut, K. and Griesheim, M. 1968. Low-temperature absorption. Rectisol process. Proceedings of the Gas Conditioning Conference, University of Oklahoma, Norman, Oklahoma, 1968.
- Hendriks, E. M., Edmonds, B., Moorwood, R. A. S. and Szczepanski, R. 1996. Hydrate structure stability in simple and mixed hydrates, *Fluid Phase Equilibria*, 117, 193-200

- Herzog, H. J., Drake, E., and Adams, E. 1997. CO₂ Capture, Reuse, and Storage Technologies for Mitigating Global Climate Change. White Paper Final Report, DOE Order NO DE-AF22-96PC01257, 66.
- Holder, G. D., Zetts, S. P., and Pradhan, N. 1988. Phase Behavior in Systems Containing Clathrate Hydrates - A Review. Chem. Eng. Reviews, 5, 1-70
- IPCC. (1996) Climate Change 1995. The Science of Climate Change. The Intergovernmental Panel on Climate Change, *Cambridge University Press*, Cambridge, UK.
- IPCC. (2001). Climate Change 2001: The Scientific Basis. Intergovernmental Panel on Climate Change, *Cambridge University Press*, Cambridge, UK.
- IPCC. (2005). "Carbon dioxide capture and storage, IPCC Special report." Intergovernmental Panel on Climate Change.
- Joshi, M. M. & Lee, S. 1996. Integrated gasification combined cycle- A review of IGCC technology, Energy Sources, 18, 537-568
- Kang, S. P., and Lee, H. 2000. Recovery of CO₂ from flue gas using gas hydrate: Thermodynamic verification through phase equilibrium measurements. Environmental Science & Technology 34, 4397-4400
- Kikkinides, E. S., Yang, R. T., and Cho, S. H. 1993. Concentration and Recovery of CO₂ from Flue-Gas by Pressure Swing Adsorption. Industrial & Engineering Chemistry Research 32, 2714-2720
- Klara, S. M., and Srivastava, R. D. 2002. US DOE integrated collaborative technology development program for CO₂ separation and capture. Environmental Progress 21, 247-253
- Komai, T., Kang, S.-P., Yoon, J.-H., Yamamoto, Y., Kawamura, T., Ohtake, M. 2004. In Situ Raman Spectroscopy Investigation of the Dissociation of Methane Hydrate at Temperatures Just below the Ice Point J. Phys. Chem. B, 108, 8062-8068
- Kumar, R., Linga, P., Moudrakovski, I., Ripmeester, J. A., Englezos, P. 2008. Structure and kinetics of gas hydrates from methane/ethane/propane mixtures relevant to the design of natural gas hydrate storage and transport facilities AIChE, 54, 2132-2144
- Larson, S. D. 1955. Phase Studies of the Two-component Carbon Dioxide - Water System, Involving the Carbon Dioxide Hydrate, PhD Thesis University of Illinois.

- Lu, H., Seo, Y., Lee, J., Moudrakovski, I., Ripmeester, J.A., Chapman, N. R., Coffin, R. B., Gardner, G., Pohlman, J. 2007. Complex gas hydrate from the Cascadia margin, *Nature*, 445, 303-306
- Makogon, Y. F. 1981. *Hydrates of Natural Gas*. Pennwell books, Tulsa, Okla. (Translated by Cieslewicz, W. J.)
- Mao, W. L., Mao, H. K., Goncharov, A. F., Struzhkin, V. V., Guo, Q. Z., Hu, J. Z., Shu, J. F., Hemley, R. J., Somayazulu, M., and Zhao, Y. S., 2002. Hydrogen clusters in clathrate hydrate. *Science* 297, 2247-2249
- Mariz, C. L., 1998. Carbon Dioxide Recovery: Large Scale Design Trends, *Journal of Canadian Petroleum Technology*, 37, 42-47
- McKee, B. (2002). "Zero Emissions Technologies – Technology status Report." OECD/IEA, Paris.
- Miller, S. L., and Smythe, W. D. 1970. Carbon Dioxide Clathrate in the Martian Ice Cap. *Science* 170, 591-594
- Moritaka, K. and Norio, I. 1989. Membrane modules for light hydrocarbon gas separation. Kokai Tokkyo Koho, JP 01043329
- Moudrakovski, I. L., McLaurin, G. E., Ratcliffe, C. I., Ripmeester, J. A. 2004. *J. Phys. Chem. B*, 108, 17591-17595.
- Moudrakovski, I. L., Sanchez, A. A., Ratcliffe, C. I., Ripmeester, J. A. 2001. Nucleation and Growth of Hydrates on Ice Surfaces: New Insights from ^{129}Xe NMR Experiments with Hyperpolarized Xenon *J. Phys. Chem. B*, 105, 12338-12347
- Natarajan, V., Bishnoi, P. R., and Kalogerakis, N. 1994. Induction Phenomena in Gas Hydrate Nucleation. *Chemical Engineering Science* 49, 2075-2087
- NETL. (2004) Gasification: world survey results 2004 (http://www.netl.doe.gov/publications/brochures/pdfs/Gasification_Brochure.pdf)
- Ng, H. J., and Robinson, D. B. 1985. Hydrate Formation in Systems Containing Methane, Ethane, Propane, Carbon Dioxide or Hydrogen Sulfide in Presence of Methanol. *Fluid Phase Equilib.* 21, 145-55
- Olsen, K., Collas, P., Boileau, P., Blain, D., Ha, C., Henderson, L., Liang, C., McKibbin, S., Huissier, L. M. Canada's greenhouse gas inventory: 1990–2000. Technical report, Environment Canada, June 2002 (http://www.ec.gc.ca/pdb/ghg/inventory_report/1990_00_report/source/031_ghgas_english5.pdf)

- Patchkovskii, S. and Tse, J. S. 2003. Thermodynamic stability of hydrogen clathrates, *PNAS- USA*, 100(25), 14645-14650
- Riemer, P. 1996. Greenhouse Gas Mitigation Technologies, an Overview of the CO₂ Capture, Storage and Future Activities of the IEA Greenhouse Gas R&D Programme, *Energy Convers. Mgmt.*, 37, 665-670
- Ripmeester, J. 2000, In 3rd International Hydrate Conference Vol. 912 (Ed, Holder, B. E.) NYAS, Salt Lake City, 2000
- Ripmeester, J. A., and Ratcliffe, C. I., 1998. The diverse nature of dodecahedral cages in clathrate hydrates as revealed by Xe-129 and C-13 NMR spectroscopy: CO₂ as a small-cage guest. *Energy & Fuels* 12, 197-200
- Ripmeester, J. A., Ratcliffe, C. I., Klug, D. D., and Tse, J. S., 1994. Molecular Perspectives on Structure and Dynamics in Clathrate Hydrates. *International Conference on Natural Gas Hydrates* 715, 161-176
- Ripmeester, J. A., Tse, J. S., Ratcliffe, C. I., and Powell, B. M., 1987. A New Clathrate Hydrate Structure. *Nature* 325, 135-136
- Robinson, D. B., and Mehta, B. R. 1971. Hydrates in the Propane-Carbon Dioxide-Water System. *J. Can. Petrol. Tech* 10, 33.
- Schicks, J. M., Ripmeester, J. A. 2004. The Coexistence of Two Different Methane Hydrate Phases under Moderate Pressure and Temperature Conditions: Kinetic versus Thermodynamic Products *Angew. Chem. Int. Ed.*, 43, 3310–3313
- Scholz, W. H., Linde A.-G. 1970 Rectisol: a low-temperature scrubbing process for gas purification. *Advances in Cryogenic Engineering*, 15, 406-414
- Sloan, E. D., 2003. Clathrate hydrate measurements: microscopic, mesoscopic, and macroscopic. *Journal of Chemical Thermodynamics* 35, 41-53.
- Sloan, E. D., Jr., 1998. *Clathrate Hydrates of Natural Gases*, Second Edition, Revised and Expanded, Marcel Dekker, NY.
- Sloan, E. D. Jr., and Koh, C. A., 2008. *Clathrate Hydrates of the Natural Gases*, Third Edition, CRC Press, Boca Raton, FL.
- Song, K. Y., and Kobayashi, R., 1987. Water Content of CO₂ in Equilibrium with Liquid Water and/or Hydrates. *SPE Formation Evaluation*, 500-508
- Spencer, D. F., 1998. Integration of an advanced CO₂ separation process with methods for disposing of CO₂ in oceans and terrestrial deep aquifers., *Proceedings of the*

- International Conference on Greenhouse Gas Control Technologies, 4th, Aug. 30-Sept. 2, 1998, 89-94
- Spencer, D. F. Tam, S. S. 1999. An engineering and economic evaluation of a CO₂ hydrate separation system for shifted synthesis gas., Proceedings of 16th Annual International Pittsburgh Coal Conference, October 11-15, 1999, 1303-1317
- Spencer, D. F. Tam, S. S., Gordon, D., Currier, R. F., Young, J. S., Anderson, G. K. 2002. Carbon dioxide separation from a high pressure shifted synthesis gas. Proceedings of 19th Annual International Pittsburgh Coal Conference, September 23, 2002 1497-1513
- Susilo, R. Moudrakovski, I. L. Ripmeester, J. A. Englezos, P. 2006. Hydrate Kinetics Study in the Presence of Nonaqueous Liquid by Nuclear Magnetic Resonance Spectroscopy and Imaging J. Phys. Chem. B, 110, 25803-25909
- Subramanian, S. Kini, R. A. Dec S. F. and Sloan E. D. Jr. 2000. Evidence of structure II hydrate formation from methane+ethane mixtures Chemical Engineering Science 55, 1981-1999
- Sum, A. K., Burruss, R. C., Sloan, E. D., Jr. 1997. Measurement of Clathrate Hydrates via Raman Spectroscopy J. Phys. Chem. B, 101, 7371-7377
- Sweny, J. W., Valentine, J. P. 1970 Physical solvent stars in gas treatment/purification. Chemical Engineering (New York, NY, United States) 77, 54-56
- Takenouchi, S., and Kennedy, G., 1965. Dissociation pressures of the phase CO₂ 5 3/4 H₂O. Geology 73, 383.
- Takahashi, T., Goldberg, D., and Mutter, J. C., 2000. International Symposium on Deep Sea Sequestration of CO₂, Tokyo, Japan.
- Uchida, T., Takeya, S., Wilson, L.D., Tulk, C.A., Ripmeester, J.A., Nagao, J., Ebinuma, T., Narita, H. 2003. Measurements of physical properties of gas hydrates and in situ observations of formation and decomposition processes via Raman spectroscopy and X-ray diffraction Can. J. Phys., 81, 351-357.
- Udachin, K. A., Ratcliffe, C. I., and Ripmeester, J. A., 2001. Structure, composition, and thermal expansion of CO₂ hydrate from single crystal X-ray diffraction measurements. Journal of Physical Chemistry B 105(19), 4200-4204.
- Udachin, K. A., and Ripmeester, J. A., 1999. A complex clathrate hydrate structure showing bimodal guest hydration. Nature 397(6718), 420-423.
- Unruh, C. H., and Katz, D. L., 1949. Gas Hydrates of Carbon Dioxide - Methane Mixtures. Petroleum Transactions, AIME, 83-86.

- von Stackelberg, M., 1949. Solid gas hydrates. *Naturwissenschaften* 11-12, 1–22
- Vos, W. L., Finger, L. W., Hemley, R. J., Mao, H.-K. 1993. Novel H₂-H₂O Clathrates at High Pressures, *Phy. Rev. Lett.*, 71, 3150-3153
- Vysniauskas, A., and Bishnoi, P. R., 1983a. A Kinetic-Study of Methane Hydrate Formation. *Chemical Engineering Science* 38, 1061-1072.
- Vysniauskas, A., and Bishnoi, P. R., 1983b. A Kinetic Study of Methane Hydrate Formation. *Chem. Eng. Sci* 38, 1061-1072.
- Vysniauskas, A., and Bishnoi, P. R., 1985. Kinetics of Ethane Hydrate Formation. *Chem. Eng. Sci.* 40, 299-303.
- WEO. (2000). "World Energy Outlook." International Energy Agency.
- Yamasaki, A., 2000, A New CO₂ Ocean Sequestration Scenario via a Crystallization Process of CO₂ Hydrate Particles," *Proceedings of DEEP SEA & CO₂ 2000, International Symposium on Deep Sea Sequestration of CO₂, February 1-2, Tokyo, Japan, pp. 2-2-1-2-1-7 (2000).*
- Yang, H., Xu, Z., Fan, M., Gupta, R., Slimane, R. B., Bland, A. E., Wright, I. 2008. Progress in carbon dioxide separation and capture: A review *Journal of Environmental Sciences*, 20, 14–27

2. INCIPIENT HYDRATE PHASE EQUILIBRIUM FOR GAS MIXTURES CONTAINING HYDROGEN, CARBON DIOXIDE & PROPANE¹

2.1. INTRODUCTION

As discussed in chapter 1, fossil fuel electric power plants are the prime targets for CO₂ capture and storage. In “post combustion” capture one has to consider separation of CO₂ from the flue gas which is essentially a CO₂/N₂ mixture. On the other hand, “pre-combustion” capture involves capturing the carbon prior to utilizing the fuel. This is an approach used for both H₂ production and electricity generation in a natural gas combined cycle power plant (NGCC) or in an integrated coal gasification combined cycle (IGCC) (Corman, 1982; Joshi and Lee, 1996). In an IGCC power station, coal is gasified or natural gas is reformed to produce synthesis gas (mixture of CO and H₂). The CO is reacted with steam in a catalytic reactor (shift converter) to produce CO₂ and more H₂. The CO₂ can then be separated from the mixture and the H₂ gas can be used in a gas turbine combined cycle plant for electricity generation, as a chemical feedstock, or in a fuel cell to produce electricity (Audus et al, 1998).

Since the energy cost is a major factor, new processes are being considered. One such process is based on gas hydrate crystallization (Kang and Lee, 2000; Klara and Srivastava, 2002). The basis for the separation is the selective partition of the target component between the hydrate phase and the gaseous phase.

¹ “A version of this chapter has been published. Kumar, R., Wu, H., Englezos, P. (2008) Incipient hydrate phase equilibrium for gas mixtures containing hydrogen, carbon dioxide and propane. Fluid Phase Equilibria, 244:167–171”

Carbon dioxide (CO_2) is known to form structure I (sI) hydrate at moderate pressures, e.g. in the range of a few MPa (Davidson, 1973). According to Mao et al. (2002) and Mao and Mao (2004), H_2 forms structure II (sII) hydrate at the high pressure of 200 MPa (or the low temperature of about 80 K). The small hydrate cages are occupied by a cluster of two H_2 molecules, whereas the large cages may have clusters of four H_2 molecules.

Zhang et al. (2000) have studied hydrate formation conditions for H_2 –hydrocarbon gas mixtures with H_2 content varying from 0 to 92 mol%. The experimental results indicate that the hydrate formation pressures of H_2/CH_4 and $\text{H}_2/\text{C}_3\text{H}_8$ gas mixtures were higher than those for pure CH_4 and pure C_3H_8 . However, there is no comment on the structure of hydrate formed by the resulting mixture. Zhang et al. (2005) studied the hydrate formation from binary gas mixtures of H_2 and CH_4 in the presence of 6-mol% tetrahydrofuran (THF). The results showed that the presence of THF in water can drastically lower the hydrate formation pressure of pure CH_4 or the H_2/CH_4 mixtures. Similarly, Florusse et al. (2004) studied H_2 hydrate formation in presence of THF. Their work was concerned with using hydrates as a media for H_2 storage. Florusse et al. reported that hydrate clusters of H_2 can be stabilized and stored at low pressure in sII binary clathrates. A single H_2 molecule or clusters of two H_2 molecules occupy small water cages, whereas large water cages are singly occupied by THF. In a more recent paper, Lee et al. (2005a) suggested that by tuning the composition of THF and H_2 in a hydrate forming mixture, it is possible that H_2 occupies both the larger and the smaller cages of the resultant sII hydrate. This tuning mechanism enhances the H_2 storage capacity of the resultant binary hydrate, while retaining the low-pressure stability.

However, after publication of this work in 2005 several studies on H₂/THF hydrate have appeared and the tuning mechanism of Lee et al., (2005a) has not been confirmed by other studies, hence H₂ storage capacity in such a hydrate is still controversial. H₂/THF hydrate is discussed in more detail in chapter 5 and in Appendix C.

Sugahara et al. (2005), based on a Raman spectroscopic study on a hydrate crystal of CO₂/H₂ hydrate reported that hydrogen does not occupy any of the cages in the resultant sI hydrate structure. Their observation was based on the fact that the Raman peak of the H–H stretching vibration mode of H₂ was detected in the gas phase but was absent in the hydrate phase. Thus, according to Sugahara et al. hydrogen behaves like a diluent gas in the formation of CO₂ hydrate. Kim and Lee (2005) used both Raman spectroscopy and NMR to determine the occupancy of hydrogen in the hydrate cages. They suggested that it is difficult to detect the hydrogen peak through Raman spectra and only NMR was able to provide two different chemical shifts of hydrogen peaks with clear distinction. Thus, they concluded hydrogen participates in the mixed structure I hydrate formed from a CO₂/H₂ mixture (20 mol% CO₂). Moreover, they reported that two H₂ molecules are found in the small 5¹² cages (double occupancy). It should be noted that the temperature and pressure conditions for hydrate formation were not reported.

Consideration of hydrate crystallization as a potential CO₂/H₂ separation process necessitates the need for relevant phase equilibrium and kinetic data. Such data will allow us to determine what pressure– temperature conditions are required for CO₂/H₂ mixtures to form hydrate at appreciable rates. Moreover, it is of interest to study the formation of hydrates from CO₂ and H₂ in the presence of a third component (*promoter*) that will decrease the hydrate formation pressure. Thus, the objectives of the work presented in

this chapter is to present phase equilibrium data for hydrates formed by: (a) CO_2/H_2 mixtures at gas concentrations relevant to the design of a “pre-combustion capture” separation process based on hydrate formation and decomposition and (b) $\text{CO}_2/\text{H}_2/\text{C}_3\text{H}_8$ mixtures, where C_3H_8 acts as hydrate promoter.

2.2. EXPERIMENTAL APPARATUS AND PROCEDURE

2.2.1. Apparatus and materials

The apparatus is shown in Fig. 2-1. It consists of a high-pressure hydrate crystallizer (CR) constructed of 316 stainless steel. The crystallizer has two circular viewing windows on the front and back. Mixing of the crystallizer contents is accomplished using a magnetic stir bar that is magnetically coupled to a set of rotating magnets (Tormag Engineering, Vancouver, BC) placed directly underneath the crystallizer. The set of magnets is driven by an electric motor (GK Heller Corp., USA, Model GT 21). Three copper–constantan thermocouples (Omega) with $\pm 0.1^\circ\text{C}$ accuracy are used to measure the temperature at the top, middle and near the bottom of the crystallizer. All pressure measurements are made with Rosemount smart pressure transducers, model 3051 (Norpac Controls, Vancouver, BC), with a range of 0–13,790 kPa and accuracy of less than 0.075% of the span. In order to measure the composition of the gas phase in the crystallizer, a VarianCX3400 gas chromatograph (GC) (Varian Canada Inc., Mississauga, Ont.) is connected on-line with the crystallizer and automated with a PC. The crystallizer is immersed in a constant temperature bath containing a 50/50 wt% ethylene glycol/water mixture. Circulating the glycol/water mixture from an external temperature-controlled bath maintains the temperature in the hydrate crystallizer and the reservoir (R) constant.

A 39.2–60.8 mol% CO₂/H₂ mixture was obtained from Praxair, Canada. Propane from Praxair was also used. All gases had 99.99% purity.

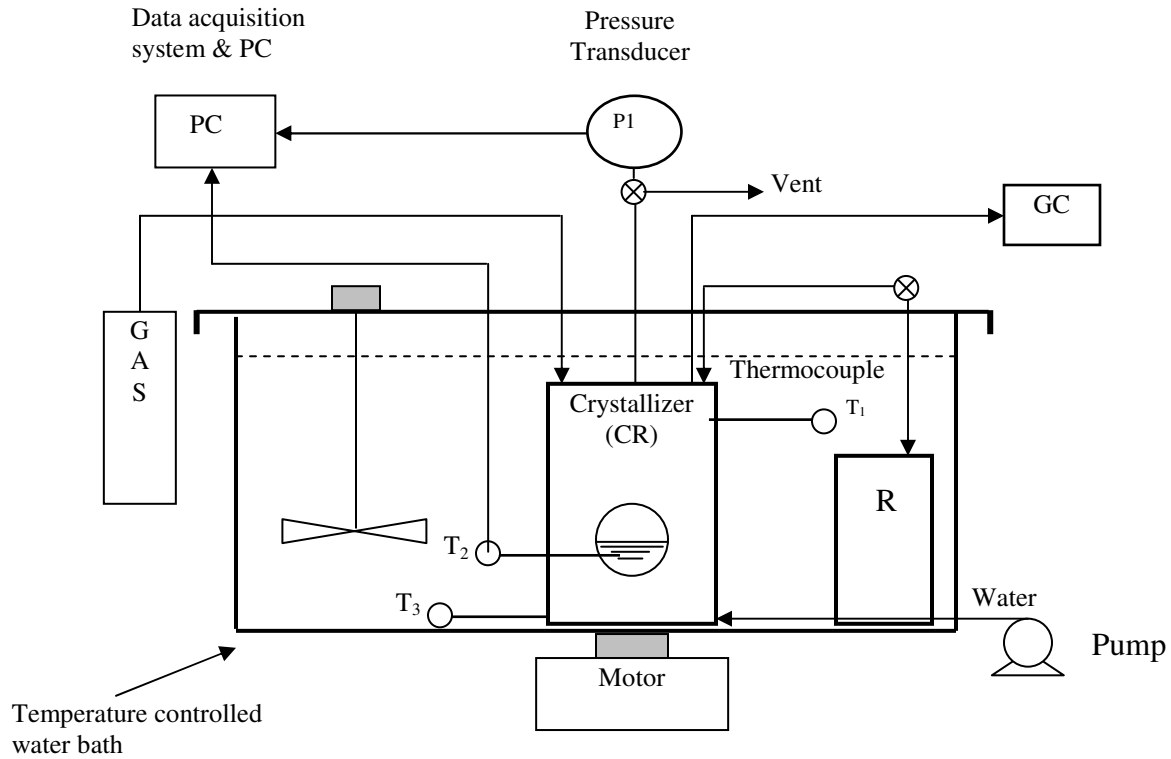


Figure 2-1: Experimental apparatus to study incipient equilibrium hydrate formation condition (adapted from Lee et al., 2005b)

2.2.2. Procedure

The isothermal pressure search method to determine the incipient equilibrium hydrate formation pressure was followed (Englezos and Ngan, 1994). For the CO₂/H₂ experiments the crystallizer was first flushed three times with pure CO₂ to get rid of any air present in the system. Subsequently, pure CO₂ and pure H₂ were charged in the crystallizer separately and were allowed to mix for 3 h. The composition of the mixture was analyzed three times after every half an hour by gas chromatography. After the dry

gas composition in the crystallizer stabilized, the gas mixture was transferred to the reservoir. The reservoir was also maintained at the experimental temperature. It is noted that for the experiments with the 39.2–60.8 mol% CO₂/H₂ mixture there was no need to mix CO₂ and H₂ because a gas cylinder from Praxair was used. For the experiments with the ternary gas mixture C₃H₈ was injected into the crystallizer containing a 39.2–60.8 mol% CO₂/H₂ mixture. The resulting composition of the ternary CO₂/H₂/C₃H₈ mixture was determined by gas chromatography (GC). The gas was then transferred to the reservoir. At a given experimental temperature the crystallizer was filled with 140 cm³ of distilled and de-ionized water through an inlet at the bottom of the crystallizer. Once the temperature of the water (inside the crystallizer) reached the desired temperature, gas from the reservoir was injected into the crystallizer and removed three times to get rid of any air present in the system. Subsequently, the crystallizer was pressurized with gas from the reservoir to a pressure well above the expected equilibrium hydrate formation pressure (1–2 MPa in excess).

After reaching thermal equilibrium, the stirring by the magnetic bar was commenced. Once a small amount of hydrate crystals formed and was visible through the viewing window the pressure was reduced to a point that ensured that the hydrate crystals completely decomposed. The process was repeated three times to get rid of any hysteresis that is known to be associated with hydrate formation (Englezos and Ngan, 1994). Moreover, forming and decomposing hydrates three times also gave an initial estimate of the equilibrium pressure at any given temperature.

Subsequently, the pressure of the system was increased to approximately 0.05–0.15MPa above the estimated equilibrium value in order to form a small amount of

hydrate. Once a small amount of hydrate formed, the pressure was quickly decreased to the expected (estimated) equilibrium value. The system was left under this condition for at least 4–5 h or over night. If there was still a very small (infinitesimal) amount of hydrate left in the system and the system pressure was constant, the pressure was noted to be the equilibrium pressure. If there was no hydrate left in the system, the current pressure of the system was below the actual equilibrium pressure. Consequently, the pressure of the system was increased and small amount of hydrate was allowed to form. The process was repeated at a new expected equilibrium pressure until an infinitesimal amount of hydrate was found to exist in equilibrium with water and gas phase for at least 4 h. Once the incipient equilibrium hydrate formation pressure has been determined a sample of 200 μL from the gas phase was injected in the gas chromatograph to determine the equilibrium composition. A gas chromatograph (Varian CX 3400) with thermal conductivity detector and PoraBOND U capillary column was used.

2.3. RESULTS AND DISCUSSION

2.3.1. Incipient phase equilibrium data

Incipient equilibrium hydrate formation conditions for the CO_2/H_2 system are shown in Table 2-1. Similar results for the ternary mixture with C_3H_8 are given in Table 2-2. The nominal composition of the ternary gas was 58.5 mol% H_2 , 38.3 mol% CO_2 and 3.2 mol% C_3H_8 . As seen in the tables, the equilibrium gas phase composition is different from the nominal composition (dry gas composition) at the start of the experiment. This is expected since the solubility of CO_2 in water is different from that of H_2 . The experimental results obtained in the current study (Table 2-1) indicate that the hydrate formation pressures from the CO_2/H_2 mixture are greater than those for pure CO_2 .

Moreover, as the relative amount of H₂ to CO₂ increases in the gas mixture the equilibrium shifts to higher pressures at a given temperature. The results obtained in the current study compare well with those presented by Sugahara et al. (2005).

Table 2-1: Incipient hydrate formation conditions from a CO₂ - H₂ gas mixture

Feed gas composition: 39.2 (mol %) CO ₂ & 60.8 (mol %) H ₂		
Temperature (K)	Pressure (MPa)	Equilibrium gas phase composition (CO ₂ : H ₂ , mol%)
273.9	5.56	30.3: 69.7
274.6	6.04	30.0: 70.0
275.1	6.41	29.1: 72.9
275.6	6.84	29.6: 70.4
276.0	7.16	29.5: 70.5
276.4	7.56	31.1: 68.9
276.7	7.95	31.0: 69.0
277.5	9.15	31.4: 68.6
277.7	9.42	31.1: 68.9
278.4	10.74	31.0: 69.0
Feed gas composition: 57.9% (mol %) CO ₂ & 42.1 (mol %) H ₂		
274.6	2.77	52.2: 47.8
277.8	4.61	50.1: 49.9
279.4	5.99	50.0: 50.0
280.7	7.41	50.2: 49.8
281.4	8.31	51.8: 48.2
Feed gas composition: 83.3% (mol %) CO ₂ & 16.7 (mol %) H ₂		
273.9	1.58	80.9: 19.1
277.1	2.45	80.6: 19.4
278.8	3.10	80.5: 19.5
280.1	3.78	80.4: 19.6
281.6	5.15	81.0: 19.0

For example, at 274.3K and a CO₂/H₂ gas mixture of 64.7% H₂ they report the equilibrium hydrate formation pressure of 5.49 MPa. Our work shows that with a 64.7% H₂ mixture at 274.6 and 273.9K the incipient equilibrium hydrate formation pressures are 6.04 and 5.56 MPa, respectively. Also at 281.9 K and 48.4% H₂ in the mixture, the

pressure reported by Sugahara et al. is 8.71 MPa, whereas in our study at 281.4 K and with 48.2% H₂ it is 8.31 MPa.

Table 2-2: Incipient hydrate formation conditions from a CO₂ - H₂ - C₃H₈ gas mixture

Feed gas composition: 38.3 (mol %) CO ₂ + 58.5 (mol %) H ₂ + 3.2 (mol %) C ₃ H ₈		
Temperature (K)	Pressure (MPa)	Eq. composition (CO ₂ : H ₂ : C ₃ H ₈)
274.0	2.51	33.0: 64.1: 2.9
274.8	2.85	32.9: 64.2: 2.9
276.5	4.03	32.1: 65.0: 2.9
277.8	5.10	31.0: 67.2: 2.8
279.0	6.30	31.0: 67.2: 2.8
279.7	7.01	31.1: 67.1: 2.8
280.6	8.15	31.8: 65.6: 2.7
282.0	9.75	31.5: 65.9: 2.7

As seen in Table 2-2, the inclusion of C₃H₈ in the gas CO₂/H₂ mixture resulted in lower pressures required to form hydrates. The equilibrium hydrate formation pressure for the gas compositions of 39.2 mol% CO₂ and 60.8 mol% H₂ was 10.74 MPa at 278.4 K. The pressure was reduced to 5.1 MPa at 277.8 K in the presence of 3.2 mol% C₃H₈ in the gas phase. As seen, there is almost 50% reduction in the required pressure to form hydrate by inclusion of 3.2 mol% C₃H₈ in the CO₂/H₂ mixture. This renders propane a potentially useful additive to reduce the hydrate formation pressure at any given temperature. It is noted that tetrahydrofuran has been proposed as a suitable additive to hydrogen hydrate forming systems (Florusse et al., 2004; Lee et al., 2005a; Zhang et al., 2005). The use of C₃H₈ as a potential promoter has the advantage that it is non-toxic and presence of small amount of C₃H₈ in the hydrate phase along with CO₂ does not create a disposal problem. Also, its presence in small amounts in the gaseous phase along with H₂ is not expected to create any potential problems in utilization of H₂ gas in IGCC turbines or in fuel cells.

2.3.2. Structural analysis from phase equilibrium data

2.3.2.1. CO₂/H₂/H₂O system

Sloan and Fleyfel (1992) proposed a heuristic to estimate the heat of hydrate dissociation (ΔH_d) at temperatures above 273.2 K. They state that, to the first approximation, the heat of dissociation above 273.2 K depends upon the type of cavity occupied and is independent of the type and concentration of the guest gas, within the size constraint. The above method indirectly suggests the resultant structure formed by the mixed gas and has been noted that the values obtained by the method are acceptable for engineering calculations. The heat of hydrate dissociation can be calculated through the use of the Clausius–Clapeyron equation, shown below:

$$\frac{d \ln P}{d \left(\frac{1}{T} \right)} = \frac{\Delta H_d}{zR} \quad (2.1)$$

where P and T are absolute pressure and temperatures of hydrate equilibrium with vapor and liquid water, R the universal constant and z is the gas compressibility. Eq. (1) indicates that the slope of the logarithm of the hydrate dissociation pressure plotted against reciprocal temperature will give the negative heat of dissociation divided by the product of the compressibility factor and gas constant. Sloan and Fleyfel (1992) have used the above equation to calculate the heat of dissociation for different gas mixtures. Fig. 2-2 shows the Clausius–Clapeyron plot from the experimental data of different gas mixtures of CO₂ and H₂ in equilibrium with hydrate. The data for pure CO₂ are also shown.

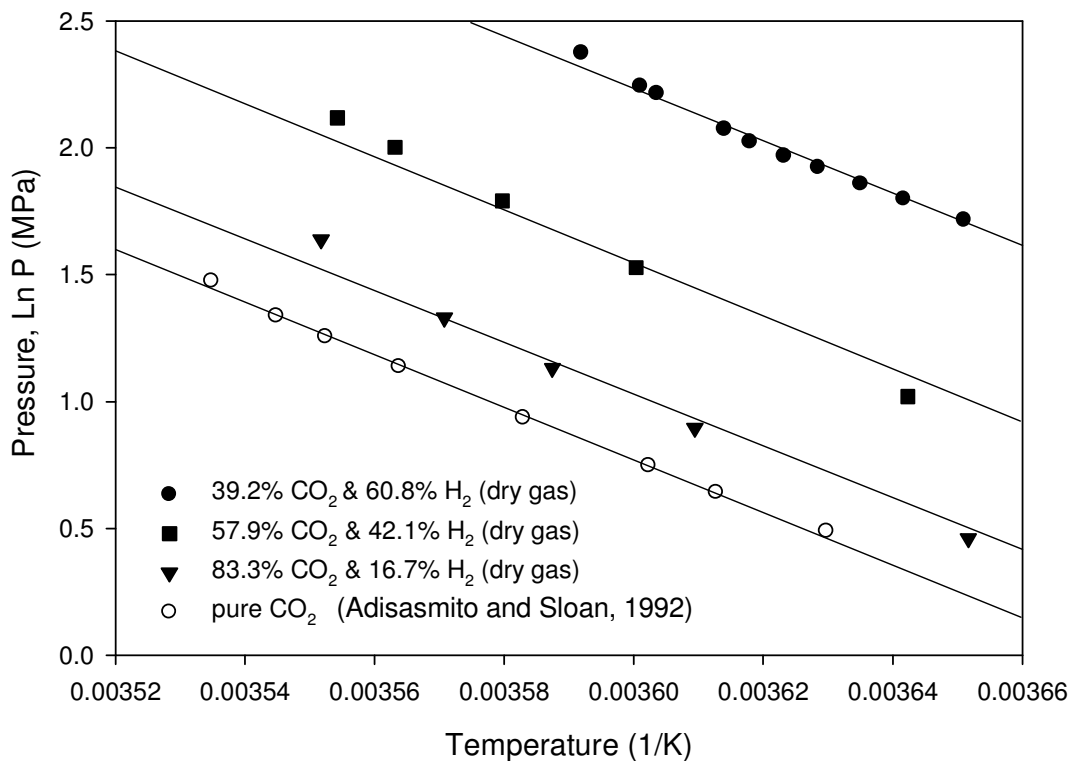


Figure 2-2: A Clausius-Clapeyron plot showing the hydrate's guest mixtures with HLV phases, with lines of same reference slope.

It is evident from Fig. 2-2 that all data points fall on the line with the same, constant slope, thereby indicating a constant heat of dissociation. The heat of dissociation calculated for all the gas mixtures was found to be within $\pm 10\%$ of a constant value of 84 kJ/mol which is within the limit as suggested by Sloan and Flyefel (1992). This suggests that all the gas mixtures studied formed structure I hydrate. As reported in the introduction, Kim and Lee (2005) indicated that H₂ molecules are included in the hydrate phase, whereas according to Sugahara et al. (2005) H₂ is not found in the hydrate phase. There appears to be a contradiction in the literature. However, after reading these publications carefully it appears that these studies are not necessarily in disagreement. Kim and Lee (2005) reported that the Raman spectra of the resultant mixed hydrate show

a peak at 4130 cm^{-1} which indicates the presence of H_2 in the hydrate phase. If one examines the spectra in Fig. 3 of the Sugahara et al. (2005) paper then one may see a peak at 4130 cm^{-1} . Perhaps, Sugahara et al. overlooked that peak. Thus, most likely both studies suggest the presence of hydrogen in the hydrate.

For this work hydrate formation experiments with CO_2/H_2 mixtures at 273.7 K and 8.5 or 7.5MPa were also carried out as discussed in chapter 3. These pressures are above the equilibrium hydrate formation pressure at 273.7K (5.1MPa) in order to have a finite crystallization rate. During the experiment which was allowed to run for 2 h the gas uptake rate and the temperature are monitored following the procedures described elsewhere (Lee et al., 2005b; Lee and Englezos 2005). After a period of 2 h of hydrate formation the crystallizer is evacuated by quickly bringing down the pressure to atmospheric. The hydrates are allowed to dissociate completely. The gas which has evolved from the hydrate and the liquid water phase is collected in the crystallizer and its composition is then determined by gas chromatography. The analysis revealed the existence of hydrogen. Interestingly, the hydrogen content increased as the pressure increased which is intuitively correct given that hydrogen forms hydrate at much higher pressures. We therefore concluded that hydrogen participates in the hydrate formed by CO_2/H_2 mixtures and as discussed above based on Clausius–Clapeyron plot most likely this gas mixture forms structure I like that formed by CO_2 alone.

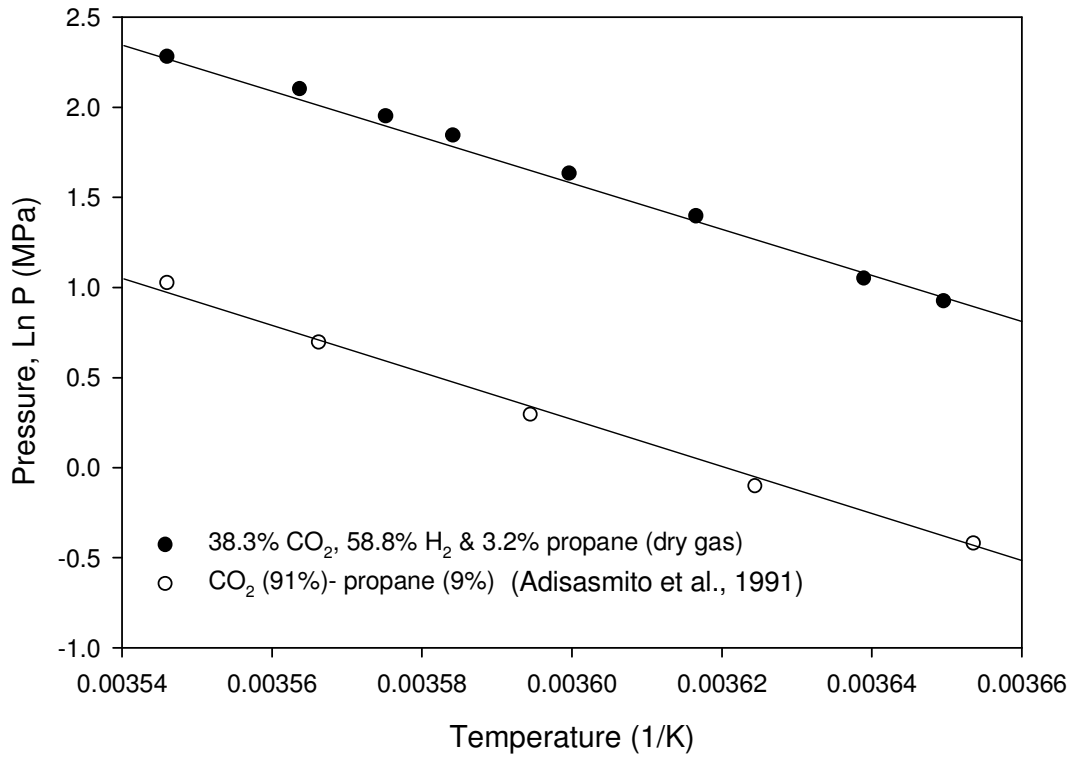


Figure 2-3: A Clausius-Clapeyron plot showing the hydrate's guest mixtures with HLV phases with line of same reference slope.

2.3.2.2. CO₂/H₂/C₃H₈/H₂O system

The incipient hydrate formation data for the CO₂/H₂/C₃H₈ gas mixture are given in Table 2-2. A Clausius–Clapeyron plot of the data in Table 2-2 is plotted in Fig. 2-3 along with the equilibrium hydrate formation data for the CO₂ (91 mol%)/C₃H₈ (9 mol%) gas mixture. This CO₂/C₃H₈ mixture is reported to form structure II hydrate (Adisasmito and Sloan, 1992). As seen from the figure the slopes for the two gas mixtures are same which again indicates a constant heat of dissociation. Based on the slope, the heat of dissociation was found to be 110 kJ/mol. This suggests that the ternary CO₂/H₂/C₃H₈ gas mixture that was used in our experiments also formed structure II hydrate. Most likely some of the large cages of structure II are occupied by CO₂ and others by C₃H₈.

molecules. It is also possible that some of the small cages of resultant structure II hydrate are occupied by H_2 . A more detail analysis of hydrate phase composition and cage occupancy of CO_2 , H_2 and C_3H_8 in the solid hydrate phase are reported in chapters 5, 6 and Appendix C.

2.4. CONCLUSIONS

Incipient equilibrium hydrate formation conditions from CO_2/H_2 and $CO_2/H_2/C_3H_8$ mixtures were determined. The results demonstrated that the hydrate formation pressures are substantially lower than those of pure H_2 . Moreover, the addition of a 3.2 mol% C_3H_8 into a CO_2/H_2 mixture reduces the pressure by 50%. An analysis of the equilibrium data based on the Clausius–Clapeyron equation indicated that the CO_2/H_2 mixtures formed structure I hydrate, whereas the ternary formed structure II. In both cases hydrogen is believed to also be present in the hydrate phase.

2.5. REFERENCES

- Adisasmito, S., Sloan, E. D. 1992. Hydrates of hydrocarbon gases containing carbon dioxide J. Chem. Eng. Data 37, 343–349
- Adisasmito, S. Frank, R. J. Sloan, E. D. 1991. Hydrates of carbon dioxide and methane mixtures. J. Chem. Eng. Data 36, 68–71
- Audus, H., Olav, K., Geoff, S. 1998. CO₂ capture by pre-combustion decarbonization of natural gas. Proceedings of the 4th International Conference on Greenhouse Gas Control Technologies, Interlaken, Switzerland, 30 August–2 September 1998, 557–562
- Corman, J.C. 1982. Coal to electricity - Integrated gasification combined cycle Appl. Energy, 10, 243–259
- Davidson, D. W., 1973. Gas Hydrates. In Water: A Comprehensive Treatise, Plenum Press, New York.
- Englezos, P., and Ngan, Y. T., 1994. Effect of Polyethylene Oxide on Gas Hydrate Phase Equilibria. Fluid Phase Equilibria 92, 271–274
- Florusse, L. J., Peters, C. J., Schoonman, J., Hester, K. C., Koh, C. A., Dec, S. F., Marsh, K. N., and Sloan, E. D., 2004. Stable low-pressure hydrogen clusters stored in a binary clathrate hydrate. Science 306, 469–471
- Joshi, M. M., and Lee, S. G., 1996. Integrated gasification combined cycle - A review of IGCC technology. Energy Sources 18, 537–568
- Kang, S. P., and Lee, H., 2000. Recovery of CO₂ from flue gas using gas hydrate: Thermodynamic verification through phase equilibrium measurements. Environmental Science & Technology 34, 4397–4400
- Kim, D.-Y., Lee, H. 2005. Spectroscopic Identification of the Mixed Hydrogen and Carbon Dioxide Clathrate Hydrate J. Am. Chem. Soc. 127, 9996–9997
- Klara, S. M., and Srivastava, R. D., 2002. US DOE integrated collaborative technology development program for CO₂ separation and capture. Environmental Progress 21(4), 247–253
- Lee, H. Lee, J.-W. Kim, D.Y. Park, J. Seo, Y.-T. Zeng, H. Moudrakovski, I.L. Ratcliffe, C.I. Ripmeester, J.A. 2005a. Tuning clathrate hydrates for hydrogen storage Nature, 434, 743–746

- Lee, J. D., Susilo, R., and Englezos, P., 2005b. Kinetics of structure H gas hydrate. *Energy & Fuels* 19, 1008-1015
- Lee, J. D., and Englezos, P., 2005. Enhancement of the performance of gas hydrate kinetic inhibitors with polyethylene oxide. *Chemical Engineering Science* 60, 5323-5330.
- Mao, W. L., Mao, H. K., Goncharov, A. F., Struzhkin, V. V., Guo, Q. Z., Hu, J. Z., Shu, J. F., Hemley, R. J., Somayazulu, M., and Zhao, Y. S., 2002. Hydrogen clusters in clathrate hydrate. *Science* 297, 2247-2249.
- Mao, W. L., Mao, H. 2004. Hydrogen storage in molecular compounds. *Proc. Natl. Acad. Sci. U.S.A.* 101, 708-710
- Sloan, E. D., Fleyfel, F. 1992. Hydrate dissociation enthalpy and guest size. *Fluid Phase Equilib.* 76, 123-140
- Sugahara, T., Murayama, S., Hashimoto, S., Ohgaki, K. 2005. Phase equilibria for $H_2 + CO_2 + H_2O$ system containing gas hydrates *Fluid Phase Equilib.*, 233, 190-193
- Zhang, S. X., Chen, G. J., Ma, C. F., Yang, L. Y., Guo, T. M. 2000. Hydrate Formation of Hydrogen + Hydrocarbon Gas Mixtures. *J. Chem. Eng. Data*, 45, 908-911
- Zhang, Q., Chen, G. J., Huang, Q., Sun, C. Y., Guo, X. Q., Ma, Q. L. 2005. Hydrate Formation Conditions of a Hydrogen + Methane Gas Mixture in Tetrahydrofuran + Water. *J. Chem. Eng. Data*, 50, 234-236

3. KINETICS OF GAS HYDRATE FORMATION FROM CO₂/H₂ MIXTURES AND SEPARATION EFFICIENCY OF HYDRATE BASED PROCESS²

3.1. INTRODUCTION

Hydrate phase equilibrium measurements, as discussed in the previous chapter, give pressure-temperature-composition bounds of a stable hydrate and thus determine a boundary to the kinetics. Gas hydrate kinetic studies have been carried out primarily through gas uptake measurements during which special care must be paid to the hydrodynamic conditions in the hydrate formation vessel (Lee et al., 2005). Kinetics is concerned with the rate at which the phase transformation occurs and the identification of the factors affecting it. Gas hydrate formation being a crystallization process consists of two major events, *nucleation* and *crystal growth*. The rate of nucleation e.g. number of hydrate crystal nuclei formed per unit time per unit volume is an extremely difficult measurement and to date there is no data reported. On the other hand the induction time marking the onset of crystallization is easily obtained experimentally. Most gas hydrate kinetic studies have focused on the gas phase coupled sometimes with measurement of the solid hydrate phase by particle size distribution (Clarke and Bishnoi, 2005; Englezos, 1993; Koh, 2002; Sloan, 1998). The rate of hydrate crystal growth is defined operationally. Thus, one may determine the gas uptake rate to describe kinetics or the rate at which a hydrate/solution interface advances. The question that arises is how an

² “A version of this chapter has been published. Linga, P., Kumar, R., and Englezos, P. (2007) Gas hydrate formation from hydrogen/carbon dioxide and nitrogen/carbon dioxide gas mixtures. Chemical Engineering Science 62:4268-4276; Linga, P., Kumar, R., and Englezos, P. (2007) The clathrate hydrate process for post and pre-combustion capture of carbon dioxide. Journal of Hazardous Materials 149: 625-629”

intrinsic rate can be distinguished from the relevant transport processes. Consequently, kinetic studies focusing on particular hydrate forming systems and hydrate vessel configurations continue to appear. An alternative approach for studying kinetics of hydrate formation is through *insitu* high-pressure static NMR spectroscopy (Susilo et al., 2006).

As discussed before in Chapter 2 hydrate based technology can be used for fuel gas separation (Aaron and Tsouris, 2005; Klara and Srivastava 2002; Englezos and Lee, 2005). The fuel gas is a mixture of H_2 and CO_2 with traces of CO and H_2S (Booras and Smelser, 1991; Hendriks et al., 1991) available at a total pressure of 2 to 7 MPa (Joshi and Lee 1996, IPCC 2005). This fuel gas mixture is pre-treated for removal of particulate matter and hydrogen sulfide. This involves cooling (cold gas cleanup at 311 K) or no cooling (hot gas cleanup at 810 K) (Zaporowski 2003). Thus, “pre combustion capture” is in fact a separation of CO_2 from a CO_2/H_2 mixture (Herzog and Drake 1996, Klara and Srivastava 2002). The pretreated fuel gas is to be used in the clathrate hydrate process for CO_2 separation. This mixture typically contains 40 % CO_2 and 60 % H_2 . The CO_2 can then be removed for disposal and the resultant H_2 could be used in fuel cells or in gas turbines (Klara and Srivastava, 2002).

Gas hydrate formation experiments from the CO_2/H_2 mixture have been carried out to identify the induction time, rate of hydrate growth and separation efficiency of the hydrate crystallization process. The results of this work are reported in this chapter. In addition, a conceptual process flowsheet for the CO_2 capture process is presented.

3.2. EXPERIMENTAL SECTION

3.2.1. Materials

The gas mixtures used in the present study were UHP grade supplied by Praxair Technology Inc. The gas compositions were chosen so that they represent the actual compositions from an IGCC power station: CO₂ (39.2)/H₂ (60.8).

3.2.2. Apparatus and procedure

A detailed schematic of the apparatus is shown in Figure 3-1. It is noted that the apparatus is the same used to obtain the equilibrium data reported in chapter 2.

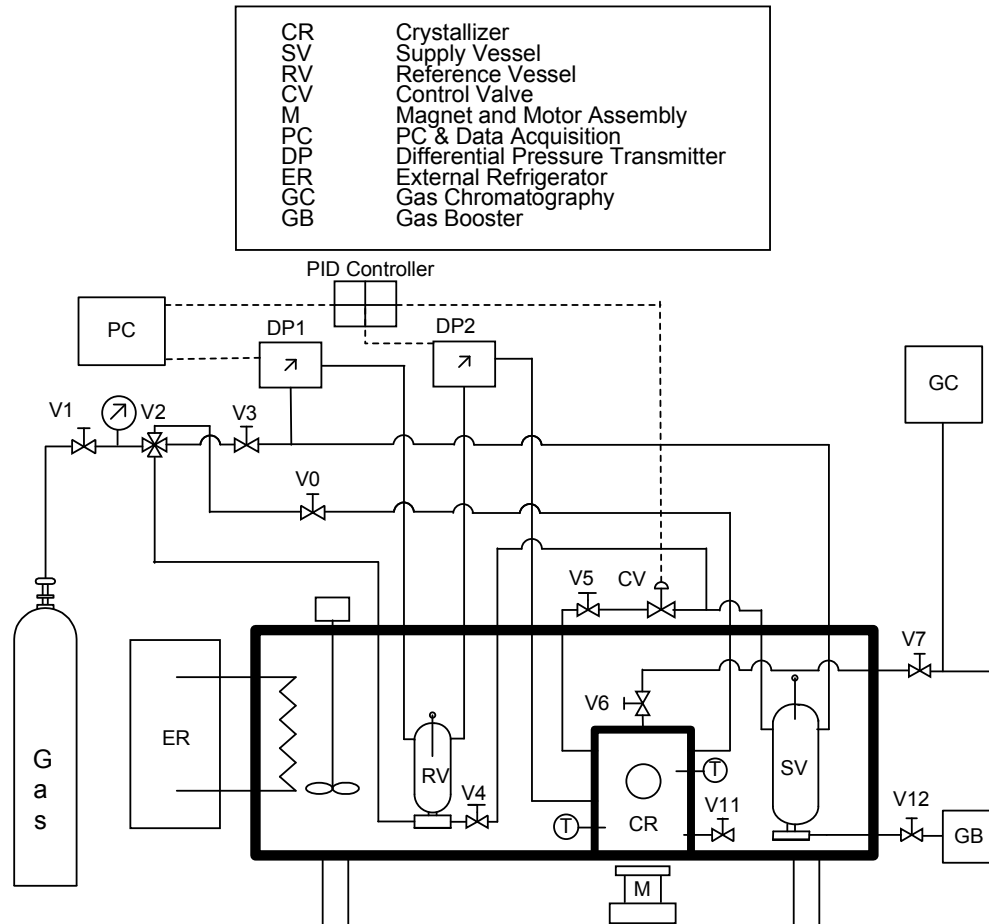


Figure 3-1: Kinetic Apparatus. (Adapted from Englezos & Ngan, 1994)

It is a versatile apparatus that also allows an accurate determination of the gas uptake into an aqueous solution under high pressure conditions. The apparatus consists of a crystallizer (CR) immersed in a temperature-controlled bath. The crystallizer is a vessel made of 316 stainless steel. It has a volume of 323 cm³. The crystallizer has two circular viewing windows made of Plexiglas on the front and back. Mixing of the crystallizer contents is accomplished using a magnetic stir bar. A baffle arrangement is used in the crystallizer in order to prevent vortex formation and to enhance mixing of the crystallizer contents. Two Rosemount smart pressure transducers, model 3051 (Norpac controls, Vancouver, BC) are employed for pressure measurement with a maximum uncertainty of 25 kPa. The temperature of the liquid phase in the crystallizer is measured using an Omega copper-constantan thermocouple with an uncertainty of 0.1 K.

The kinetics of hydrate formation was studied through gas uptake measurements following a technique pioneered at Bishnoi's laboratory (Vysniauskas and Bishnoi, 1983; Englezos et al., 1987a, b). The procedure followed in this work is described in detail elsewhere (Lee et al. 2005). Essentially, one measures the amount and composition of hydrate forming gas consumed in the crystallizer under constant temperature and pressure. The key to obtaining meaningful results is an accurate measurement of the amount of gas consumed and the control of the mixing conditions in the crystallizer. The first requirement is satisfied through accurate pressure measurements, a pressure control system and a reference gas reservoir. The second requirement is satisfied through a baffle placed in the vessel as described by Lee and Englezos (2005).

The crystallizer was filled with 140 cm³ of water. Any air present was flushed out by repeating three pressurizations (with the experimental gas mixture) and depressurizations to atmospheric pressure. Subsequently, the crystallizer was filled with hydrate forming gas until the desired pressure is reached. Once the temperature was stabilized (typically within 2 min) the gas phase composition is measured and the stirrer in the crystallizer was started. This is time zero. It is assumed that the amount of gas dissolved in water up to this point is negligible because the time is very small for mass transfer as diffusion into the quiescent liquid water is not significant. As the gas in the crystallizer was consumed for hydrate formation, additional gas was supplied and the pressure was maintained constant with a PID controller. All kinetics experiments were carried out at pressures above equilibrium so that a finite rate of crystallization is obtained. The deviation of the experimental pressure (P_{exp}) from the equilibrium pressure (P_{eq}) is frequently called *driving force*. It should be noted that the magnitude of this driving force may change during the course of an experiment. For example when hydrates form from a gas mixture the phase composition may change during hydrate formation (Kumar et al. 2008). This results in a change in equilibrium hydrate formation pressure (P_{eq}) and thus the driving force.

3.2.3. Calculation of the amount of gas consumed

Since the experiments are performed in a closed system at any given time, the total number of moles ($n_{T,i}$) in the system remains constant and equal to that at time zero ($n_{T,0}$). The system includes the crystallizer (CR), the supply vessel (SV) and the connecting tubing. The total number of moles at any given time is the sum of the number of moles

(n_{SV}) in the supply vessel, the number of moles (n_G) in gas phase (G) of the crystallizer and the number of moles (n_H) consumed to form hydrate (H) or dissolved in water.

$$n_{G,0} + n_{SV,0} + n_{H,0} = n_{G,t} + n_{SV,t} + n_{H,t} \quad (3.1)$$

The number of moles that have either gone into the water or been consumed for hydrate formation can then be calculated as follows.

$$n_{H,t} - n_{H,0} = n_{G,0} - n_{G,t} + n_{SV,0} - n_{SV,t} \quad (3.2)$$

or

$$\Delta n_H = n_{H,t} - n_{H,0} = \left(\frac{PV}{zRT} \right)_{G,0} - \left(\frac{PV}{zRT} \right)_{G,t} + \left(\frac{PV}{zRT} \right)_{SV,0} - \left(\frac{PV}{zRT} \right)_{SV,t} \quad (3.3)$$

Where z is the compressibility factor calculated by Pitzer's correlation (Pitzer., 1973).

During the kinetic experiment, the composition of the gas phase is determined by gas chromatography. At any given time by knowing the composition of the gas mixture in the crystallizer, the number of moles of the individual gas component consumed for hydrate formation can be calculated by the component mass balance.

$$\begin{aligned} \Delta n_H^i &= n_{H,t}^i - n_{H,0}^i = \left(y^i \frac{PV}{zRT} \right)_{G,0} - \left(y^i \frac{PV}{zRT} \right)_{G,t} + \left(y^i \frac{PV}{zRT} \right)_{SV,0} - \left(y^i \frac{PV}{zRT} \right)_{SV,t} \\ &= V_G \left[\left(y^i \frac{P}{zRT} \right)_{G,0} - \left(y^i \frac{P}{zRT} \right)_{G,t} \right] + y_{SV}^i V_{SV} \left[\left(\frac{P}{zRT} \right)_{SV,0} - \left(\frac{P}{zRT} \right)_{SV,t} \right] \end{aligned} \quad (3.4)$$

Superscript "i" refers to component of the gas mixture. The uncertainties in the mole numbers due to the uncertainties in the measurement of pressure, temperature and

composition were calculated by Linga (2009), the uncertainty in the induction time and during the first 10-20 min is $\pm 10\%$ and it decreases as the number of moles consumed increases.

3.2.4. Gas phase analysis

A Varian CX-3400 gas chromatograph (GC) with a Thermal conductivity detector and flame ionization detector along with a CP-PoraPLOT U capillary column were used. Ultra high purity He was used as carrier gas. The gas sample was transferred from the crystallizer to a 1/8" stainless steel sampling tube. The volume of the sampling tube is 300 μL . considering that the volume of crystallizer is 323 mL it is reasonable to assume that the amount in the sample does not affect the mass balance calculations. The sampling tube was flushed out three times with He before collecting a sample for analysis. The gas from the sampling tube was injected into the GC through a 6-port valve which had 100 μL of sampling loop.

3.3. HYDRATE CRYSTAL/ GAS SEPARATION

When gas hydrate crystals are formed from a CO_2/H_2 mixture the concentration of these gases in the hydrate crystals is different than that in the original gas mixture. This is the basis for the utilization of clathrate hydrate formation/decomposition as a separation process. Figure 3-2 illustrates the basic idea behind the gas separation using gas hydrate technology. A CO_2/H_2 mixture is fed in to the process where it comes into contact with water at suitable temperature and pressure conditions and forms hydrate crystals. The crystals are separated and subsequently decomposed to create the CO_2 -rich stream while the rest constitute the CO_2 -lean one.

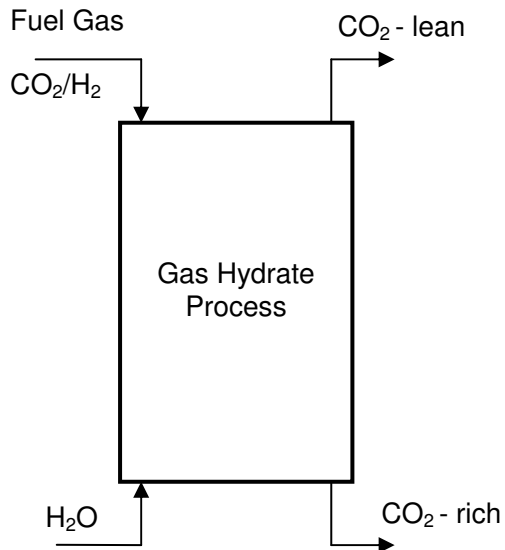


Figure 3-2: Simplified schematic of hydrate based gas separation process

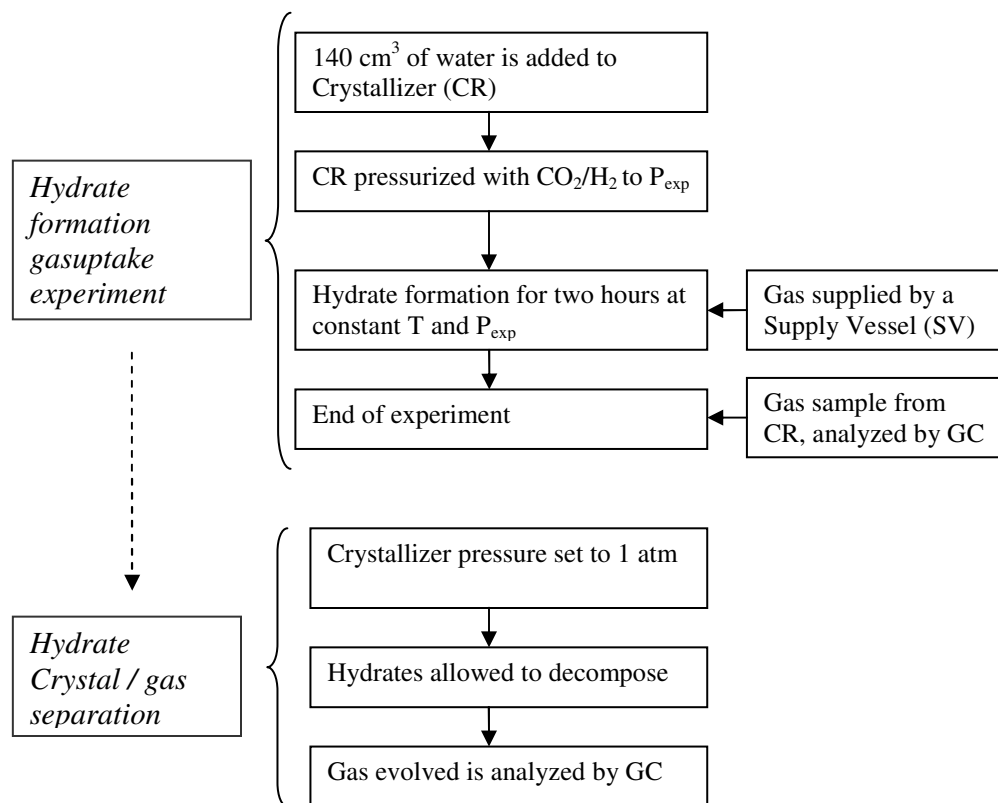


Figure 3-3: Block diagram of the experimental methods for the hydrate formation kinetic and separation experiments

Following the hydrate formation (gas uptake experiment as discussed above) for about 120 min, a hydrate crystal/gas separation was carried out. The pressure in the crystallizer was quickly brought down to atmospheric pressure and the hydrates were allowed to completely dissociate. The gas which evolved from the decomposed hydrate and that released from the liquid water phase (dissolved amount at the higher pressure) was collected and analyzed by gas chromatography. The procedures for the hydrate formation and separation experiments are shown as a block flow diagram in Figure 3-3.

3.3.1. CO₂ recovery and separation factor

The following quantities are introduced in order to provide appropriate metrics for the separation. Their values are calculated based on the kinetic (gas uptake) and separation experiments. The CO₂ *recovery* or *split fraction* (S.Fr.) of carbon dioxide in gaseous and hydrate phases is calculated as follows

$$\text{S.Fr.} = \frac{n_{\text{CO}_2}^{\text{H}}}{n_{\text{CO}_2}^{\text{Feed}}} \quad (3.5)$$

where $n_{\text{CO}_2}^{\text{Feed}}$ is defined as number of moles of CO₂ in feed gas and $n_{\text{CO}_2}^{\text{H}}$ is the number of moles of CO₂ in hydrate phase at the end of the experiment. The split fraction or CO₂ recovery in Equation 3.5 has a range of 0 to 1. The split fraction of 0 would mean no CO₂ from the gas phase goes to the hydrate phase while a split fraction of 1 would mean all the CO₂ in the gas phase goes into the hydrate phase at the end of the experiment.

In addition, the *separation factor* (S.F) is given by

$$S.F. = \frac{n_{CO_2}^H \times n_{H_2}^{gas}}{n_{H_2}^H \times n_{CO_2}^{gas}} \quad (3.6)$$

where $n_{CO_2}^{gas}$ is the number of moles of CO₂ in the gas phase at the end of the kinetic experiment, $n_{H_2}^{gas}$ is the number of moles of H₂ in the gas phase at the end of the kinetic experiment and $n_{H_2}^H$ is the number of moles of H₂ in the hydrate phase. The separation factor can range from 1 to as high as infinity. A high separation factor would mean it is favorable for CO₂ to occupy the hydrate phase compared to H₂. Equation 3.4 was used for calculating the number of moles of CO₂ and H₂ in the hydrate phase.

3.4. RESULTS AND DISCUSSION

The incipient equilibrium hydrate formation pressure (P_{eq}) for CO₂/H₂ (39.2:59.8 mol ratio) hydrate at 273.7 K was found to be 5.1 MPa by following the procedure described in chapter 2. Gas uptake measurements were carried out at 273.7 K and at 7.5 and 8.5 MPa which correspond to 2.4 and 3.4 MPa above the hydrate equilibrium pressure. This ensures a finite rate of hydrate crystallization. Experiments with fresh water as well as with memory water were conducted. Memory refers to the situation where water that is used in the experiment has experienced hydrate formation (Visniauskas and Bishnoi, 1983). The water obtained is used three hours after hydrate decomposition. Table 3-1 summarizes the results.

Table 3-1: Experimental conditions along with measured induction times and hydrate formation rates for CO₂/H₂/H₂O system at 273.7 K.

System	Experiment No	Sample State	Driving force ^a [MPa]	P _{exp} [MPa]	Induction Time [min]	Final moles consumed	R _f ^b [mol/min]	Water conversion to hydrate ^c [%]
CO ₂ /H ₂ /H ₂ O	1	Fresh	3.4	8.5	5.0	0.012	0.0068	~11
	2	Memory	3.4	8.5	3.7	0.014	0.0056	~13
	3	Fresh	2.4	7.5	7.7	0.010	0.0035	~10
	4	Memory	2.4	7.5	5.3	0.011	0.0071	~10
	5	Fresh	3.4	8.5	9.7	0.017	0.0069	~14
	6	Fresh	2.4	7.5	9.7	0.015	0.0048	~13

^a Driving force = P_{exp} - P_{eq} (at the start of the experiment)

^b Rate of hydrate growth (gas consumption rate for the first 5 min after nucleation)

^c Hydration number obtained in chapter 5 is used for this calculation

A typical gas consumption or gas uptake curve for a period of two hours is shown in Figure 3-4. The gas uptake curve and the temperature profile inside the reactor is plotted with respect to time. As seen, the temperature inside the reactor rises once due to heat of mixing of CO₂ and water and then due to hydrate nucleation (an exothermic event) which takes place within 10 minutes from the start of the mixing. The temperature is gradually brought down because the temperature controller brings back the temperature to the set point value. The rate of gas uptake increases significantly just after nucleation and denotes significant hydrate crystal growth. The rates of hydrate growth along with other information are given in Table 3-1.

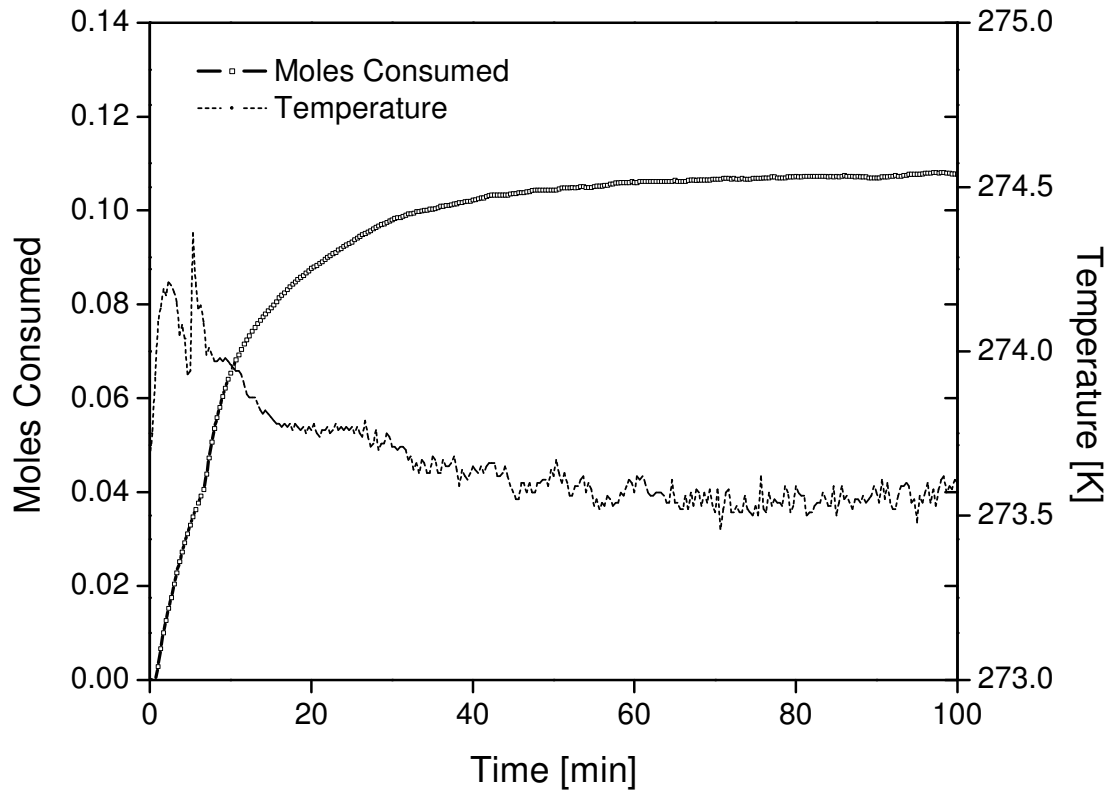


Figure 3-4: A typical gas uptake measurement curve together with the temperature profile in the aqueous phase. This is experiment 4 (Table 3-1).

The rate of hydrate growth (R_f) is defined as the slope of the gas uptake curve during the first 5 min after the induction time. The justification for this choice is the visual observation that the hydrate particles are well-dispersed in the water phase (Lee et al. 2005). Visual observations of the crystallizer contents allow the experimenter to approximately identify when the state of extensive hydrate formation commences. During this phase, the hydrate particles are well suspended in water and appear as shown in section C of Figure A-4. After 15 minutes of hydrate growth, particle agglomeration and growth results in accumulation of gas hydrate crystals at the gas/liquid interface of the laboratory apparatus as shown in section D of Figure A-4. This prevents more gas from coming into contact with the water (Linga, 2009).

Figure 3-5 shows the gas uptake curve of hydrate formation at two different pressure at 273.7 K. (The gas uptake curves for other experiments are given in Appendix A.) It is evident that the rate of hydrate formation (R_f) at higher pressure or higher driving force (at the start of experiment) is significantly higher than the one for lower driving force. The calculated rates, R_f , (Table 3-1) indicate that in general the rate decreases with decreasing driving force. While one should be careful not to generalize these observations the observed rates indicate the relative speed of the phase change in the different hydrate forming systems. It should be pointed out that kinetics through gas uptake measurements and macroscopic techniques in general are in reality “average kinetics” over the whole sample because the conversion to hydrate is quite an inhomogeneous process and that the observation of gradual conversion in bulk samples only arises as a result of averaging over many local environments (Moudrakovski et al., 2004). Susilo et al. (2006) employed Nuclear Magnetic Resonance (NMR) spectroscopy and imaging (MRI) to monitor the kinetics of structure I and H methane hydrate growth and found that the results agree with the results from gas uptake measurements obtained by Lee et al. (2005). It has been suggested before that there is a weak correlation between induction time and driving force (Bishnoi and Natarajan, 1996). In general, the induction time is shorter as the driving force increases. This is seen in experiments 1 to 4 as reported in Table 3-1 and in Figure 3-5.

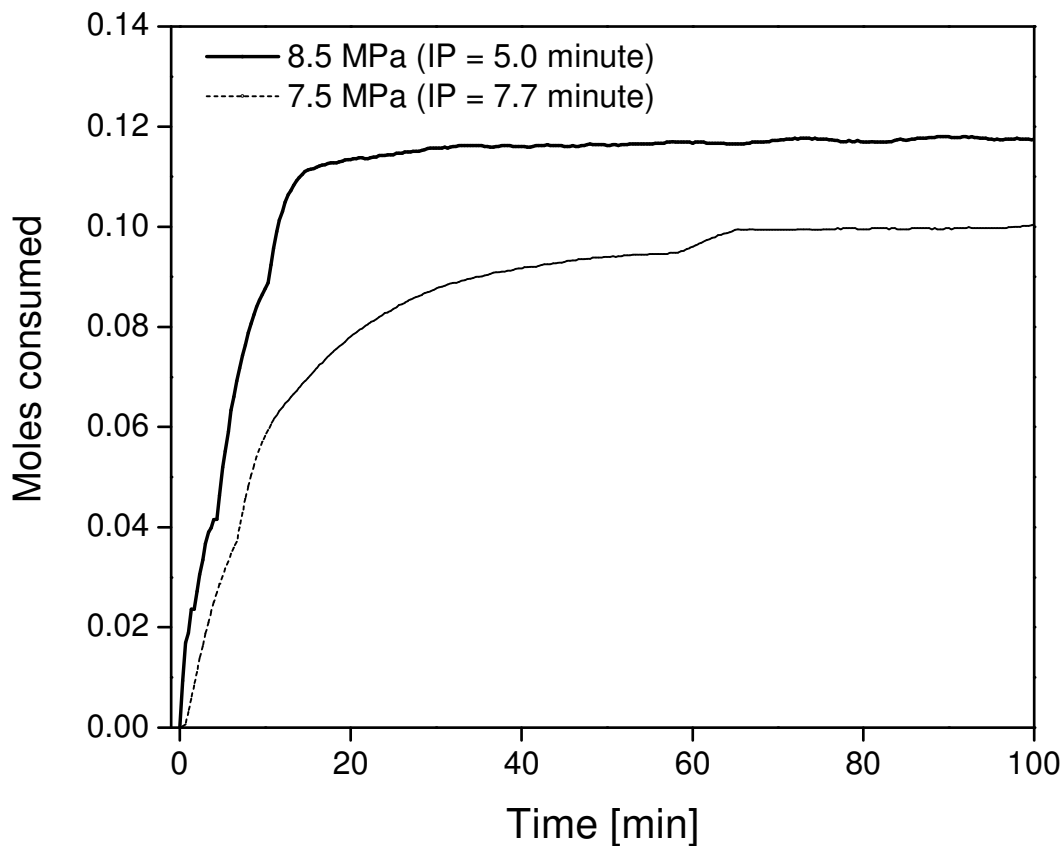


Figure 3-5: Gas uptake curves for CO₂/H₂ at 8.5 MPa (Experiment 1, Table 3-1), and 7.5 MPa (Experiment 3, Table 3-1) with the corresponding induction point.

It is generally accepted that hydrate formation from memory water is shorter (Lee et al., 2005; Uchida et al., 2000). This is what was also found in this work. For example, as it can be seen in Table 3-1, the induction time was shortened from 7.7 min (Experiment 3) to 5.3 min (Experiment 4) for a driving force of 7.5 MPa. It is noted that the observed memory-related phenomena have not been explained yet. Buchanan et al. (2005) concluded that there is no significant difference between the structure of water before hydrate formation and the structure of water after hydrate decomposition, nor is there any significant change to the methane hydration shell.

The conversion of water to hydrate for all the kinetic experiments is given in Table 3-1. There is certainly an increasing trend in the conversion with the increase in the driving force for hydrate formation, a similar trend can be seen visually in Figure 3-5, which shows higher gas uptake for hydrate formation at 8.5 MPa. Overall, the conversion of water to hydrate is low (~10-13% conversion, Table 3-1) because of the mass transfer resistance in the existing laboratory scale apparatus which employs mixing the liquid contents using a magnetic stirrer bar coupled with an electric motor. Recall that, visual observations of the crystallizer contents allow the experimenter to identify the state of extensive hydrate crystal agglomeration which results in accumulation of crystals as stagnant pockets at the gas/water interface. This prevents more gas from coming into contact with the water. Eventually, the gas uptake slows down with time due to the formation of bulk hydrate at the interface between the water and gas which hinders further growth of hydrate formation

Table 3-2: Vapor phase composition during hydrate formation from CO₂/H₂ mixture.

CO ₂ /H ₂ /H ₂ O at 8.5 MPa (Experiment 1, Table 3-1)		CO ₂ /H ₂ /H ₂ O at 7.5 MPa (Experiment 4, Table 3-1)		CO ₂ /H ₂ /H ₂ O at 7.5 MPa (Experiment 6, Table 3-1)	
Sampling time (min)	CO ₂ mole fraction in CR (y_{CO_2})	Sampling time (min)	CO ₂ mole fraction in CR (y_{CO_2})	Sampling time (min)	CO ₂ mole fraction in CR (y_{CO_2})
0.0	0.392	0.0	0.392	0.0	0.392
5.0	0.298	5.0	0.287	5.0	0.286
15.0	0.256	15.0	0.254	10.0	0.260
30.0	0.250	30.0	0.236	20.0	0.251
60.0	0.249	60.0	0.220	40.0	0.232
300.0	0.239	100.0	0.219	60.0	0.223
-	-	-	-	100.0	0.218
-	-	-	-	180.0	0.207

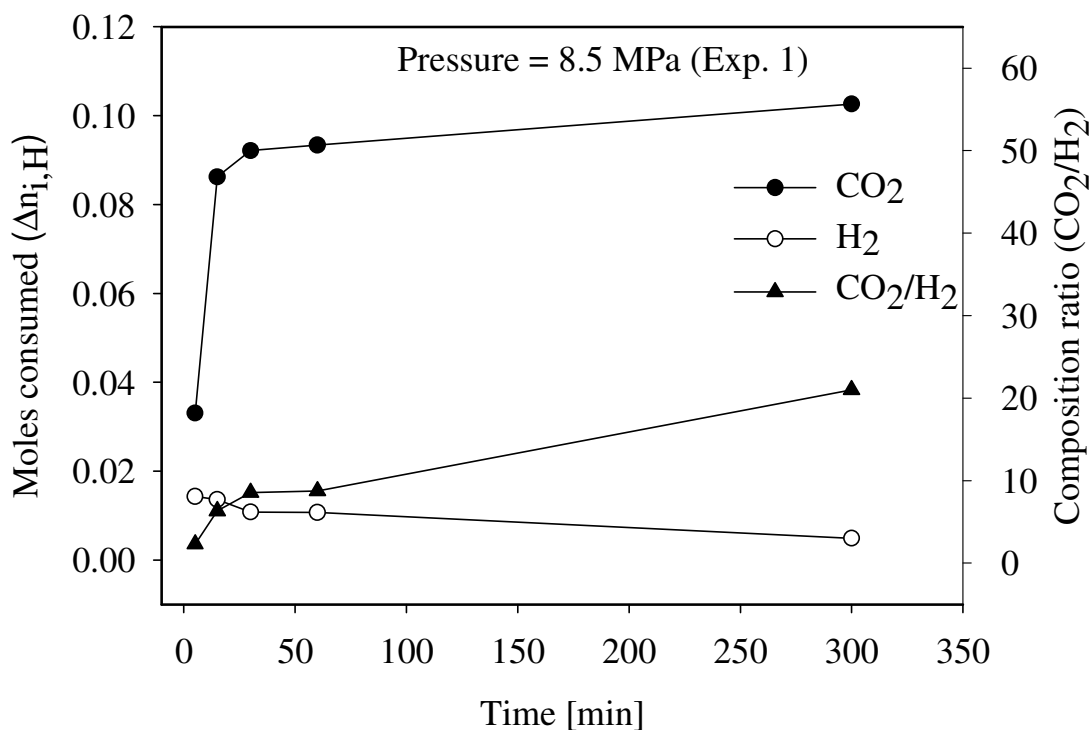


Figure 3-6: Mole consumption and molar ratio for the CO₂/H₂/H₂O system at 8.5 MPa

Gas phase analysis during gas uptake experiment was also conducted. The results for experiments 1, 4 and 6 are shown in Table 3-2. It is evident that the gas phase CO₂ content decreases as the experiment proceeds, which indicates a preferential incorporation of CO₂ into hydrate. The number of moles of CO₂ and H₂ consumed for hydrate formation were also calculated using equation 3.4 and the results are shown in Figures 3-6 and 3-7. As seen, the CO₂/H₂ ratio after 80 min is about 55 at 8.5 MPa and 65 at 7.5 MPa. The decrease in the CO₂/H₂ ratio at higher pressure can be attributed to the fact that, at higher driving force H₂ competes with CO₂ for cage occupancy. These results indicate incorporation of some H₂ into the hydrate. This was confirmed by spectroscopic studies and is presented in chapter 5. The fact that CO₂ is preferentially incorporated into

the hydrate phase proves the conceptual process for CO₂ separation from fuel gas mixtures and the recovery of H₂.

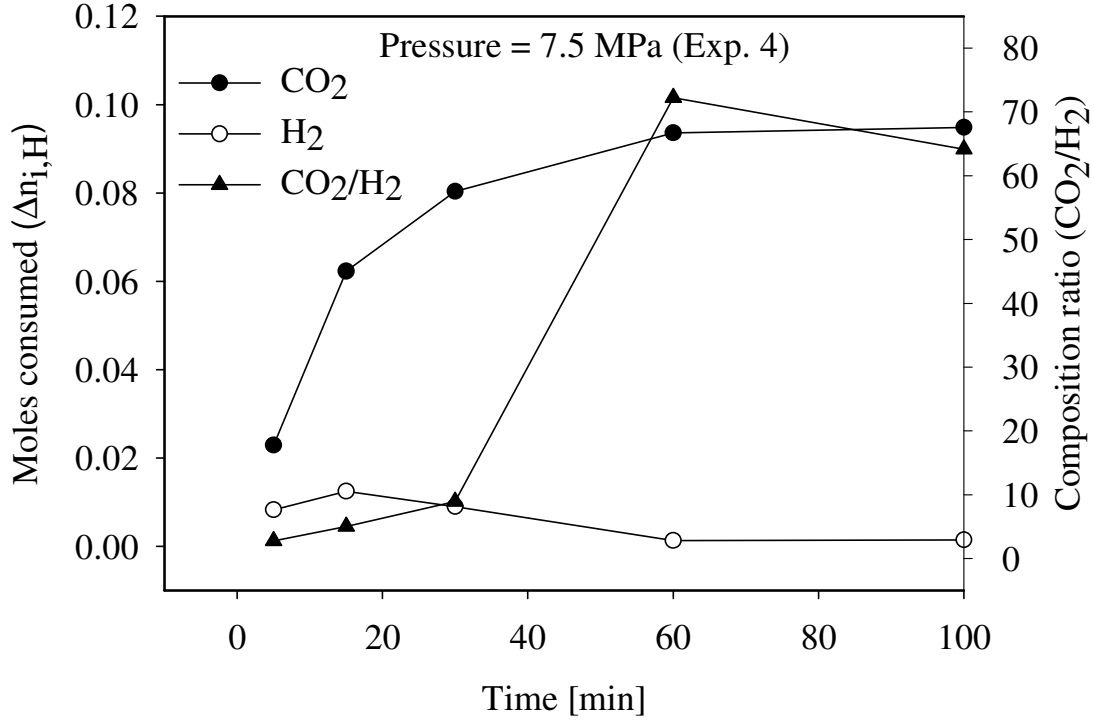


Figure 3-7: Mole consumption and molar ratio for the CO₂/H₂/H₂O system at 7.5 MPa

3.4.1. Gas separation efficiency

The gas separation experiments were carried out at the end of each kinetic experiment (gas uptake measurement) as explained in the experimental section. Figure 3-8 shows the CO₂ content in the CO₂/H₂ gas mixture (initial composition), the hydrate formed and the residual gas phase (final composition). As seen, the hydrate formed contains ~ 86% CO₂, the rest H₂. The split fraction or CO₂ recovery was calculated using Equation 3.5 and was found to be 0.42 at 7.5 MPa and 273.7 K. The separation factor for the above experiment calculated from Equation 3.6 is 98.7. For a similar gas separation experiment at 8.5 MPa

and 273.7 K the values obtained for split fraction and separation factor are 0.36 and 32.4 respectively. The experiment performed at 8.5 MPa (higher driving force) shows a decrease in the CO₂ recovery compared to a lower driving force of 7.5 MPa. The decrease of split fraction at higher driving force can be explained by the fact that at higher pressure H₂ gas competes with carbon dioxide for cage occupancy which results in lower occupancy of carbon dioxide in the hydrate phase. A sharp decrease in separation factor from 7.5 MPa to 8.5 MPa can also be explained similarly as at higher pressure more number of H₂ gas occupies hydrate cages and in turn reduces the relative concentration of CO₂ in the hydrate phase.

3.4.2. Hydrate-membrane process for CO₂ recovery from fuel gas

In order to minimize compression costs during hydrate formation the smallest possible operating pressure is desired. The above results indicate the lower operating pressure of 7.5 MPa is also better in terms of CO₂ recovery and separation factor. Therefore, a conceptual hydrate based separation process was designed which has been shown in Figure 3-9. Figure 3-8 shows that hydrate contains more than 85 % CO₂ at 7.5 MPa, which would be the output from the first hydrate (formation/decomposition) stage. In the conceptual process, it is proposed to add one more stage and obtain a further concentrated CO₂ stream. The equilibrium hydrate formation pressure of a CO₂/H₂ gas mixture with 83.3 % CO₂ and the rest hydrogen is 1.4 MPa at 273.7 K (as shown in chapter 2). The second hydrate formation vessel would operate at a lower pressure compared to the first one since the equilibrium pressure is lower by about 3.7 MPa. For a second stage in the process diagram a hydrate separation experiment was carried out with 83.3 % CO₂ and the rest hydrogen at 3.8 MPa and 273.7 K. The new CO₂-rich mixture (hydrate

composition in second stage) contains more than 96% CO₂ in the hydrate phase. As shown in Figure 3-9, a hybrid process is proposed to purify the H₂-rich streams by a membrane based separation unit. Table 3-3, shows the split fraction and separation factors for the two stages in CO₂/H₂ separation. It is also possible that by recycling the CO₂ from the membrane process to the second gas hydrate process a 98-99 mol % of CO₂ stream can be obtained.

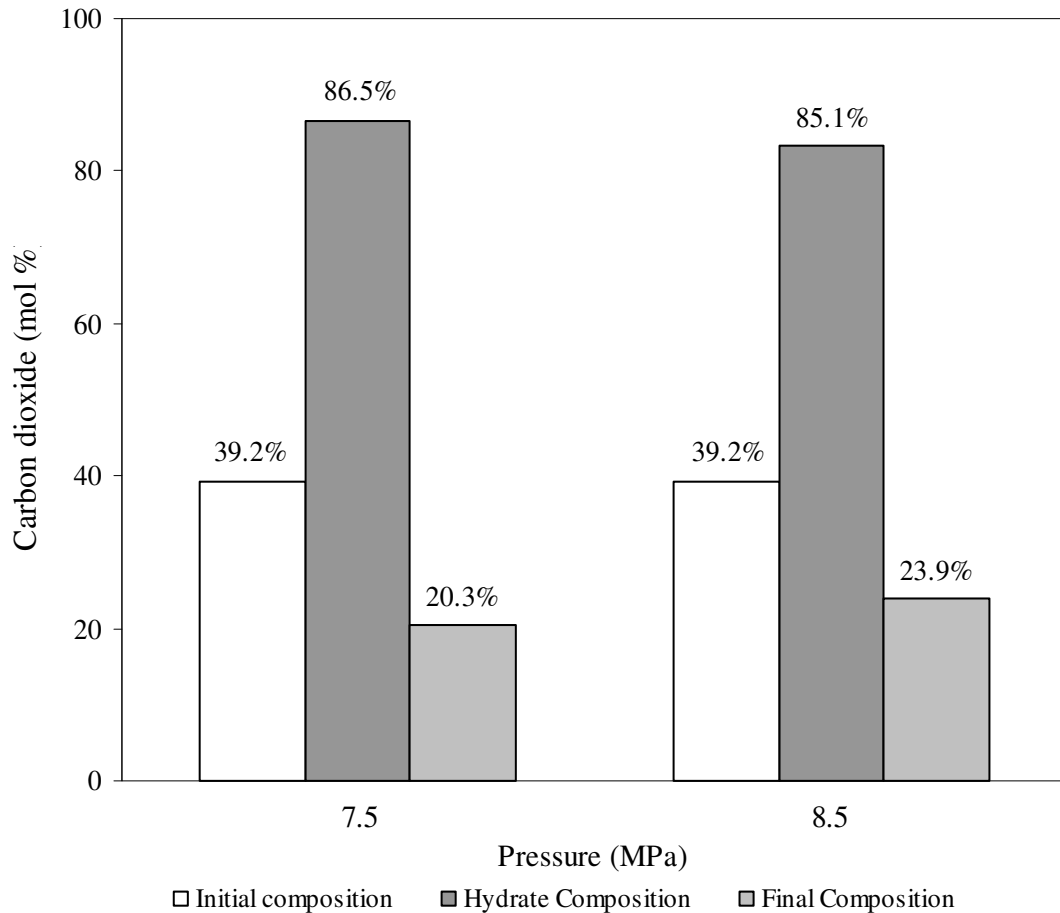


Figure 3-8: Hydrate based separation for CO₂ (39.2 mol %) – H₂ (60.8 mol %) gas mixture, Temperature = 273.7 K

The major disadvantage of the above processes is the high pressure required specially in the first stage. The above-illustrated processes show the feasibility of the

concept but not the economic viability. Clearly, from an economic viewpoint, lower pressures are required, which can be achieved by adding proper additives to reduce the hydrate formation pressure at any given temperature without compromising the CO₂ recovery and separation efficiency. As was mentioned in Chapter 2, addition of a small amount of propane in the fuel gas mixture would reduce the hydrate formation pressure considerably. However, the hydrate formation rate and separation efficiency for CO₂/H₂/C₃H₈ system has to be studied and this is discussed in the next chapter.

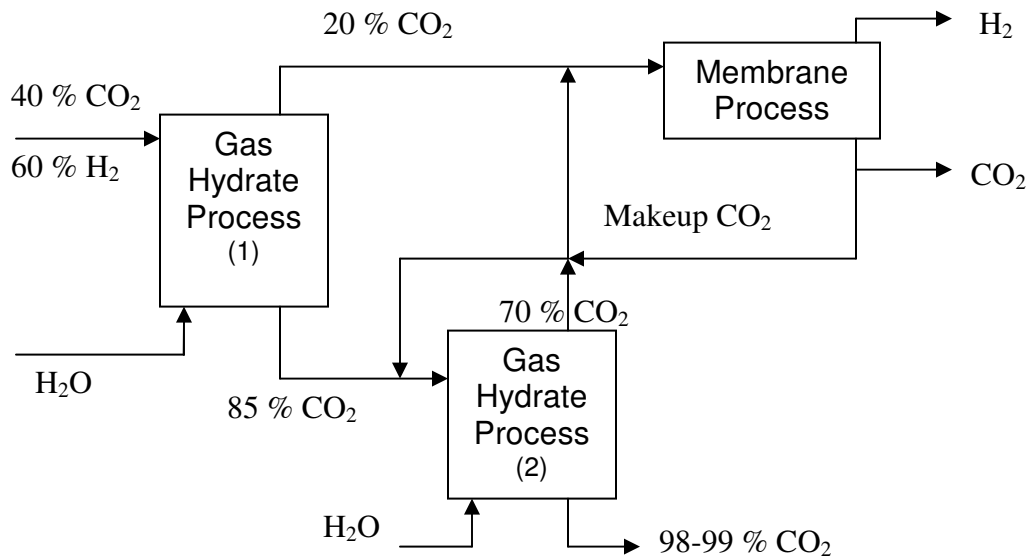


Figure 3-9: A hybrid hydrate-membrane process for CO₂ recovery from fuel gas

Table 3-3: Split fraction and separation factors for the two stages for CO₂/H₂ separation

System	Experimental conditions	Split fraction or CO ₂ recovery	Separation factor
CO ₂ (39.2%)/H ₂	P _{exp} = 7.5 MPa, P _{eq} = 5.1 MPa	0.42	98.7
CO ₂ (85%)/H ₂	P _{exp} = 3.8 MPa, P _{eq} = 1.4 MPa	0.38	94.7

3.5. CONCLUSIONS

Gas hydrate formation experiments were carried out in a crystallizer operating in a semi-batch mode with a fixed amount of water and a continuous supply of gas to maintain constant pressure. Hydrates from CO₂/H₂ gas mixtures were formed at 273.7 K and the hydrate growth was correlated with the gas uptake. CO₂ is preferentially incorporated into the hydrate offering the possibility to separate CO₂ and H₂ from a fuel gas mixture. Two metrics, CO₂ recovery and a separation factor were proposed in order to assess the separation efficiency of the CO₂ capture process. CO₂ recovery of ~ 40% and separation factor ~100 were obtained in one stage operating at ~8 MPa and 273.7K. Based on this a conceptual process, a flowsheet for a hybrid hydrate-membrane processes was developed. However, the high operating pressure in the first stage of hydrate formation makes this process uneconomical.

3.6. REFERENCES

- Aaron, D., and Tsouris, C. 2005. Separation of CO₂ from flue gas: A review. *Separation Science and Technology*, 40, 321-348
- Bishnoi, P. R., and Natarajan, V., 1996. Formation and decomposition of gas hydrates. *Fluid Phase Equilibria* 117, 168-177
- Booras, G. S., Smelser, S. C. 1991. "An engineering and economic evaluation of CO₂ removal from fossil-fuel-fired power plants". *Energy*, 16, 1295–1305
- Buchanan, P., Soper, A. K., Thompson, H., Westacott, R. E., Creek, J. L., Hobson, G., and Koh, C. A., 2005. Search for memory effects in methane hydrate: Structure of water before hydrate formation and after hydrate decomposition. *J Chem Phys*, 123, 164507/1-164507/7
- Clarke, M. A., and Bishnoi, P. R. 2005. Determination of the intrinsic kinetics of CO₂ gas hydrate formation using in situ particle size analysis. *Chem Eng Sci*, 60, 695-709
- Englezos, P. 1993. Clathrate Hydrates. *Ind & Eng Chem Res* 32, 1251-1274
- Englezos, P.; Ngan, Y. T., 1994. Effect of Polyethylene Oxide on Gas Hydrate Phase Equilibria. *Fluid Phase Equilibria* 92, 271-288
- Englezos, P., Kalogerakis, N., Dholabhai, P. D., and Bishnoi, P. R. 1987a. Kinetics of Formation of Methane and Ethane Gas Hydrates. *Chem Eng Sci*, 42, 2647-2658
- Englezos, P., Kalogerakis, N., Dholabhai, P. D., and Bishnoi, P. R., 1987b. Kinetics of Gas Hydrate Formation from Mixtures of Methane and Ethane. *Chem Eng Sci*, 42, 2659- 2666
- Englezos, P., and Lee, J. D. 2005. Gas hydrates: A cleaner source of energy and opportunity for innovative technologies. *Korean J Chem. Eng.*, 22, 671-681
- Fidel-Dufour, Gruy, F., and Herri, J. M. 2006. Rheology of methane hydrate slurries during their crystallization in a water in dodecane emulsion under flowing, *Chem Eng Sci*, 61, 505-515
- Hendriks, C., Blok, K., Turkenburg, W. C. 1991. "Technology and cost of recovering and storing carbon dioxide from an integrated-gasifier, combined-cycle plant". *Energy*, 16, 1277–1293
- Herzog, H. J., Drake, E. M. 1996. "Carbon dioxide recovery and disposal from large energy systems" *Annu. Rev. Energy Environ.*, 21, 145–66

- IPCC. (2005). "Carbon dioxide capture and storage, IPCC Special report." Intergovernmental Panel on Climate Change.
- Joshi, M. M. Lee, S. G. 1996. Integrated gasification combined cycle - A review of IGCC technology, *Energy Sources*, 18, 5 537-568
- Klara, S. M., and Srivastava, R. D. 2002. US DOE integrated collaborative technology development program for CO₂ separation and capture. *Environmental Progress*, 21, 247-253
- Koh, C. A. 2002. Towards a fundamental understanding of natural gas hydrates. *Chemical Society Reviews*, 31, 157-167
- Kumar, R., Linga, P., Moudrakovski, I., Ripmeester, J. A., Englezos, P. 2008 Structure and kinetics of gas hydrates from methane/ethane/propane mixtures relevant to the design of natural gas hydrate storage and transport facilities *AIChE*, 54, 2132-2144
- Lee, J. D., and Englezos, P. 2005. Enhancement of the Performance of Gas Hydrate Kinetic Inhibitors with Polyethylene Oxide. *Chem Eng Sci* 60, 5323-5330
- Lee, J. D., Susilo, R., and Englezos, P. 2005. Kinetics of structure H gas hydrate. *Energy & Fuels* 19, 1008-1015.
- Linga, P. 2009. Separation of Carbon Dioxide from Flue Gas (Post-Combustion Capture) via Hydrate Crystallization, PhD Thesis, University of British Columbia, Vancouver BC Canada
- Moudrakovski, I. L., McLaurin, G. E., Ratcliffe, C. I., and Ripmeester, J. A., 2004. Methane and carbon dioxide hydrate formation in water droplets: Spatially resolved measurements from magnetic resonance microimaging. *Journal of Physical Chemistry B* 108, 17591-17595
- Pitzer, K. S., 1973. Thermodynamics of Electrolytes .1. Theoretical Basis and General Equations. *Journal of Physical Chemistry* 77, 268-277
- Sloan, E.D. 1998. *Clathrate Hydrates of Natural Gases*, Second Edition, Revised and Expanded, Marcel Dekker, NY
- Susilo, R., Moudrakovski, I. L., Ripmeester, J. A., Englezos, P. 2006. Hydrate Kinetics Study in the Presence of Nonaqueous Liquid by Nuclear Magnetic Resonance Spectroscopy and Imaging *J. Phys. Chem. B*, 110, 25803-25909
- Uchida, T., Ebinuma, T., Narita, H. 2000. Observations of CO₂-hydrate decomposition and reformation processes. *J Crystal Growth* 217, 189-200

Vysniauskas, A., Bishnoi, P. R. 1983. A Kinetic-Study of Methane Hydrate Formation. Chem Eng Sci, 38, 1061-1072.

Zaporowski, B. 2003 Analysis of energy-conversion processes in gas-steam power-plants integrated with coal gasification, Appl Energ, 74, 297-30

4. KINETICS OF GAS HYDRATE FORMATION FROM CO₂/H₂/C₃H₈ MIXTURES AND SEPARATION EFFICIENCY OF THE HYDRATE BASED PROCESS³

4.1. INTRODUCTION

Based on kinetics of hydrate formation from a CO₂/H₂ mixture it was found and presented in Chapter 3 that the hydrate crystals contained a higher percent of CO₂ in the solid hydrate phase. As a result a hybrid gas separation process, combining the advantages of hydrate crystallization process (high selectivity) and membranes (small size) (Kaldis et al. 2004) was proposed for separating CO₂ and H₂ (from an IGCC power station). However, the high operating pressure requires significant energy for compression. One way to alleviate this is the use of additives that will lower the hydrate formation conditions without affecting the kinetics and the separation efficiency or CO₂ & H₂ recovery to a greater extent. Based on the hydrate phase equilibrium studies presented in Chapter 2 it is evident that addition of a small amount of propane (3.2 mol%) in the fuel gas mixture reduces the minimum hydrate formation pressure by half. Hashimoto et al. (2006) studied the effect of tetrahydrofuran (THF) as an additive on mixed hydrate of CO₂ and H₂. Their result reveals that the equilibrium pressure is considerably reduced with a small amount of THF. It is noted that the use of THF was proposed by Kang and Lee (2000) to be used in a hydrate process for post-combustion capture of CO₂. The use of C₃H₈ as a potential promoter has the advantage that it is not

³ “A version of this chapter has been published. Kumar, R., Linga, P., Ripmeester, J. A., Englezos, P. (2009) A two-stage clathrate hydrate/membrane process for pre-combustion capture of carbon dioxide and hydrogen. J. Envir. Engrg. 135, 411-417”

toxic and presence of small amount of C_3H_8 in the hydrate phase along with CO_2 does not create a disposal problem. Also, its presence in small amounts in the gas phase along with H_2 is not expected to create any potential problems in utilization of H_2 gas in IGCC turbines or in fuel cells.

The objective of the current study is to determine the CO_2 and H_2 separation efficiencies and recoveries from a fuel gas (CO_2/H_2) mixture in the presence of 2.5 mol % propane. This C_3H_8 concentration was chosen such that the equilibrium pressure is reduced substantially and at the same time not all large cavities are occupied by C_3H_8 . In addition, the kinetics of hydrate formation will be studied and will be compared with kinetics obtained for the CO_2/H_2 hydrate. As reported in Chapter 3, kinetic studies involve measurement of the induction time for crystallization and determination of the rate of hydrate crystal growth. Based on this information a medium-pressure hydrate based hybrid process will be proposed.

4.2. EXPERIMENTAL SECTION

Gas uptake measurements on a desired gas mixture are performed at constant temperature and pressure conditions for two hours (gas uptake or kinetic measurements). At the end of this period (usually two hours) the residual gas is removed from the crystallizer. This is followed by decomposition of the hydrate and compositional analysis of the evolved gas (separation). The $CO_2/H_2/C_3H_8$ (38.1% CO_2 , 59.4 % H_2 & 2.5 mol% C_3H_8) gas mixture used in the present study was UHP grade gas supplied by Praxair Technology Inc. Canada. The water used is distilled and de-ionized. The details of the experimental procedures as well as the relevant schematics are presented in chapter 3. Briefly, the gas uptake experiment proceeds as follows, a fixed amount of water is used and gas is

supplied continuously from a reservoir into the hydrate formation vessel (crystallizer) with the help of a feedback control system that regulates the pressure in the crystallizer. The drop in the reservoir pressure is recorded for quantifying the gas consumed during hydrate growth. In addition, the gas phase composition was also determined during the experiment with a Varian CX-3800 gas chromatograph (GC) equipped with a thermal conductivity detector. After the end of the gas uptake or the kinetic part of the experiment, the pressure in the crystallizer was quickly brought down to atmospheric pressure and the hydrates were allowed to dissociate completely. The gas which evolved from the decomposed hydrate and that released from the liquid water phase (dissolved amount at the higher pressure) was collected and analyzed by gas chromatography.

As explained in Chapter 3, before starting a kinetic experiment, knowledge of equilibrium hydrate formation temperature and pressure (the minimum pressure at any given temperature to form hydrate crystals) condition for that particular gas mixture is necessary. Equilibrium hydrate formation condition for CO₂/H₂/C₃H₈ gas mixture has been reported in chapter 2. A temperature of 273.7 K was chosen as the operating temperature (similar to that of CO₂/H₂ experiment reported in chapter 3). All gas uptake experiments were carried out at pressures (P_{exp}) above the equilibrium pressure (P_{eq}) so that a finite rate of crystallization is obtained. The deviation of the experimental pressure from the equilibrium pressure ($P_{\text{exp}}-P_{\text{eq}}$) is frequently called *driving force*. Experiments with fresh water as well as with memory water were conducted. Table 4-1 provides the list of the experimental conditions. Each experiment was conducted twice.

Table 4-1: List of experimental conditions along with measured induction times and hydrate formation rates at temperature $T = 273.7$ K.

Hydrate	Exp. No.	Sample State	Driving force ^a [MPa]	P_{exp} [MPa]	Induction Time [min]	Final moles consumed	R_f^b [mol/min]	Water conversion to hydrate ^c (%)
CO ₂ -38.1% + H ₂ - 59.4% + C ₃ H ₈ -2.5%	1	Fresh	2.7	4.8	14.1	0.1090	0.0005	~14
	2	Memory	2.7	4.8	13.0	0.0697	0.0006	~10
	3	Fresh	2.7	4.8	11.0	0.0750	0.0006	~10
	4	Memory	2.7	4.8	5.0	0.1043	0.0007	~14
	5	Fresh	1.7	3.8	31.0	0.0680	0.0002	~10
	6	Memory	1.7	3.8	28.3	0.0615	0.0003	~9
	7	Fresh	1.7	3.8	33.0	0.0618	0.0002	~9
	8	Memory	1.7	3.8	19.0	0.0790	0.0003	~11
CO ₂ -80.0% + H ₂ - 18.8% + C ₃ H ₈ -1.2 %	9	Fresh	1.9	3.5	11.0	0.1113	0.0015	~10*

^a Driving force = $P_{exp} - P_{eq}$ (at the start of the experiment)

^b Rate of hydrate growth (gas consumption rate for the first 5 min after nucleation)

^c Hydration number obtained in chapter 5 is used for calculation

* Hydration number of 7.0 has been used for calculation

4.2.1. CO₂ recovery and efficiency

Two metrics to assess the hydrate based separation processes have been defined in Chapter 3. The CO₂ *recovery* or *split fraction* (S.Fr.) of carbon dioxide in the gas and hydrate phase are calculated by Equation 3.5 which requires the number of moles of CO₂

in feed gas ($n_{\text{CO}_2}^{\text{Feed}}$) and the number of moles of CO_2 in the hydrate phase at the end of the experiment ($n_{\text{CO}_2}^{\text{H}}$). These quantities are calculated based on the experimental information. In addition, the *separation factor* (S.F) is determined by Equation 3.6. Which requires, $n_{\text{H}_2}^{\text{gas}}$, the number of moles of H_2 in the gas phase at the end of the kinetic experiment, $n_{\text{H}_2}^{\text{H}}$, the number of moles of H_2 in the hydrate phase and $n_{\text{CO}_2}^{\text{gas}}$ the number of moles of CO_2 in the gas phase at the end of the kinetic experiment. Equation 3.4 is used to calculate some of these quantities.

4.3. Results and Discussion

The minimum pressure to form hydrates crystals from the gas mixture containing 2.5% C_3H_8 , 38.1% CO_2 and the rest hydrogen was determined by following the procedure explained in Chapter 2 and was found to be 2.1 MPa at 273.7 K. Kinetic (gas uptake) experiments were conducted at 273.7 K and two pressures (3.8 and 4.8 MPa). Table 4-1 shows the measured induction or nucleation times and the estimated rates of hydrate growth. As expected, the induction times increase with decreasing driving force (Bishnoi and Natarajan 1996). A short induction time is definitely desirable from a practical standpoint to speed up the process, but the drawback of increasing the pressure is higher compression costs. It can be seen that induction times with memory water are smaller than those with fresh water, as expected. As explained in Chapter 3, the rate of hydrate growth (R_f) is defined as the slope of the gas uptake curve during the first 5 min after the induction time.

Figure 4-1 compares the gas uptake curve of hydrate formation from fresh and memory water at a driving force of 2.7 MPa. The curves show the general characteristics exhibited by gas uptake curves (Bishnoi and Natarajan 1996). It can be seen that the amount of gas consumed after 120 minutes is greater in the case of hydrate formed from

fresh water as compared to hydrate formed from memory water. The same trend is observed with the repeated run. However, for the driving force of 1.7 MPa as shown in Figure 4-2, there is no significant difference in moles consumption between hydrate formation from fresh or from memory water for runs 5, 6 and 7. Run 8 give a slightly higher overall consumption.

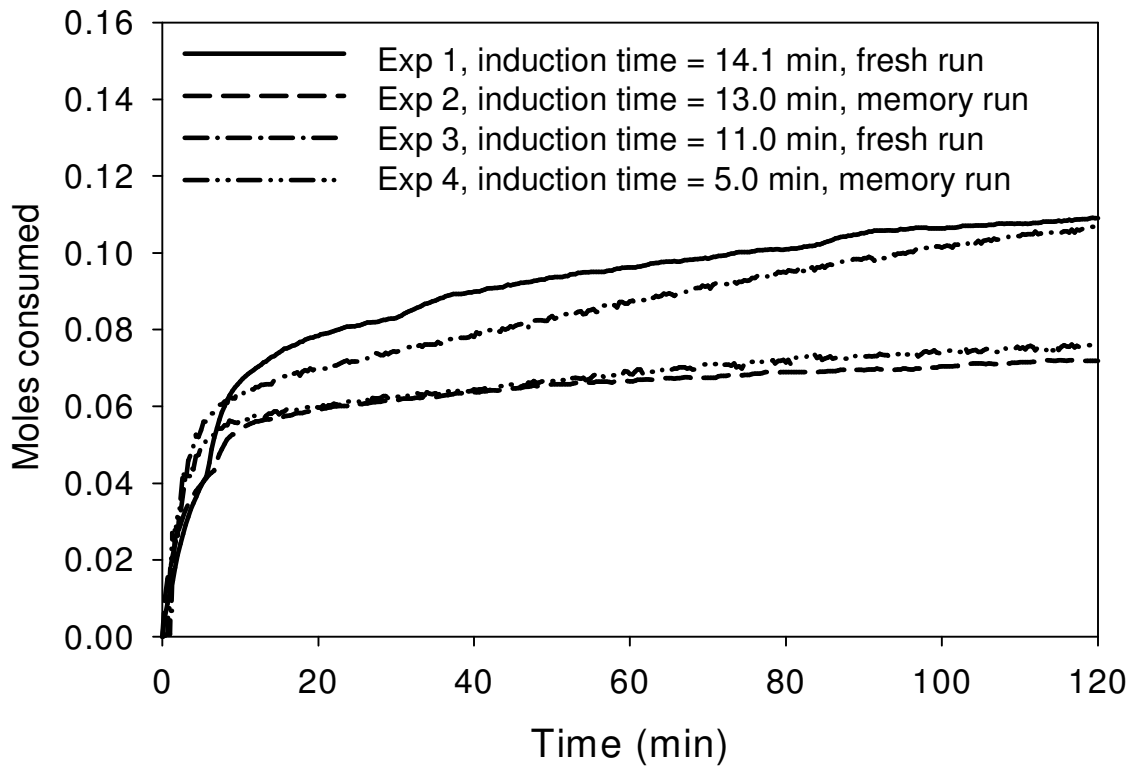


Figure 4-1: Gas uptake measurement curves for hydrate formation from fresh water and from memory water at $P_{\text{exp}}=4.8$ MPa and 273.7 K. The equilibrium hydrate formation pressure P_{eq} is equal to 2.1 MPa.

It can also be seen from Figure 4-1 and Figure 4-2 that, although the total number of moles consumed at higher driving force is slightly higher compared to lower driving force, the difference is not significant. Hence, a lower driving force of 1.7 MPa is preferable which would substantially reduce the compression cost.

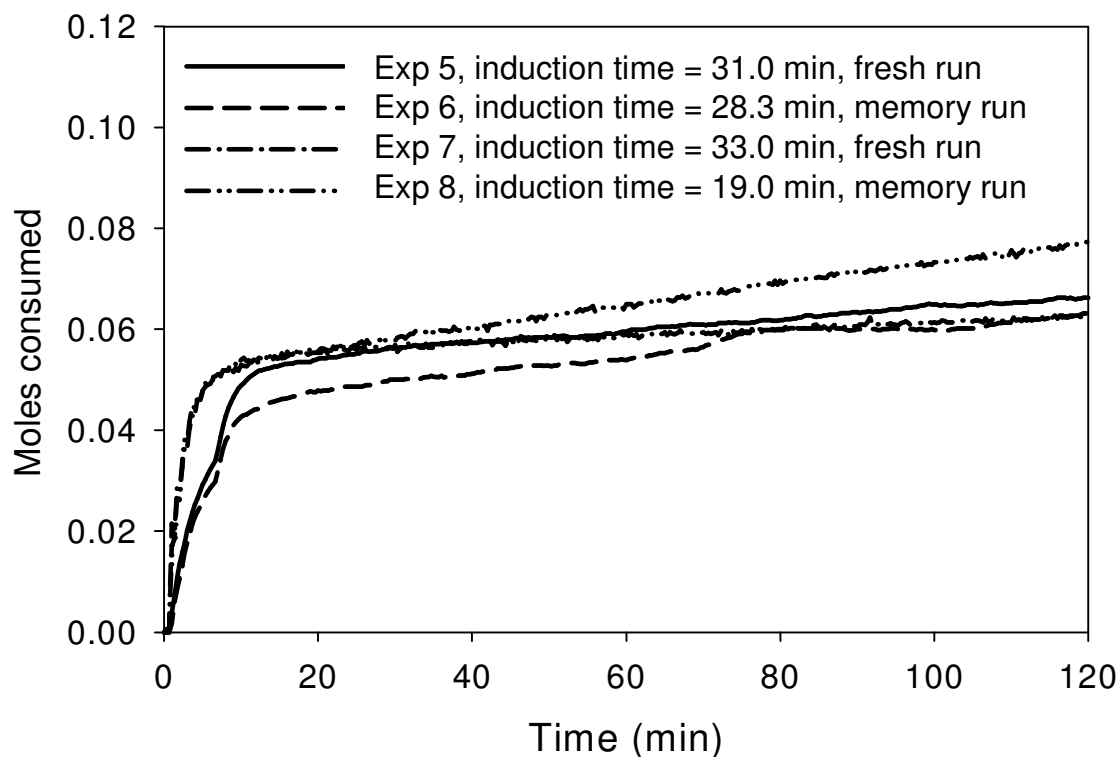


Figure 4-2: Gas uptake measurement curves for hydrate formation from fresh water and from memory water at $P_{\text{exp}}=3.8$ MPa and 273.7 K. The equilibrium hydrate formation pressure P_{eq} is equal to 2.1 MPa.

Figure 4-3 shows a comparison of the gas uptake curve for the system with the presence of propane and the one without propane as reported in Chapter 3. It can be seen from the Figure that the total number of moles consumed at the end of the experiment for the system without propane is higher than that of the system in the presence of propane. It should be noted however that the initial driving force for the system with propane is 1.7 MPa (see Table 4.1) which is less than that for the system without propane (2.4 MPa, Table 3.1). The rate of hydrate formation for the system in presence of propane (0.0003 mol/min) is also slower than CO_2/H_2 (0.0035 mol/min) system. A slower rate of hydrate formation for the $\text{CO}_2/\text{H}_2/\text{C}_3\text{H}_8$ mixture as compared to the CO_2/H_2 mixture is one of the

reasons behind the lower gas uptake for the ternary system after 120 minutes of hydrate formation. Thus, the addition of propane is beneficial because it reduces the operating pressure, but on the other hand it has a drawback because it decreases the rate of hydrate formation. Overall, the benefit from the reduction in pressure outweighs the kinetic penalty because the compression cost reduction is significant.

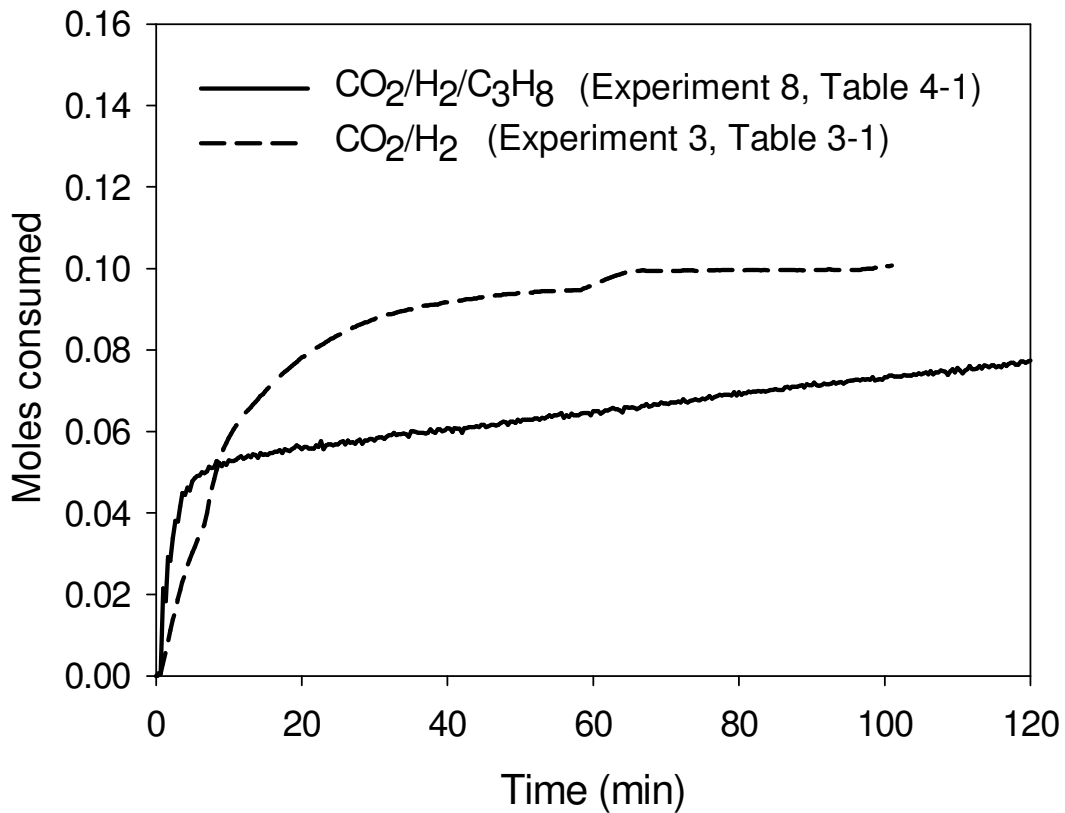


Figure 4-3: Comparison of gas uptake curves for the system with 2.5% propane and the system without propane (Chapter 3).

The results of the gas phase analysis for experiments 1, 6 and 9 are shown in Table 4-2. It is evident that the gas phase CO₂ contents decreases as the experiment proceeds indicating a preferential incorporation of carbon dioxide gas into hydrate. Based on the propane concentration in the gas phase it can be said that propane also occupies

the hydrate cages preferentially. The number of moles of CO₂ and H₂ consumed for hydrate formation was calculated by using the procedure established in chapter 3. The results are shown in Figures 4-4 and 4-5.

Table 4-2: Gas phase analysis during hydrate formation at T = 273.7 K

System	P _{exp} [MPa]	Sampling Time [min]	Gas phase composition (volume %) (Uncertainty ±0.1%)		
			CO ₂	H ₂	C ₃ H ₈
CO ₂ (38.1%)/H ₂ (59.4%)/ C ₃ H ₈ (2.5%)/H ₂ O (Experiment No. 1)	4.8	1	31.7	65.4	2.9
		5	31.0	66.1	2.9
		15	25.9	71.3	2.8
		60	24.5	73.9	1.6
		120	23.1	75.5	1.4
CO ₂ (38.1%)/H ₂ (59.4%)/ C ₃ H ₈ (2.5%)/H ₂ O (Experiment No. 6)	3.8	1	32.6	64.5	2.9
		5	29.0	67.8	3.2
		15	27.6	69.4	3.0
		60	25.3	72.6	2.1
		120	24.1	74.1	1.8
CO ₂ (80.0%)/H ₂ (18.8%)/ C ₃ H ₈ (1.2 %)/H ₂ O (Experiment No. 9)	3.5	1	72.3	26.0	1.7
		5	69.5	28.6	1.9
		15	66.6	31.6	1.8
		45	65.0	33.3	1.7
		80	64.3	33.8	1.9

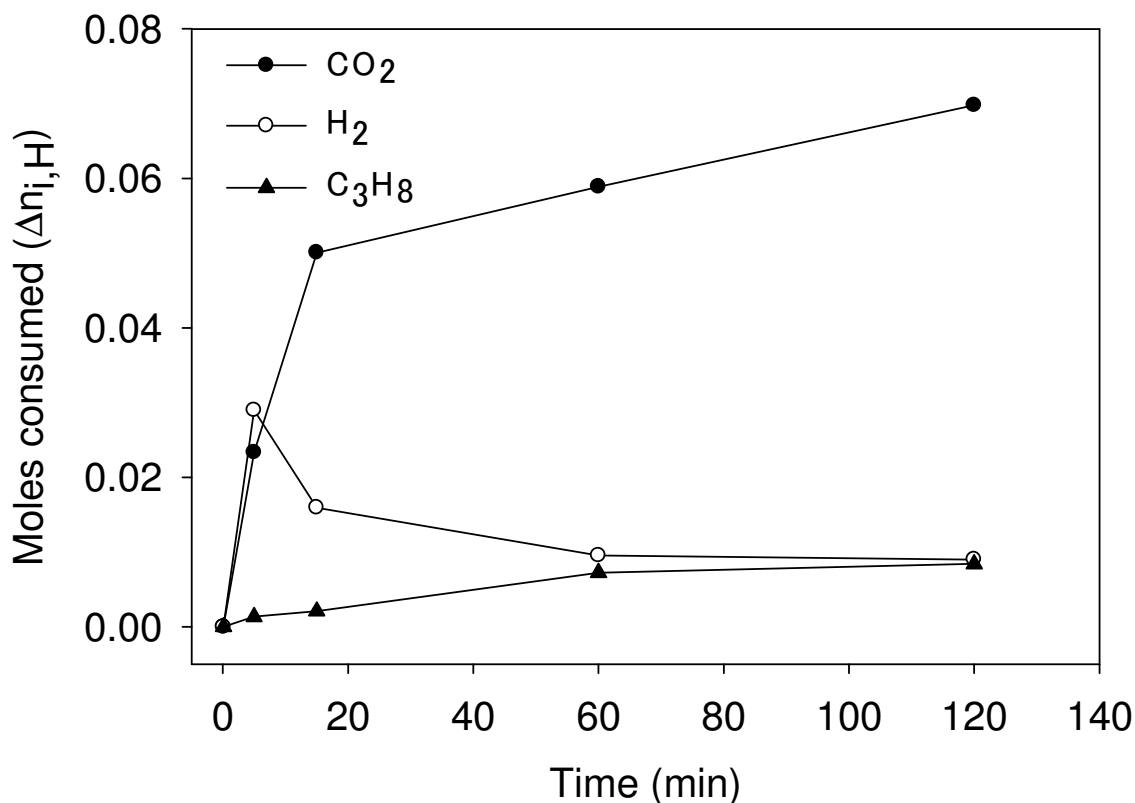


Figure 4-4: Mole consumption for the $\text{CO}_2/\text{H}_2/\text{C}_3\text{H}_8/\text{H}_2\text{O}$ system at 4.8 MPa and 273.7 K. (experiment 1). The induction time was 14.1 min.

As seen, these results indicate incorporation of some H_2 into the hydrate and that the occupancy of carbon dioxide is slightly higher at higher driving force. In both the figures it can be seen that number of moles of H_2 consumed increases, but after some time it begins to decrease. This kind of behavior suggests that hydrogen is exchanged over time with carbon dioxide. Similar behavior was observed with hydrates formed from the fuel gas mixture in the absence of propane (Chapter 3). Overall, as the hydrate formation proceeds the percent H_2 content in the gas phase increases as seen in Table 4-2. It is noted that H_2 can occupy hydrate cages at low pressures when mixed with a hydrate former (Hashimoto et al. 2006; Florusse et al. 2004; Kim and Lee 2005).

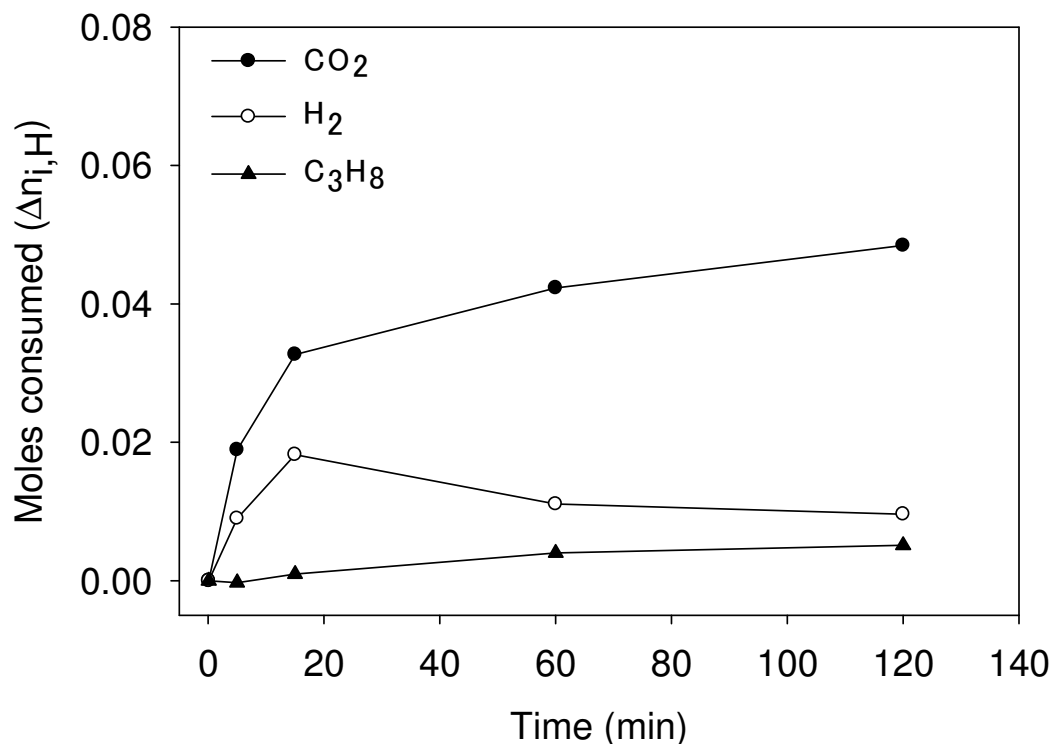


Figure 4-5: Mole consumption for the CO₂/H₂/C₃H₈/H₂O system at 3.8 MPa and 273.7 K (experiment 6). The induction time was 28.3 min.

The separation efficiency of the hydrate formation was determined by calculating the split fraction (Eq. 3.5) and separation factor (Eq. 3.6). The split fraction or CO₂ recovery and the separation factor were found to be 0.423 and 33.346 respectively at 4.8 MPa and 273.7 K. For a similar gas separation experiment at 3.8 MPa and 273.7 K the values obtained for CO₂ recovery and separation factor are 0.475 and 27.841 respectively.

Thus, the presence of propane in the ternary mixture does not affect the CO₂ recovery in comparison to the binary CO₂/H₂ mixture. The CO₂ recovery value reported here for CO₂/H₂/C₃H₈ is better than for the CO₂/H₂ system where CO₂ recoveries of 0.42 and 0.38 were obtained for stage one and two respectively. However, the presence of C₃H₈ slightly reduces the separation factor in comparison to that for the CO₂/H₂ system,

which is closer to 100 as reported in chapter 3. It is possible that in the $\text{CO}_2/\text{H}_2/\text{C}_3\text{H}_8$ system C_3H_8 competes with CO_2 for large cage occupancy and hence reduces the separation factor. Molecular level studies have been done on these system (Chapter 5) using powder-XRD, Raman and NMR spectroscopy. These results suggest that CO_2 shares large cages with C_3H_8 and small cages with H_2 in the resultant structure II hydrate synthesized at 3.8 MPa and 274.3 K.

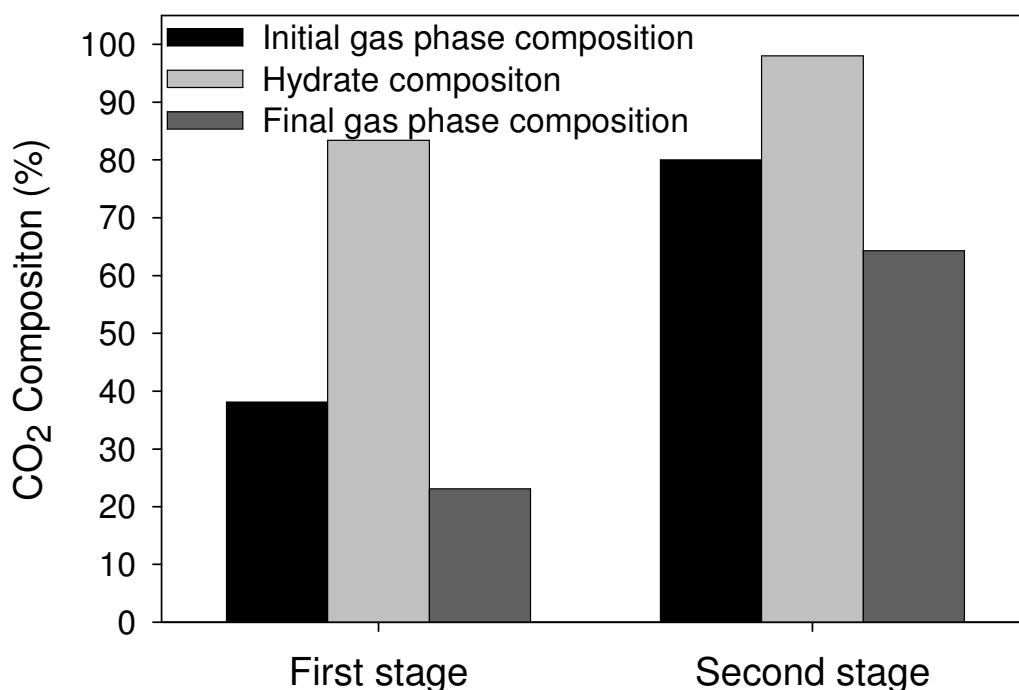


Figure 4-6: CO_2 content in the gas phase (initial composition), hydrate phase and residual gas phase (final composition) for two stages. The first stage operates at 3.8 MPa and the second at 3.5 MPa.

The above results indicate that following a one stage hydrate formation/decomposition process for fuel gas mixture in 2.5 mol% of propane, a CO_2 -rich gas is obtained which contains approximately 83.7 mol % CO_2 as shown in Figure 4-6, while the composition of propane and hydrogen are 6.5 % and 9.8 % respectively.

Since the objective is to obtain a highly concentrated CO₂ stream and pure H₂, a second hydrate formation/decomposition stage is required to treat this CO₂-rich stream. In addition a membrane stage is proposed to treat the CO₂-lean stream. The feed to the second stage of hydrate crystallization will be a mixture that consists of approximately 80% CO₂/ 18.8% H₂ and 1.2% C₃H₈. The above gas mixture is obtained by recycling part of the gas mixture from the residue side of a membrane separation unit and part from the CO₂-lean stream from the second crystallizer. The proposed flow sheet will be discussed later.

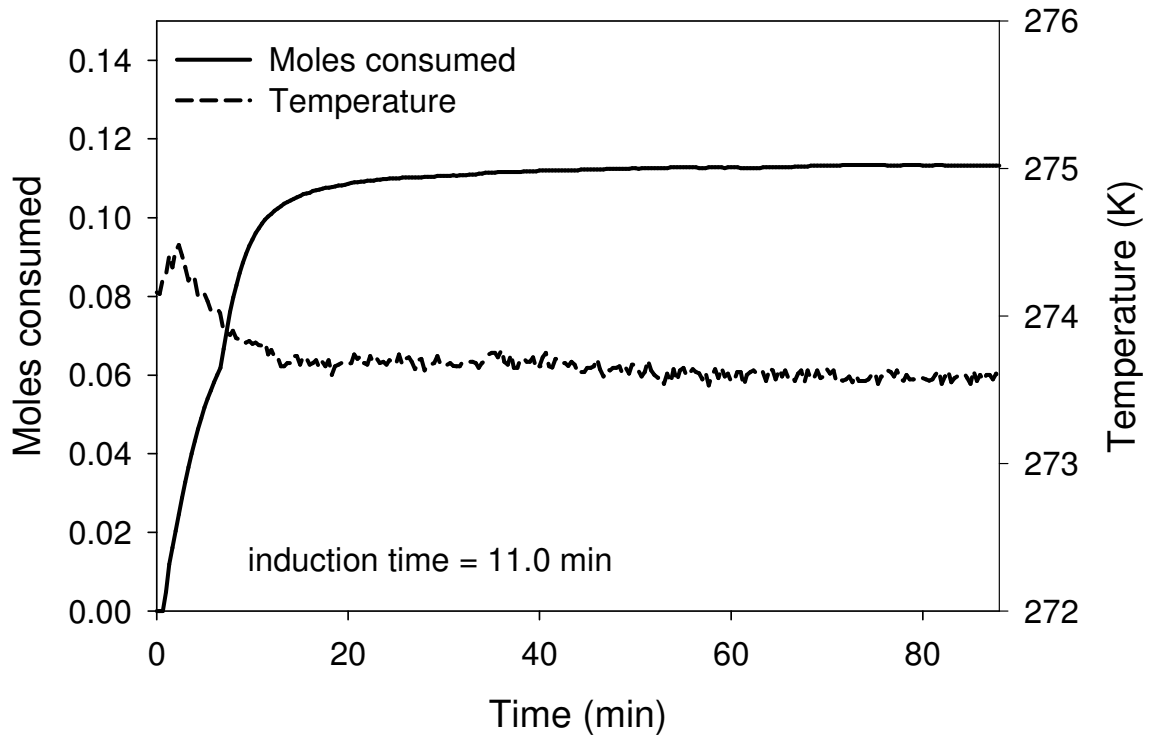


Figure 4-7: Gas uptake curve for hydrate formation for second stage CO₂ (80%) /H₂ (18.8%) /C₃H₈ (1.2%)-H₂O system at 273.7 K and 3.5 MPa (experiment 9). The induction time was 11.0 min. The equilibrium hydrate formation pressure P_{eq} is equal to 1.6 MPa.

Hydrate formation for the feed mixture in the second stage was carried out at 3.5 MPa at 273.7 K. The hydrate equilibrium for 80% CO₂/ 18.8% H₂ and 1.2% C₃H₈ mixture was determined by following the procedure explained in chapter 2 and was found to be 1.6 MPa at 273.7 K. The gas uptake measurement curve obtained for the second stage is shown in Figure 4-7. The rate of hydrate growth and gas phase composition analyzed during the kinetic experiment are given in Tables 4-1 and 4-2 respectively.

The second stage shows a better growth rate compared to the first one, mainly due to higher concentration of CO₂ in the gas mixture. The temperature in the water phase is also shown in the figure. The rise in temperature profile during the first few minutes of hydrate formation is due to the heat of mixing (solution) of CO₂ and water; however the temperature is gradually brought down because the temperature controller restores the temperature to the set point value.

Table 4-3: Split fraction and separation factor for the two CO₂ recovery stages

System	Experimental conditions	Split fraction or CO ₂ recovery	Separation factor
CO ₂ (38.1%)/H ₂ (59.4%)/ C ₃ H ₈ (2.5%)/H ₂ O (Experiment No 6)	Stage 1 P _{exp} = 3.8 MPa, P _{eq} = 2.1 MPa	0.47	27.84
CO ₂ (80.0%)/H ₂ (18.8%)/ C ₃ H ₈ (1.2 %)/H ₂ O (Experiment No 9)	Stage 2 P _{exp} = 3.5 MPa, P _{eq} = 1.5 MPa	0.32	91.19

At the end of 80 minutes from the start of the experiment, when further hydrate accumulation is minimal, a separation experiment was carried out similar to the one for

the first stage as explained earlier in the chapter. The hydrate phase composition at the end of the second stage is 98% CO₂/ 0.7% C₃H₈ and the rest hydrogen. Following the separation experiment from the second stage, separation efficiency were calculated using equation 3.5 and 3.6, Table 4-3 reports the separation efficiency values for both the stages, which suggest that, in two stages CO₂ and H₂ can be separated from a fuel gas mixture. A block flow diagram for the process is shown in Figure 4-8.

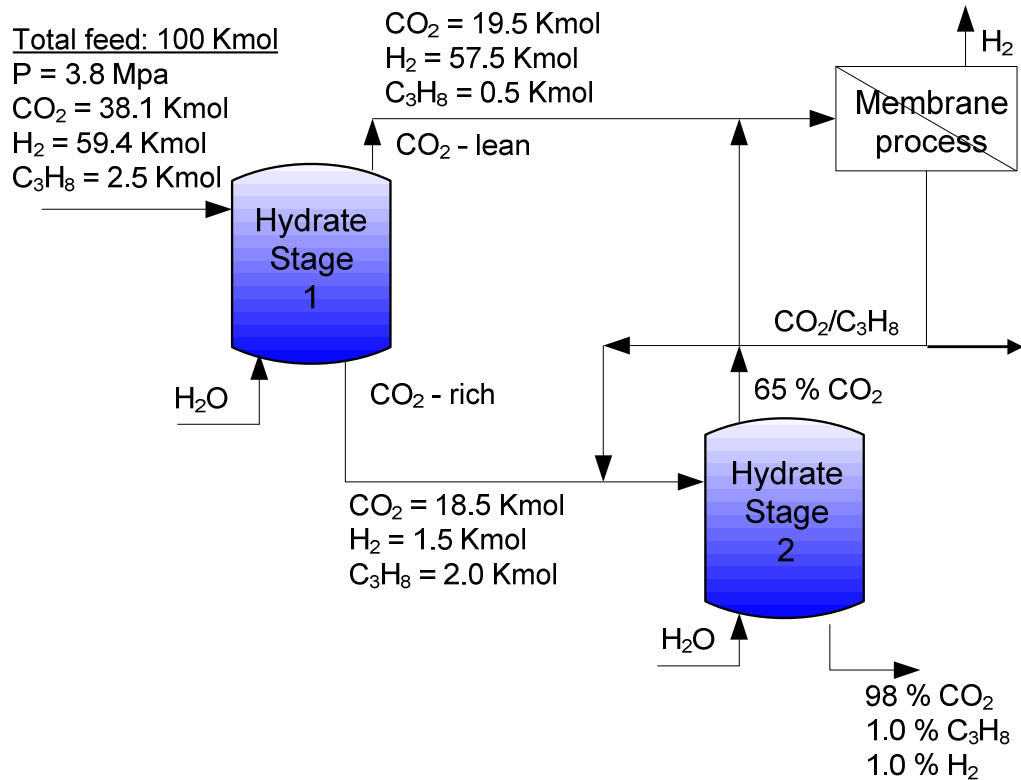


Figure 4-8: Block flow diagram for a hybrid hydrate-membrane process for CO₂ recovery from fuel gas in presence of propane. Hydrate stage 1 operates at 3.8 MPa and the second at 3.5 MPa. Both operate at 273.7 K.

Two hydrate formation stages are required. They operate at temperature 273.7 K and pressure of 3.8 MPa and 3.5 MPa respectively. The reduction in operating pressure

achieved by introducing 2.5 mol % propane compared to the pressure required by the process proposed in chapter 3 would reduce the compression cost for hydrate formation. Compression costs were calculated for the first stage of a hydrate process to deal with the fuel gas mixture coming out from a 500 MW IGCC power plant (MIT 2007), in order to pressurize the fuel gas from 2.5 MPa and 26 °C to 3.8 MPa and 1 °C. It was found that one compression stage is required (calculations given in Appendix B). The power penalty for first stage of hydrate process was found to be 12.5 MW, which is approximately 2.5% of the power output. It was reported recently that a 7% energy penalty is imposed when a hydrate based separation process for separating fuel gas mixture of CO₂/H₂ is employed (Yang et al., 2008).

If hydrate formation takes place in a mechanically agitated vessel then the electrical energy required for stirring must also be taken into account. This may be a significant cost component and should be calculated before scaling up the process. An alternative approach would be to study other gas water contact modes such as a fixed bed silica sand column (Linga, 2009) or a fixed bed silica gel column (Adebola, 2008) which eliminates the need of stirring and hence the associated cost.

The proposed process also requires an additional gas separation step other than hydrate crystallization. It is proposed that this is a membrane stage. Membrane separation is believed to be one of the promising methods to separate CO₂/H₂ gas mixtures, but currently this process is not suitable for such a huge load that comes from a commercial power generation station. A hybrid gas separation process, combining the advantage of high selectivity (hydrate crystallization) and small size (membranes) is a worthwhile alternative, especially for an IGCC power station. In the current conceptual process,

when membrane separation is used in conjunction with hydrate separation processes, it only takes the load of the residual gas phase from stage one and a small membrane separation unit will be very efficient and economical to operate.

4.3.1. Membrane separation unit

Membranes can be classified into organic, inorganic and hybrids of organic/inorganic systems. Selectivity and permeation rate are clearly the most basic properties of a membrane. However, a membrane's durability and mechanical integrity under the operating conditions must be balanced against cost issues. Gas separation using polymeric membranes was first reported over 180 years ago by Mitchell in a study with a hydrogen and carbon dioxide mixture (Mitchell, 1831). Hydrogen separation from gases, such as methane, carbon monoxide, carbon dioxide, is easy to achieve by polymeric membranes. Even though solubility factors are not favorable for hydrogen the relatively high diffusion coefficient of hydrogen due to its small size, dominates and hence the overall high selectivity (Freeman and Pinnau 1997). Polymeric membranes have been used for hydrogen separation in industries, particularly for low temperature applications for many years (Baker, 2001; Gardner et al. 1977). However, the high temperature stability problem limits its applications when separation at high temperature is required and hence inorganic membranes are used instead.

As shown in Figure 4-8, the gas phase from stage 1 has to be sent to a membrane separation unit, which would produce pure H_2 on the permeate side and pure CO_2 on the residue side. Since the gas mixture going to the membrane process is at low temperature, an organic polymeric membrane would be suitable for this separation. Polymeric membranes are economical compared to inorganic ceramic/metal membrane (Feron and

Jansen, 2002; Paul and Yampolskii, 1994). Also in this case, the gas mixture is available at high pressure and with high H₂ concentration; a polymeric membrane would give higher selectivity and higher flux for H₂ separation (Paul and Yampolskii, 1994). Based on a paper presented by Kaldis et al (2004) and given that our CO₂/H₂ gas mixture is highly concentrated in H₂, a single stage membrane unit would be sufficient to get almost pure H₂ in the permeate side and the gas mixture from the residue side can be recycled back to the second stage of hydrate formation. This enables the process to obtain nearly pure CO₂ from the second hydrate crystallization stage.

4.4. CONCLUSIONS

The fuel gas (CO₂/H₂) mixture is mixed with propane to achieve 2.5 mol % propane content and then is subjected to gas hydrate crystallization at 273.7 K and 3.8 MPa. The resulting CO₂-rich stream is directed to a second hydrate crystallization stage operating at 3.5 MPa and same temperature whereas the CO₂-lean stream is fed to a membrane separation unit. The two stages together with the membrane enable the recovery of nearly pure CO₂ and H₂ streams. The role of the propane is to reduce the operating pressures from 7.5 MPa (in a system without propane, chapter 3) to 3.8 MPa in the first stage thus reducing the compression requirements. It is interesting that the addition of propane does not compromise the separation efficiency. The only drawback is the fact that the rate of hydrate crystallization was smaller.

4.5. REFERENCES

- Adebola, A. 2008. Post combustion capture of carbon dioxide through hydrate formation in silica gel column, MASc Thesis, University of British Columbia, Vancouver BC Canada
- Baker, R. 2001. Future directions of membrane gas-separation technology, *Membrane Technology*, 138, 5-10
- Bishnoi, P. R., and Natarajan, V. 1996. Formation and decomposition of gas hydrates. *Fluid Phase Equilibria*, 117, 168-177
- Feron, P. H. M., Jansen, A. E. 2002. CO₂ separation with polyolefin membrane contactors and dedicated absorption liquids: performances and prospects. *Separation and Purification Technology*, 27, 231–242
- Florusse, L. J., Peters, C. J., Schoonman, J., Hester, K. C., Koh, C. A., Dec, S. F., Marsh, K. N., and Sloan, E. D. 2004. Stable low-pressure hydrogen clusters stored in a binary clathrate hydrate. *Science*, 306, 469-471
- Freeman, B. and Pinnau, I. 1997. Separation of gases using solubility-selective polymers *Trends in polymer science*, 5, 167-173
- Gardner, R.G., Crane, R. A. and Hannan, J. F. 1977. "Hollow fiber permeator for separating gases" *Chem. Eng. Prog.*, 73, 76
- Hashimoto, S., Murayama, S., Sugahara, T., and Ohgaki, K. 2006. Phase equilibria for H₂ plus CO₂ plus tetrahydrofuran plus water mixtures containing gas hydrates. *Journal of Chemical and Engineering Data*, 51, 1884-1886
- Kaldis, S. P., Skodras, G., Sakellariopoulos, G. P. 2004. Energy and capital cost analysis of CO₂ capture in coal IGCC processes via gas separation membranes. *Fuel Processing Technology*, 85, 337-346
- Kang, S. P., and Lee, H. 2000. "Recovery of CO₂ from flue gas using gas hydrate: Thermodynamic verification through phase equilibrium measurements." *Environmental Science & Technology*, 34(20), 4397-4400
- Kim, D. Y., and Lee, H. 2005. Spectroscopic identification of the mixed hydrogen and carbon dioxide clathrate hydrate. *Journal of the American Chemical Society*, 127, 9996-9997
- Linga, P. 2009. Separation of Carbon Dioxide from Flue Gas (Post-Combustion Capture) via Hydrate Crystallization, PhD Thesis, University of British Columbia, Vancouver BC Canada

- Mitchell, J. K. 1831. "Polymeric gas separation membrane" Philadelphia *J. Med. Sci.* 9 36.
- Paul, D. R., Yampolskii, Y. P. 1994. Polymeric gas separation membranes CRC press., Boca Raton, Florida.
- Yang, H., Xu, Z., Fan, M., Gupta, R., Slimane, R. B., Bland, A. E., Wright, I. 2008. Progress in carbon dioxide separation and capture: A review *Journal of Environmental Sciences*, 20,14–27

5. STRUCTURAL AND COMPOSITIONAL CHARACTERIZATION OF HYDRATES FORMED FROM CO₂/H₂ AND CO₂/H₂/C₃H₈ GAS MIXTURES⁴

5.1. INTRODUCTION

It is evident from Chapter 3 and 4 that gas uptake measurements alone cannot give information on cage filling dynamics of the solid hydrate phase. Uchida et al. (2005) illustrated how hydrate produced from a CO₂/CH₄ mixture shows variable composition with time. More recently Kumar et al., (2008) by using gas uptake measurements and *in-situ* Raman spectroscopy analysis on the solid hydrate phase of CH₄/C₂H₆/C₃H₈ hydrate showed how the gas and hydrate phase composition changes with time during hydrate growth.

In Chapters 3 and 4 it was shown how the difference in hydrate formation pressure of CO₂ and H₂ hydrates can be exploited to preferentially incorporate CO₂ in the hydrate cages from a CO₂/H₂ mixture, thus partitioning the gas components. Based on these studies, it was concluded that H₂ occupies the hydrate phase. The observation made in this study (based on gas uptake measurement) that H₂ occupies some of the hydrate cages in the solid hydrate phase is in agreement with the work by Kim and Lee (2005) in which it was shown that a 20/80 mol % CO₂/H₂ gas mixture forms structure I hydrate and H₂ is included in the hydrate. However, Sugahara et al. (2005 & 2008) reported that H₂ behaves like a diluent gas and thus does not take part in hydrate formation. Hasimoto et

⁴ “A version of this chapter has been published. Kumar, R., Moudrakovski, I., Ripmeester, J. A., Englezos, P. (2009) Structure and composition of CO₂/H₂ and CO₂/H₂/C₃H₈ hydrate in relation to simultaneous CO₂ capture and H₂ production. AIChE J. 55, 1584-1594.”

al (2006) report sII hydrate formation from CO₂/H₂/THF hydrate with H₂ and CO₂ occupying the small cages and THF going into the large cages. Therefore, two references in favor and two references against the candidacy of H₂ in the hydrate cages of CO₂/H₂ hydrate, warrant a detailed molecular level study.

It must also be noted that, the controversy about H₂ occupying the hydrate cages goes a step further where the exact capacity of the hydrate cages for H₂ is still controversial (Mao et al., 2002; Mao and Mao, 2004, Lee et al., 2005; Struzhkin et al., 2007). Several studies done on THF/H₂ hydrate point towards single occupancy of hydrogen in the small hydrate cages, whereas multiple hydrogen was found to occupy the large cages (Anderson et al., 2007; Hester et al., 2006; Lokshin et al., 2004; Strobel et al., 2006). A detailed account of cage occupancy in simple and binary hydrates of H₂ and storage capacity of these hydrates is presented by Strobel (2008).

The objective of our work in this chapter is to determine the structure and cage occupancies of the hydrates formed by the CO₂/H₂ and the CO₂/H₂/C₃H₈ gas mixtures by employing analytical techniques like powder-XRD, Raman, Infrared and NMR spectroscopies. This information will aid in the further development of the clathrate process for simultaneous pre- combustion capture/ hydrogen production.

The determination of the cage occupancies for the mixed hydrates in this study represents considerable challenges. As mentioned earlier the exact capacity of the hydrate cages for H₂ is still controversial (Struzhkin et al., 2007). One reason why it has been difficult to confirm the occupancy limits of the hydrate cages is that so far there are no reliable direct methods. Powder diffraction is limited by the data/parameter ratio in fitting any but the simplest models, Raman spectroscopy is not quantitative, as scattering

cross sections for the different cavities remain unknown and there is also ortho-para conversion, making the spectrum time dependent on the scale of days to weeks. On the NMR side, the calculated chemical shift scale for H_2 is very small, and again there are problems with ortho-para spin conversion (Senadheera and Conradi, 2007). The problem is further complicated by the fact that hydrogen diffuses rather easily through the six rings of hydrate cages, less readily through the five rings, so that the detailed temperature history of a sample becomes important for all methods of analysis (Alavi & Ripmeester, 2007; Okuchi et al., 2007)

For CO_2 cage occupancies there are also some difficulties. Raman spectroscopy does not distinguish CO_2 in large and small cages (Murphy and Roberts; 1995), and for NMR spectroscopy it is not completely straightforward either as one must use the anisotropic chemical shift patterns. Infrared spectroscopy does offer opportunities, and we explore a new approach, FTIR attenuated total reflection (ATR) spectroscopy *in-situ* at high pressure to distinguish CO_2 in large and small cavities. This work is presented in chapter 6.

5.2. Experimental Section

A (40/60) mol % (CO_2/H_2) and a (38.2/59.2/2.6) mol % $CO_2/H_2/C_3H_8$ were used. Approximately five grams of fresh-ground ice particles ($d < 63 \mu m$) were poured by gravity into a 50 mL pressure vessel (reactor). Ice was ground at liquid nitrogen temperature and the particle size was determined by passing the ground ice through an ASTM 230 sieve at $-20^\circ C$. The loading procedure was performed in a freezer at $-20^\circ C$ to prevent melting of the ice. The vessel was then immersed in a constant temperature water-methanol (50:50 by mass) bath and connected to a valve and pressure transducer.

Before the start of the experiment the vessel was evacuated to eliminate the presence of air. The time-zero of the measurement was recorded as the vessel was pressurized to the desired pressure of 8.0 MPa (for CO₂/H₂ mixture) at -20°C and 3.8 MPa for the CO₂/H₂/C₃H₈ mixture. All experiments were performed at -20 °C for about 24 h. At the end of the 24h period the temperature was increased to a point above the ice point (1°C) within 5 min to enhance the conversion of ice into hydrate. It is well known that temperature ramping through the ice point enhances the conversion to hydrate. The temperature was then brought back to -20°C for further hydrate formation. The starting pressures were well into the stability region of sI hydrate to ensure there was sufficient driving force for hydrate formation. As the experiment was conducted in batch mode, the pressure decreased continuously as hydrate formed. The, final pressure was ~ 1.0 MPa lower than the starting pressure. The experiments were stopped when a significant pressure drop was no longer observed. Hydrate samples were collected under liquid nitrogen temperature (~80 K) at the end of the experiment and kept in liquid nitrogen for subsequent analysis.

Crystal structures and lattice constants were obtained from powder x-ray diffraction (PXRD). The PXRD measurements were performed by a $\theta/2\theta$ step scan mode with a counting time of 47.3 s/step and a step width of 0.041° in the 2θ range of 5-60 ° (40 kV, 40 mA; BRUKER axs model D8 Advance). The PXRD measurements were done using Cu-K α radiation ($\lambda=1.5406$ Å) at -110°C to prevent hydrate dissociation. The temperature deviation of the sample during measurement was within $\pm 1.0^\circ\text{C}$.

¹H and ¹³C NMR measurements were carried out on a Bruker DSX-400 NMR spectrometer (magnetic field of 9.4 T). The ¹H and ¹³C Larmor frequencies were 400.1

and 100.63 MHz, respectively. For some of the NMR measurements hydrates were also synthesized with deuterated ice (D_2O) to reduce the proton signals for quantitative analysis of the solid hydrate phase. Similarly for some of the measurements instead of natural CO_2 , ^{13}C enriched CO_2 was used for a better signal to noise ratio for ^{13}C NMR measurement. A BL7 MAS probe with stretched spinners was used for all of the analyses. Hydrate samples were kept and loaded into the spinners in liquid nitrogen to avoid any decomposition of hydrate at atmospheric pressure. All of the NMR measurements were performed with a spinning speed of 2500-4000 Hz at $-100^\circ C$ maintained by a Bruker BT 3000 temperature controller. ^{13}C data were acquired in Bloch decay mode (^{13}C $\pi/2$ pulse of 5 μs) with high power composite pulse proton decoupling. The delay between the scans was set at 80-100s, which was sufficient for a complete relaxation of all the signals and quantitative measurements. 100 and 300 scans were commonly acquired to obtain a sufficient signal-to-noise ratio. Due to a strong proton background signal, the 1H spectra were acquired as spin-echoes synchronized with the rotation of the sample. Because of this procedure, quantitative intensity measurement required accurate T_2 (spin-spin relaxation time) measurement for each resonance. Only 16 or 32 scans were required for a good signal-to-noise ratio. For absolute quantitative measurements a sample of THF hydrate of known composition was used as a quantitative standard and its 1H and ^{13}C spectra were obtained under conditions identical to those used for the hydrates studied. All of the acquisition parameters were set to ensure that the measurements were quantitatively accurate. Tetramethylsilane was used as an external chemical shift reference for both ^{13}C and 1H .

The hydrate samples were also analyzed using Raman spectroscopy. An Acton Raman spectrograph with fiber optics and equipped with a 1200 grooves/mm grating and an externally cooled CCD detector was used in this study. An Ar-ion laser was used as the excitation source emitting at 514.53 nm. The laser was focused on the sample by 10x microscope objective on a sample area of 2-3 μm^2 . The spectrograph was controlled with a computer and the spectra were recorded with a 1s integration time over 100 to 500 scans. In order to determine the composition of the gas phase and the gas evolved from the decomposition of the hydrate sample at the end of the experiment, an SRI 8610 C gas chromatograph (GC) is used.

In order to monitor the mass numbers of effluent gas from a decomposing hydrate sample at atmospheric pressure, an MKS Instruments Cirrus quadrupole mass spectrometer with a heated capillary inlet line was used. Finally, a Fourier Transform Infrared Spectrometer (FTIR) coupled with an Attenuated Total Reflection (ATR) optical unit, was used for analyzing hydrate samples. The experimental section and procedure for FTIR analysis is given in chapter 6.

5.3. RESULTS AND DISCUSSION

Figure 5-1 shows a typical plot of the gas consumed (left axis) versus time during hydrate formation. The temperature is also shown on the right axis. As seen, a period of rapid hydrate growth during the first two hours is followed by a more gradual decrease in pressure: because of this pressure drop the driving force diminishes (driving force can be excess pressure at constant temperature, or sub-cooling at constant pressure). Also, a hydrate film will have covered the ice surface (Wang et al., 2002) thus the reaction

becomes limited by the diffusion of guest gas molecules across the hydrate film and the reaction at the ice-hydrate interface. The ramping of temperature above the ice point increased the pressure before this dropped back down again. As the temperature increases above the melting point of ice the rate of hydrate growth increases considerably. This phenomenon is well known and is due to the melting of the ice, which in turn induces fracturing of the hydrate layer, and this allows better contact between gas and water or ice (Moudrakovski et al., 1999; Susilo et al., 2006 & 2007). It is also seen that the rate of gas consumption becomes constant after some time, most likely due to a decreased driving force, which can be brought back to higher values by reducing the temperature to -20 °C and which results in additional hydrate being formed. Based on the gas uptake measurement the conversion of the ice to hydrate was found to be approximately 95%. This result was confirmed from the ice peak intensities shown in the powder-XRD pattern.

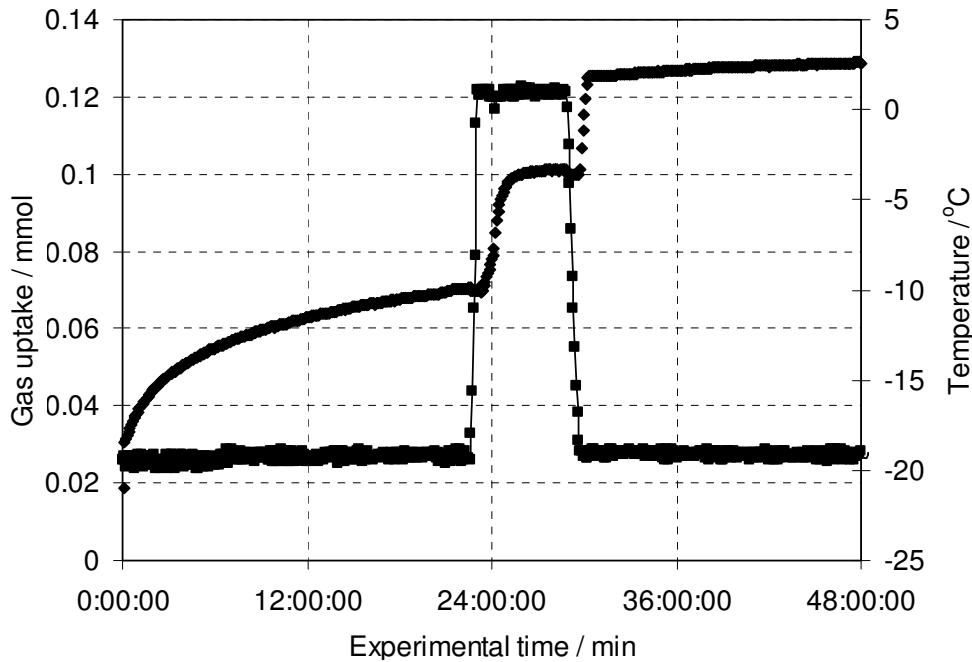


Figure 5-1: Gas uptake profile during hydrate formation from ice powder and the CO₂/H₂ mixture synthesized at 8 MPa.

Figure 5-2 shows the x-ray powder diffraction pattern for hydrate synthesized from the CO₂/H₂ mixture. The hydrate sample analyzed at -110°C and atmospheric pressure can be indexed in the regular cubic space group $Pm\bar{3}n$, with a unit cell parameter of 11.89 (±0.01) Å and cell volume of 1681 (±10) cubic Å. This result matches with the reported values for the unit cell parameter of pure structure I CO₂ clathrate hydrate (Henning et al., 2000). The presence of ice is indicated by the asterisk on top of the ice reflections. It was found that this gas mixture always formed structure I hydrate under the temperature and pressure conditions used.

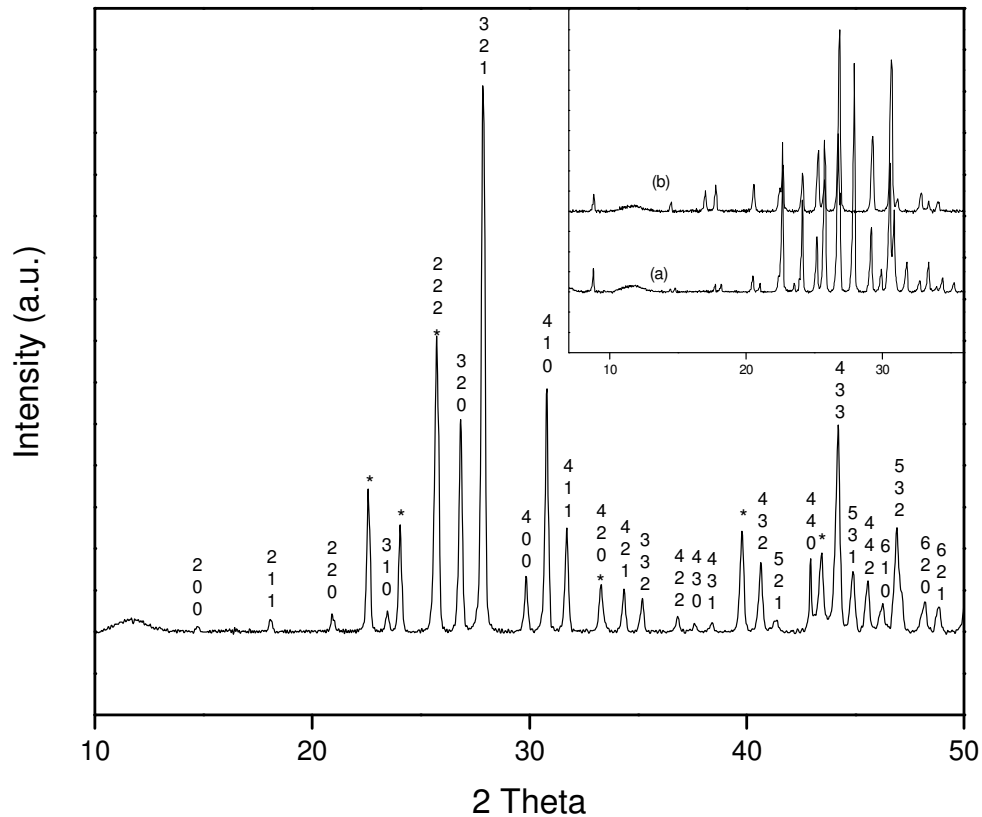


Figure 5-2: The X-ray diffraction pattern of the (40/60 mol%) CO₂/H₂ hydrate. The X-ray powder diffraction data were collected at -110 °C and atmospheric pressure. CO₂/H₂ forms sI hydrate whereas the CO₂/H₂/C₃H₈ mixture forms hydrate of sI & sII at 5.0 MPa (a) and only sII hydrate at 3.8 MPa (b). The composition of the CO₂/H₂/C₃H₈ gas mixture is given in Table 5-1.

Table 5-1: Phase composition at the start and end of the experiment as analyzed by gas chromatography

Description	CO ₂ (mol %)	H ₂ (mol %)	C ₃ H ₈ (mol %)
CO₂/H₂ mixture			
Feed gas composition (start)	40.1 (±0.1)	59.9 (±0.1)	-
Gas phase composition (end)	20.0 (±0.2)	80.0 (±0.2)	-
Hydrate phase composition	91.8 (±0.2)	8.2 (±0.2)	-
CO₂/H₂/C₃H₈ mixture			
Feed gas composition (start)	38.2 (±0.2)	59.2 (±0.2)	2.6 (±0.2)
Gas phase composition (end)	23.2 (±0.2)	76.4 (±0.2)	0.4 (±0.2)
Hydrate phase composition	74.2 (±0.2)	11.2 (±0.2)	14.6 (±0.2)

The powder-XRD pattern obtained from the hydrate formed with the ternary CO₂/H₂/C₃H₈ (38.2/59.2/2.6 mol %) mixture is shown as an insert in Figure 5-2. Figure 5-2(a) shows the powder pattern of the synthesized hydrate at 5.0 MPa, whereas Figure 5-2(b) shows the pattern of the hydrate synthesized at 3.8 MPa. The powder patterns show that the hydrate formed at 5.0 MPa is a mixture of structure I and structure II hydrate, whereas that at 3.8 MPa is pure structure II hydrate. It is noted that hydrates in both cases were synthesized for 20 hours at -20°C followed by 4 hours at 1°C and then bringing back the temperature to -20°C for another 20 hours. Additional experiments were performed during which hydrate samples were formed and analyzed after two and ten hours. These additional experiments confirmed the above structural findings which are consistent with expectations from thermodynamics. Thus, when the hydrate is synthesized at 3.8 MPa, thermodynamically it is possible to form only structure II hydrate with propane occupying the large cages. However, when the CO₂/H₂/C₃H₈ mixture is used for hydrate formation at 5 MPa and -20°C, thermodynamically it is possible to form structure I (with

only CO₂ and H₂ occupying the hydrate cages) and structure II (with all the three gases occupying the hydrate cages) hydrate.

It was found that C₃H₈ preferentially occupies the large cage of sII and tends to enhance the stability of the hydrate. However, the Langmuir constant for CO₂ in the large cage of structure I is greater than it is for that of sII. Thus, CO₂ would preferentially occupy the large cage of sI over that of sII for the same fugacity of CO₂ in the vapor phase. It is also more efficient for CO₂ to occupy the large cages of structure I, as sI has more large cages than sII for a given volume, and hence there is a greater opportunity for CO₂ to become incorporated in the large cages of sI. Therefore, at 5 MPa a hydrate which is a mixture of structure I and structure II forms. It is important to note that all the hydrates of CO₂/H₂/C₃H₈ analyzed for characterization purpose were synthesized at 3.8 MPa to ensure that the hydrate is pure structure II. It would be impossible to characterize the composition and cage occupancy of a hydrate mixture without knowing the amounts of sI and sII. Also the first stage of the hydrate based separation process for CO₂/H₂/C₃H₈ mixture as shown in chapter 4 operates at 3.8 MPa.

Figure 5-3 shows the PXRD pattern of the dissociating hydrate of CO₂/H₂ (from structure I to ice) as temperature is increased from -110°C to 5°C in steps of 5°C with a 2θ scan time of 2.5 minute. The result shows the stability of synthesized hydrate at atmospheric pressure. The rate of increase in temperature was approximately 2.0°C per minute during the diffraction test. Peak intensities assigned for ice increase with temperature and the peak intensity assigned to hydrate becomes smaller. This indicates that dissociating hydrate is transformed into ice. The insert in Figure 5-3 shows the intensity ratio of the hydrate peaks (2θ from 20 to 32) at any time to the hydrate peaks at

zero time as a function of temperature. It can be seen from the insert that the hydrate obtained from the CO_2/H_2 mixture with or without C_3H_8 starts decomposing at approximately -100°C . In the case of the $\text{CO}_2/\text{H}_2/\text{C}_3\text{H}_8$ hydrate (structure II) the dissociation of hydrate proceeds in one step up to around -60°C where all the hydrate has been completely transformed into ice. However, the dissociation of CO_2/H_2 hydrate (structure I) proceeds in stages. It was also interesting to note that there was almost 40% hydrate left at -10°C , which only decomposed completely once the temperature reached the melting point of ice. The above observation matches well with the self-preservation phenomena reported in the literature for CO_2 hydrate (Takeya and Ripmeester, 2008).

Stepwise dissociation of CO_2/H_2 hydrate is possible if the hydrate synthesized is actually a mixture of pure CO_2 hydrate (structure I) and CO_2 & H_2 hydrate (structure I). If such a hydrate sample stored at liquid nitrogen temperature were decomposed by gradually heating the hydrate at atmospheric pressure, it is expected that CO_2/H_2 hydrate would decompose at lower temperature (being less stable compared to pure CO_2 hydrate) compared to pure CO_2 hydrate. In order to examine whether the hydrate synthesized from CO_2 and H_2 was a mixture of pure CO_2 hydrate and hydrate of CO_2/H_2 a sample was decomposed at atmospheric pressure by gradually increasing the temperature and allowing the gas evolved to pass through a mass spectrometer with a heated capillary inlet line.

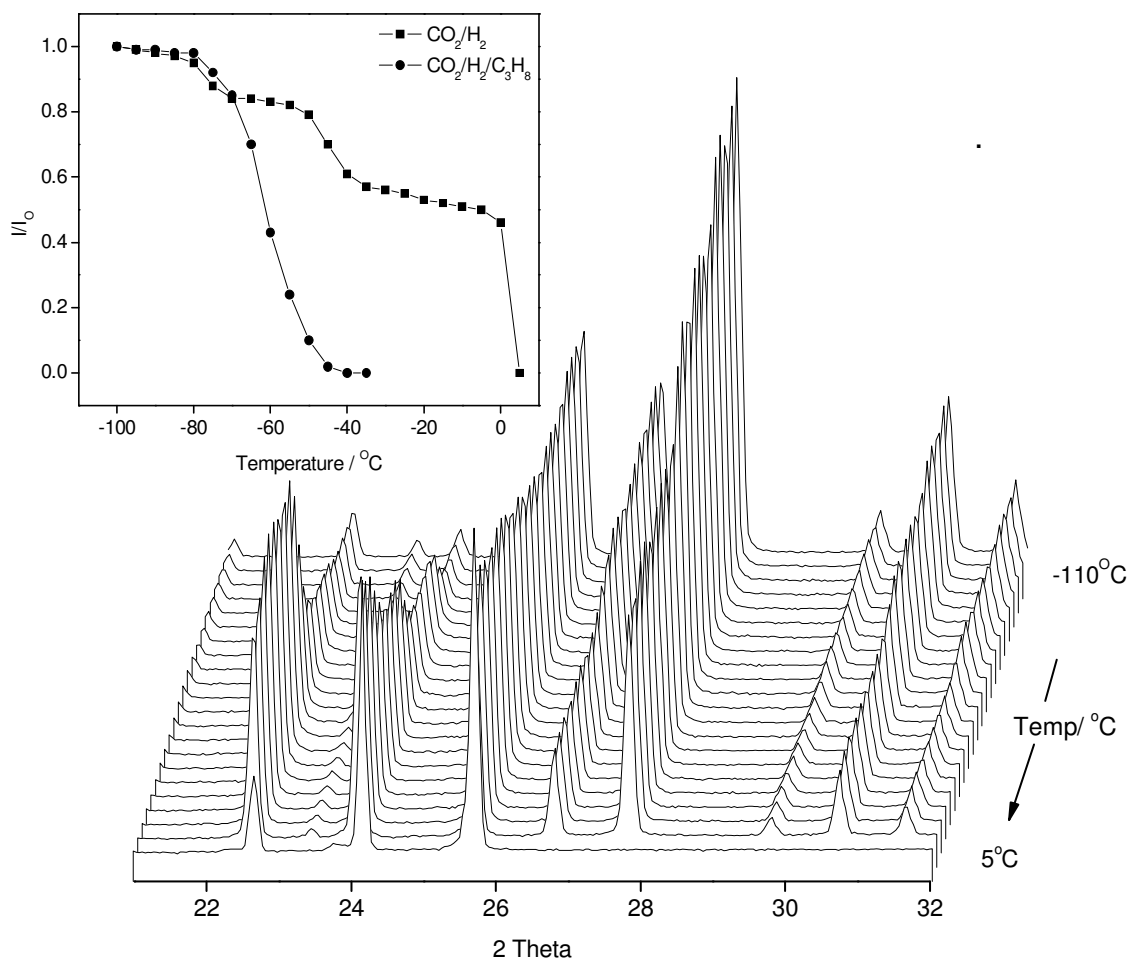


Figure 5-3: Temperature dependent PXRD profile for (40/60 mol%) CO₂/H₂ hydrate from -110°C to 5 °C. Inset shows intensity ratio of hydrate peak as a function of temperature during transformation of CO₂/H₂ hydrate (8 MPa & -20°C) and CO₂/H₂/C₃H₈ hydrate (3.8 MPa & -20°C) into ice.

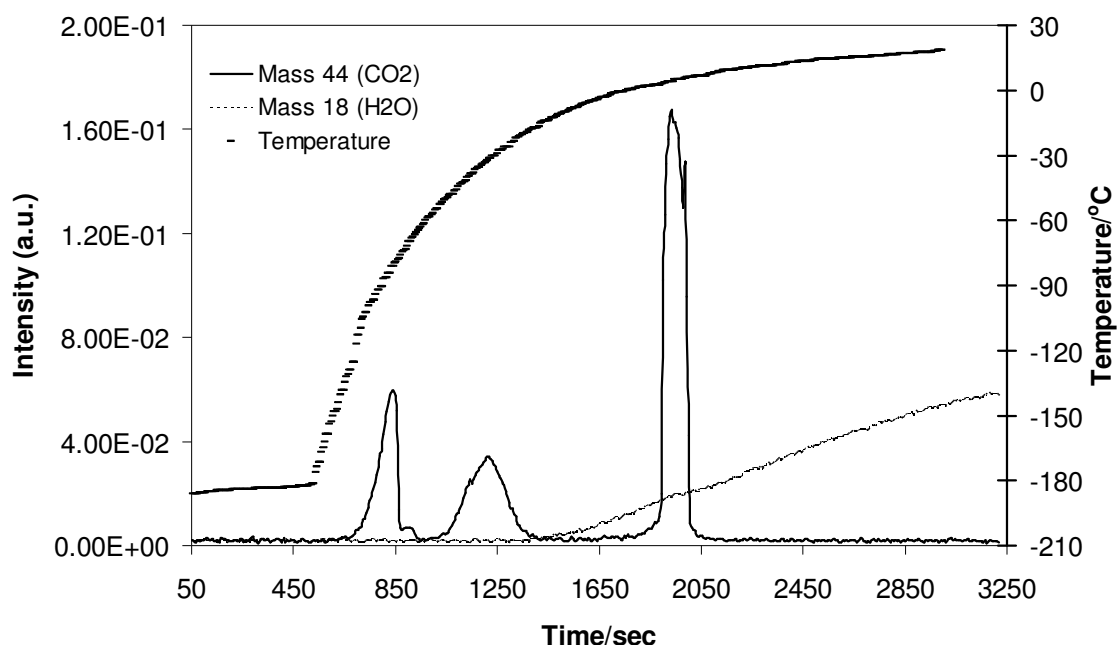


Figure 5-4: Mass of decomposed gas coming out of (40/60 mol%) CO₂/H₂ hydrate with respect to time.

Figures 5-4 and 5-5 shows the gas obtained from the decomposition of the hydrate as a function of time. The temperature is also shown. As seen in Figure 5-4, the first peak of carbon dioxide appears at about -80°C, which coincides with the melting point of dry ice. Dry ice is accumulated in the system when a hydrate reactor pressurized with the CO₂/H₂ mixture is quenched at liquid nitrogen temperature to recover the hydrate. As can be seen from Figure 5-4, CO₂ release stops until the temperature of hydrate sample is increased to -55 °C. At temperatures close to -30 °C a peak corresponding to the CO₂ from the decomposed hydrate is seen. However, as the temperature increases further, CO₂ release is not observed until the temperature reaches close to 0°C, where another CO₂ peak is seen. It is likely that due to the self-preservation effect hydrates are kinetically stable above the theoretical equilibrium point and a portion of the hydrate decomposes

close to 0°C. Figure 5-4 also shows that water vapor can be detected at a temperature as low as -15°C.

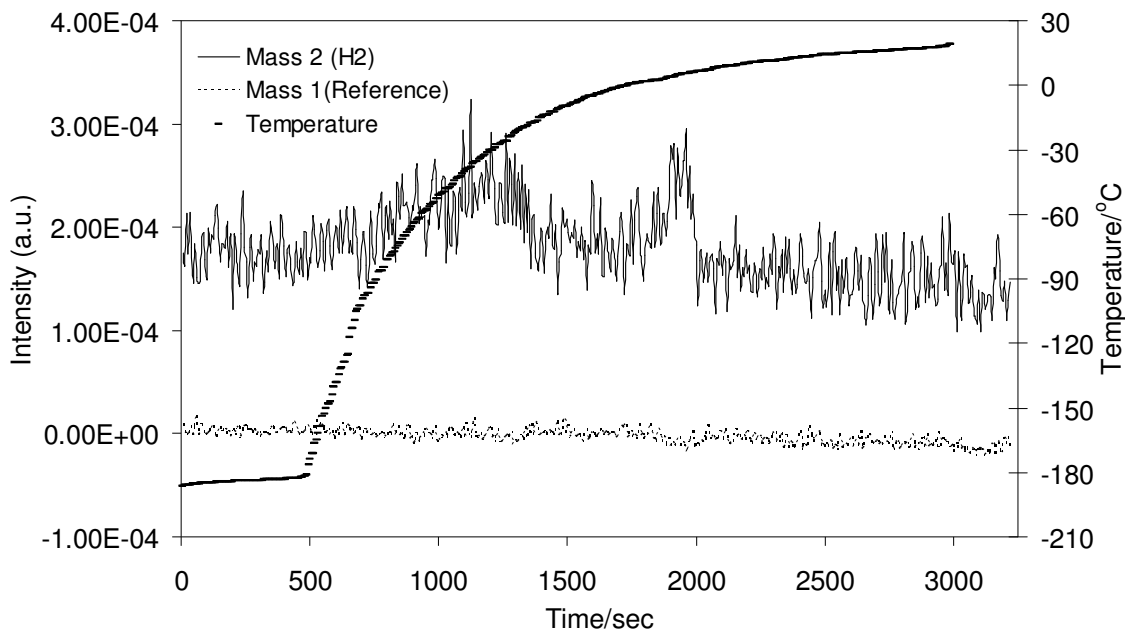


Figure 5-5: Mass of decomposed gas coming out of (40/60 mol%) CO₂/H₂ hydrate with respect to time. Mass number 2 is for hydrogen leaving the hydrate lattice on decomposition, mass 1 is shown as a reference.

Figure 5-5 shows the pattern of hydrogen escaping from the hydrate cages. The temperature dependence of species with mass number 1 is also plotted in Figure 5-5, which acts as a reference line for mass 2 (H₂). The amount of hydrogen present in the hydrate cages is at least an order of magnitude less than CO₂ hence; a relatively smaller peak for H₂ is seen. However, it is evident that hydrogen release also follows the decomposition pattern shown by CO₂ since the majority of H₂ from the hydrate phase accompanies CO₂, once at -60°C to -30°C and then again at a temperature closer to the melting point of ice. These observations indicate that the hydrate synthesized and analyzed was a CO₂/H₂ hydrate. We note that this H₂ release pattern is quite different

than those for sII mixed hydrates ($\text{CO}_2/\text{H}_2/\text{C}_3\text{H}_8$ mixture). In the latter hydrate, the small cavities form continuous layers by face sharing of the D cages (5^{12} cages), thus a continuous diffusion path is available for hydrogen to leave the hydrate (Senadheera and Conradi, 2007). In sI hydrate, the small cavities are surrounded by the T cages ($5^{12}6^2$ cages) which contain CO_2 molecules, thus blocking diffusion pathways for H_2 (Alavi and Ripmeester, 2007). Moreover, the hydrate exhibits the self-preservation effect similar to that for CO_2 hydrate (Takeya and Ripmeester, 2008), thus it is possible to store H_2 quite effectively in sI hydrate, although there is far less capacity because of the small number of D cages. Once the PXRD and mass spectroscopic measurements confirmed that the solid phase contained homogeneous hydrate, the hydrate phase composition was obtained by gas chromatography. Table 5-1 shows the gas/hydrate composition at each stage for both systems. This result is in agreement with the gas uptake measurement performed and presented in Chapters 3 and 4.

Raman spectra for the rotational and vibrational stretching regions (vibrons) of hydrogen were recorded to find the signature of hydrogen in the hydrate cages. The low-frequency spectra from hydrogen are usually dominated by the rotational excitations of the hydrogen molecules which appear at $300\text{--}850\text{ cm}^{-1}$. The vibron (molecular vibration) region for hydrogen in the hydrate phase appears at $4100\text{--}4200\text{ cm}^{-1}$. Figure 5-6 shows a typical Raman spectrum from the $\text{CO}_2/\text{H}_2/\text{C}_3\text{H}_8$ sII hydrate synthesized at 3.8 MPa. The spectrum was obtained by focusing the laser on the solid hydrate phase at atmospheric pressure and liquid nitrogen temperature. The signatures of all the three gases in the hydrate phase are seen. Hydrogen rotational bands in the hydrate phase can be seen at 355 cm^{-1} and 585 cm^{-1} (Struzhkin et al., 2007). It has to be noted that hydrogen from the

gas phase appears at 359 cm^{-1} and 590 cm^{-1} (shown in appendix C, Figure C-1). This suggests that the peaks associated with the hydrogen rotational bands are red shifted in the hydrate phase by almost 5 cm^{-1} and that these frequencies are not greatly perturbed for hydrogen in the cages. Raman frequencies for gases trapped in the hydrate phase are generally shifted (propane is an exception, Kumar et al., 2008) to lower wave numbers, as in the case of CO_2 , shown as an insert in Figure 5-6. The two largest peaks, one at 1278 cm^{-1} and the other 1382 cm^{-1} in Figure 5-6 correspond to the Fermi diad of CO_2 in the hydrate cages.

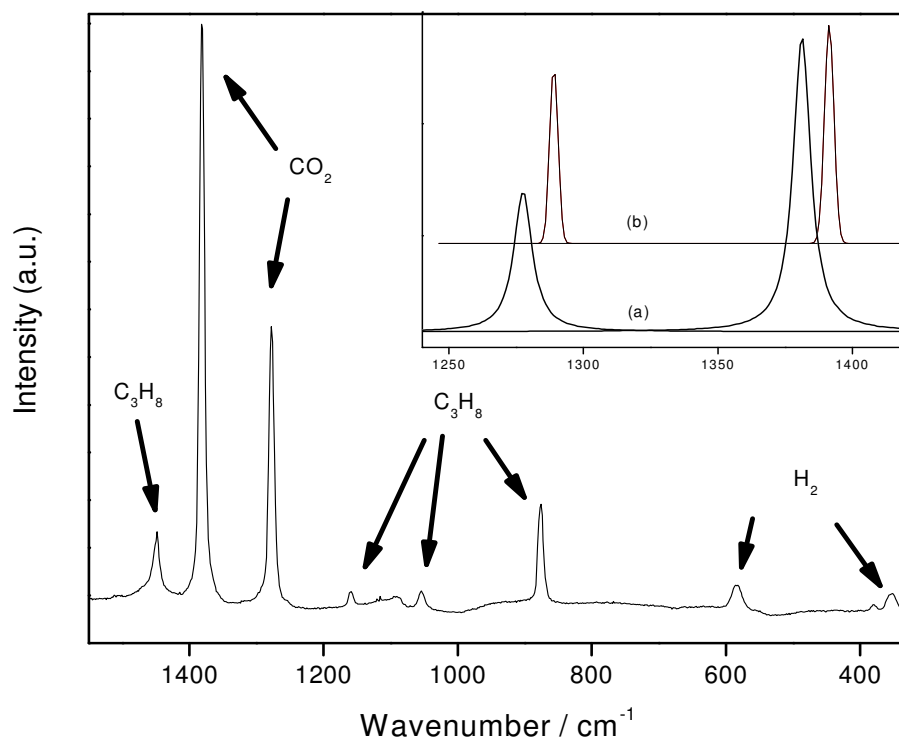


Figure 5-6: Raman spectrum for the Fermi diad of CO_2 incorporated into hydrate phase from the $\text{CO}_2/\text{H}_2/\text{C}_3\text{H}_8$ gas mixture. Note the rotational modes for H_2 occupying the hydrate cages and several C-C stretching modes of C_3H_8 . The figure in the inset suggests the broadening and red shift of CO_2 incorporated in hydrate phase (a) compared to CO_2 in gas phase (b)

Figure 5-6 (a) shows the Fermi diad positions of CO₂ in the hydrate phase and (b) shows the Fermi diad positions of CO₂ in the gas phase. It has been reported previously that Raman spectra for pure CO₂ hydrate do not show peak splittings (Murphy and Roberts, 1995) even though CO₂ occupies both the small and large cages (Udachin et al., 2001). Peak splitting has been observed with infrared spectroscopy (Fleyfel and Devlin, 1991) and this is discussed in Chapter 6. Propane shows several peaks in the C-C stretching region and the most prominent one appears at about 878 cm⁻¹ (Figure 5-6). Propane only occupies the large cage of structure II hydrate and hence, does not show any peak splitting for guests in different cages. It is noted that CO₂/H₂ hydrate, which forms structure I also shows similar Raman spectra (included in Appendix C, Figure C-2) in this region. The peak positions for CO₂ and H₂ in structure I and structure II hydrate remain unchanged (within ± 1 wavenumber).

Figure 5-7 shows Raman spectra in the hydrogen vibron region of the gas and the hydrate phases. Hydrogen gas at ambient conditions shows four visible peaks $Q_1(0)$, $Q_1(1)$, $Q_1(2)$, and $Q_1(3)$ which appear at 4161, 4155, 4144, and 4126 cm⁻¹ respectively. The even number in parenthesis denotes the para- state of hydrogen (total nuclear spin of zero) whereas the odd number denotes the ortho- state of hydrogen (total nuclear spin of 1). Under ambient conditions, the ratio of ortho- to para- hydrogen is 3:1 which results in a larger ortho- peak at 4155 cm⁻¹ compared to para- peak at 4161 cm⁻¹ (H₂ gas in Figure 5-7). However, at liquid nitrogen temperatures at equilibrium the ratio of ortho hydrogen to para hydrogen is close to 1:1 (Senadheera and Conradi, 2007).

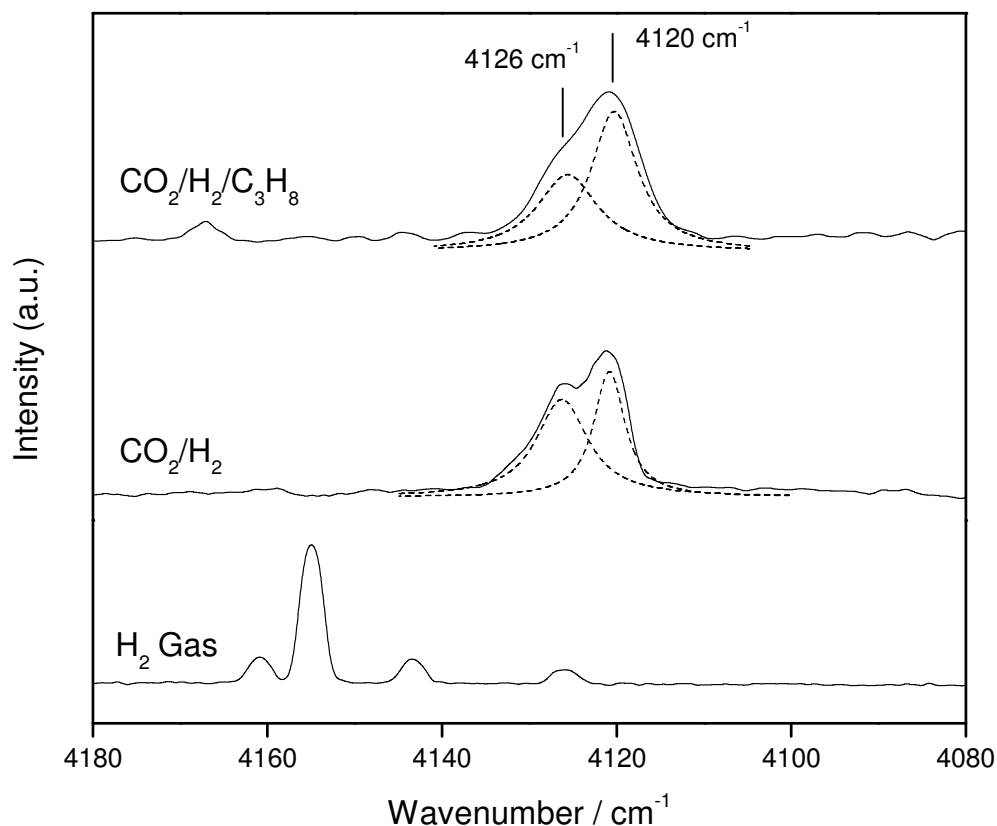


Figure 5-7: Raman spectra of the vibron region for H₂ gas and H₂ incorporated into hydrates of CO₂/H₂ and CO₂/H₂/C₃H₈. H-H stretching of H₂ gas was recorded at room temperature whereas H-H stretching of H₂ in hydrate phase was recorded at liquid nitrogen temperature. It is noted that the CO₂/H₂ mixture forms structure I hydrate whereas CO₂/H₂/C₃H₈ mixture forms structure II hydrate.

In the hydrate phase the H₂ signature appears as a doublet with maxima at 4120 cm⁻¹ and 4126 cm⁻¹. The shift to lower frequency for each Q band in the hydrate phase is attributed to changes in the H-H stretching mode when H₂ is enclathrated. (Florusse et al., 2004) Moreover, the H₂ vibron bands at 4120 & 4126 cm⁻¹ consist of relatively broad peaks typical of enclathrated guests in the hydrate cavities. The enclathrated hydrogen gives rise to a strong signal even at atmospheric pressure and ~-190°C, owing to its higher density of H₂ in the hydrate phase. It is clear from Figure 5-7 that in the presence of help

gases like CO₂ and C₃H₈, H₂ occupies the small cages of structure I and II hydrate, respectively, even at moderate pressures (further information is provided in appendix C).

Even though Raman spectroscopy shows the presence of different gases in hydrate cages it fails to i) provide the ratio of CO₂ in large and small cages ii) determine whether H₂ is present as a single molecule in the small cages of structure I and structure II or as a cluster of two H₂ molecules. In this study, infrared spectroscopy was used to identify CO₂ in large and small cages in the hydrate structure and NMR spectroscopy was used to determine the hydrogen occupancy in the hydrate cages. Generally, it is agreed that for pure CO₂ hydrate, CO₂ molecules occupy essentially all of the large cages in structure I as well as a fraction (60-80%) of the small cages (Udachin et al., 2001). However, unlike methane hydrate where the peaks of methane in the small and large cages are separated by almost ten wavenumbers (Kumar et al., 2008), Raman spectroscopy does not show a split peak for CO₂ in large and small cages. On the other hand FTIR work by Fleyfel and Devlin (1991) conducted at lower temperature indicated two separate peaks of CO₂ in large and small cages in sI and sII hydrates of CO₂.

Pure CO₂, CO₂/H₂, CO₂/C₃H₈ and CO₂/H₂/C₃H₈ hydrates were synthesized for this study to find the frequencies for CO₂ in the small and large cages, chapter 6 presents this work in detail. In brief, it was found that for CO₂/H₂ hydrate most of the CO₂ in the hydrate phase is present in the larger 5¹²6² cages and a very small amount of CO₂ is present in the small cages of the resultant structure I hydrate. However, in the ternary mixture of CO₂/H₂/C₃H₈ hydrate it can be said that CO₂ occupies a higher percentage of small cages as compared to CO₂/H₂ hydrate. With just 2.6 mol% C₃H₈ (less than stoichiometric requirement for full occupancy of large cages) in the CO₂/H₂/C₃H₈ gas

mixture the large cages in the resulting structure II hydrate are shared by C₃H₈ and CO₂ and a significant amount of CO₂ occupies the smaller 5¹² cages, along with H₂.

¹³C MAS NMR confirmed that the hydrate prepared from the CO₂/H₂ mixture is structure I as was found by PXRD. Only one signal (isotropic shift 124.95 ppm) can be resolved in the ¹³C MAS spectrum for CO₂/H₂ hydrate. The observed spectral pattern is characteristic of chemical shift anisotropy (CSA), as one may expect for pure CO₂ hydrate in sI (Ratcliffe and Ripmeester, 1986), where the spectrum reflects partial averaging of the CSA tensor for CO₂ in the anisotropic environment of the sI large cage at low temperature (Ratcliffe and Ripmeester, 1986, 1998; Udachin et al., 2001). In this study for the CO₂/H₂ hydrate sample, ¹³C MAS spectra show that the total integrated intensity of the CO₂ signal corresponds to $2.74 \pm 0.35 \times 10^{21}$ CO₂ molecules per gram of hydrate, which is very close to complete occupancy of the large cages. This leaves a large number of small cages that can be filled with hydrogen in agreement with results obtained by infrared spectroscopic data for CO₂/H₂ hydrate. The ¹³C MAS NMR spectrum for CO₂/H₂ hydrate is given in chapter 6 (Figure 6-2).

In the case of hydrate prepared from the CO₂/H₂/C₃H₈ mixture at 3.8 MPa, a structure II hydrate is formed which is reflected in its ¹³C spectrum (Figure 5-8). The two closely spaced and most intense signals at 17.25 and 16.8 ppm are from the methyl (CH₃) and methylene carbon (CH₂) groups of propane in the large cages, respectively. The intensity of the signals corresponds to 6.92×10^{20} C₃H₈ molecules per gram of hydrate, which is less than the number required for full occupancy of the large cages. The remaining large cages have to be occupied by CO₂ in order to form a stable hydrate, considering that complete filling of the large cages in sII is a criterion for stability. The signal of CO₂

appears as a center band and a set of spinning sidebands (similar to CO₂/H₂ hydrate) with an isotropic shift of 125.06 ppm. The spectral pattern is once more indicative of the partially averaged CSA tensor for CO₂ in the small cages plus a contribution from the isotropic resonance for CO₂ in the large cage (Ratcliffe and Ripmeester, 1986). The intensity of the CO₂ signal in this hydrate corresponds to 1.7×10^{21} CO₂ molecules per gram of hydrate, which is lower than the total amount of CO₂ present in the hydrate cages of CO₂/H₂ hydrate.

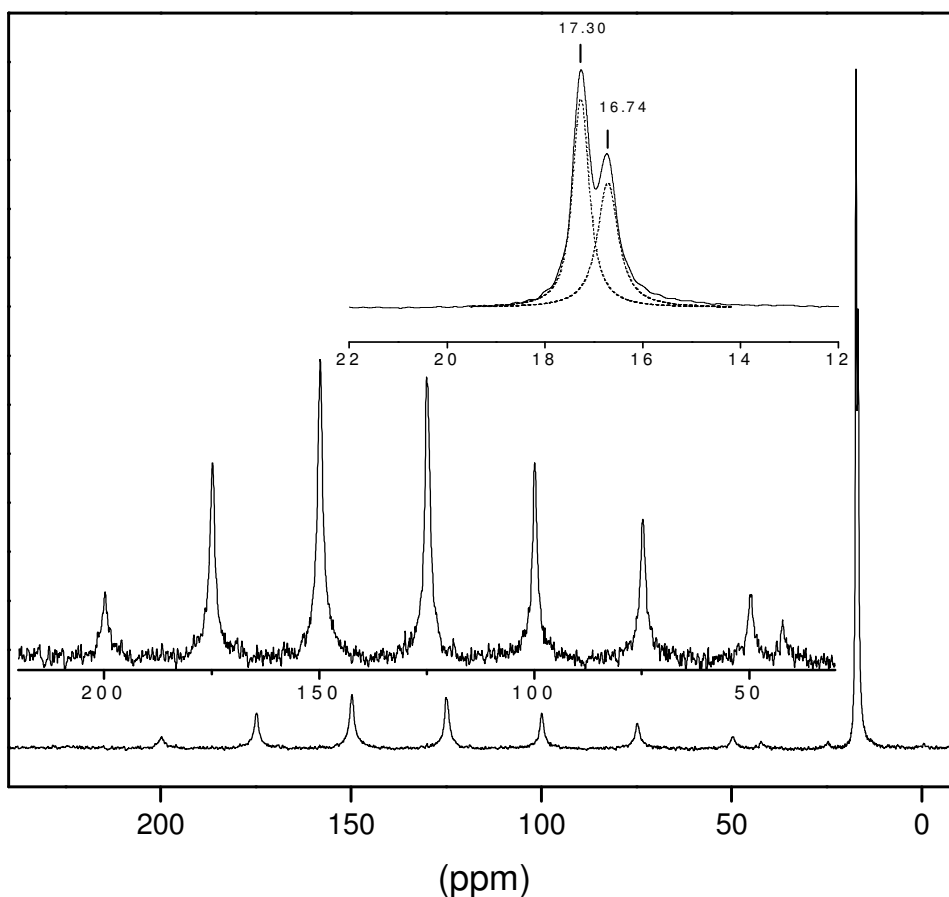


Figure 5-8: ¹³C CP MAS NMR spectra for CO₂/H₂/C₃H₈. Upper inset shows the expanded signal of C₃H₈ in large cages of resultant sII hydrate. T=173K, spinning speed of 2500 Hz

Figure 5-9 shows a ^1H MAS spectrum of CO_2/H_2 hydrate in D_2O recorded as a spinner-synchronized spin-echo. Three signals can be seen in the spectrum. The broader line at 6.59 ppm, based on its position and its presence in the spectrum of pure $\text{CO}_2/\text{D}_2\text{O}$ hydrate, can be assigned to the residual protons in the D_2O that was used in the hydrate preparation to reduce the intensity of the water proton signal. A prominent signal at 4.26 and a shoulder at 4.09 ppm are from H_2 molecules trapped in the hydrate cages. The assignment is based on the chemical shift of the signals, which is close to the shift of molecular hydrogen. This is also supported by the slow decrease of the signal intensity with the time (Moudrakovski et al., 2008). The latter likely is due to decomposition of hydrate at -100°C . In the course of three hours, the combined intensity of the two signals was reduced by about 30%. Integration of the spectrum gives the relative intensities of the H_2 signals as 3:1 (Moudrakovski et al., 2008).

As mentioned above, at ambient conditions hydrogen molecules exist in the form of two-spin isomers ortho- and para- hydrogen, with only the ortho-isomer being observable by proton NMR. There have been very few studies regarding ortho and para hydrogen in hydrates (Senadheera and Conradi, 2007; Ulivi et al., 2007) and quantitative studies have not been carried out on spin conversion between ortho- and para- states. Since only the ortho-isomers are being observable by proton NMR, it is possible that the signals at 4.09 and 4.26 ppm in Figure 5-9 originate from H_2 molecules in singly and doubly occupied small cages as all the large cages are filled by CO_2 .

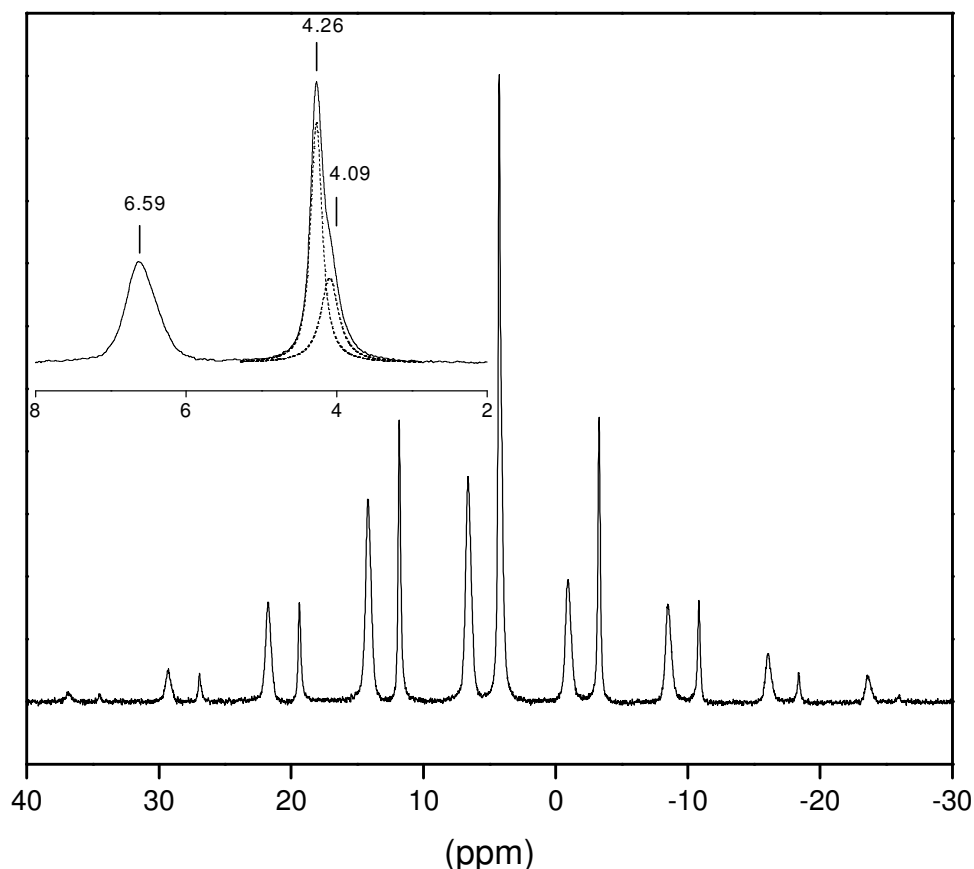


Figure 5-9: ^1H MAS ($T=173\text{K}$, 3000 Hz) of CO_2/H_2 hydrate prepared in D_2O . The inset shows expanded central region of the spectrum without spinning sidebands. The peak at 6.59 ppm is due to the proton impurity in D_2O .

It is not surprising that ^1H MAS spectra shows evidence of doubly occupied (two H_2 molecules) small cages. Based on ^1H MAS NMR spectra Kim and Lee (2005) have also reported double occupancy of H_2 in the small cages of CO_2/H_2 hydrate. However, they observed a single resonance at 4.2 ppm . In our work, two peaks differing by 0.16 ppm were seen and this is in close agreement with the calculations of Alavi et al. (2005) who reported a difference of 0.1 ppm in the peak position of doubly occupied H_2 to that of singly occupied H_2 in the small cages. Considering that the small cage in structure I hydrate have a slightly different shape than those in structure II hydrate there are possibilities that in CO_2/H_2 hydrate a number of small cages are occupied by two H_2

molecules. So far, there is no other evidence of doubly occupied small cages except that from the NMR assignments.

Figure 5-10 shows a ^1H MAS spectrum of hydrate prepared from $\text{CO}_2/\text{H}_2/\text{C}_3\text{H}_8$ mixture at 3.8 MPa. The two most intense signals at 0.64 and 1.07 ppm with relative intensity ratio 3:1 are from CH_3 and CH_2 groups of propane occupying the large cage. No signal from residual protons in D_2O was observed in this sample. The difference likely can be attributed to a difference in dynamic states of the water molecules in the hydrates with the water in the CO_2 hydrate being more mobile and hence giving greater averaging of dipolar couplings and a sharper ^1H resonance. The third signal in the spectrum at 3.93 ppm can be assigned to molecular hydrogen in the hydrate cage. Small cages are the most likely location for this hydrogen since the large cages in this hydrate are well occupied by C_3H_8 and CO_2 (see ^{13}C data). Based on the peak position at 3.93 ppm and the broad nature of the peak we cannot comment on the presence of doubly occupied small cages in this structure II hydrate. Moreover, comparing the absolute intensity of the H_2 peak at 3.93 ppm with that of the C_3H_8 peak in the same hydrate, the hydrogen is present at about 11-12 mol % of the enclathrated propane. This is significantly less than what is found from gas hydrate decomposition just after hydrate synthesis. This difference likely is due to H_2 leaking from the hydrate cages over a period of time on storage and during the NMR analysis at 173 K (Alavi and Ripmeester, 2007; Okuchi et al., 2007)

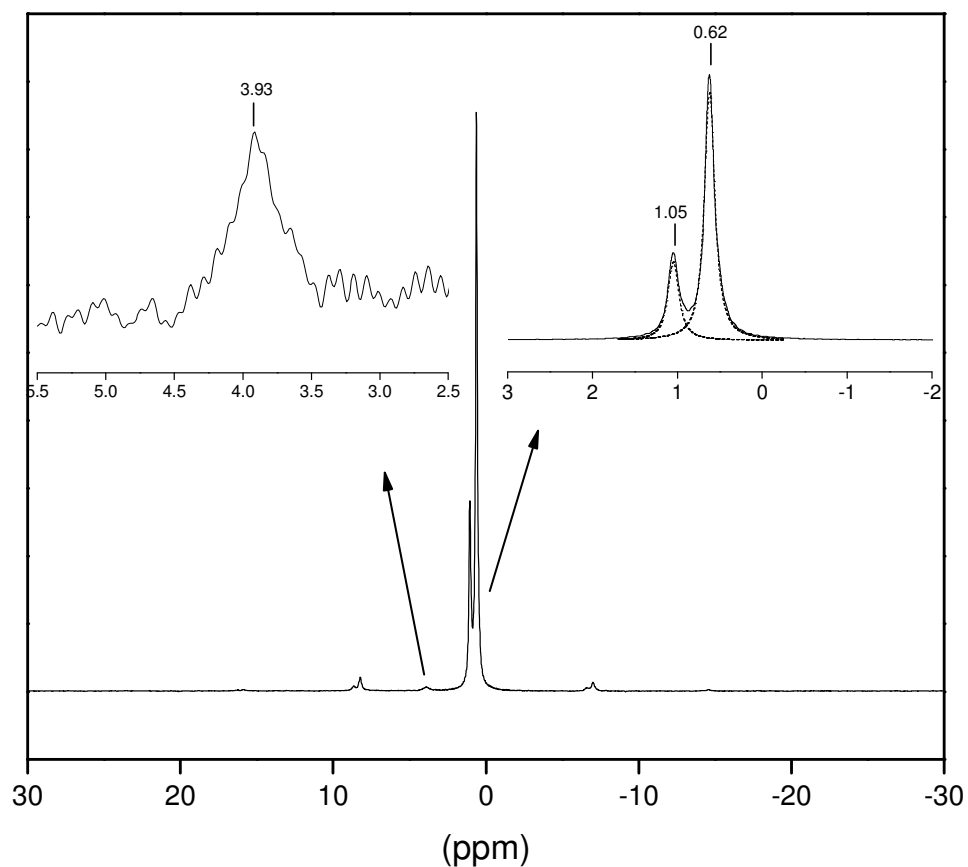


Figure 5-10: ^1H MAS ($T=173\text{K}$, 3000 Hz) of $\text{CO}_2/\text{H}_2/\text{C}_3\text{H}_8$ hydrate in D_2O . Expanded signals for propane are shown on the right inset along with a weak signal from H_2 on the left inset.

5.3.1. Determination of cage occupancy

In most cases NMR can provide accurate quantitative data on cage occupancies. For example, in a similar study (which is not part of this thesis) on $\text{CH}_4/\text{C}_2\text{H}_6/\text{C}_3\text{H}_8$ fractionation we carried out ^{13}C NMR analysis of the resultant hydrate, where methane occupies small as well as large cages, results in two well-separated signals at -8.2 ppm (large cage) and -4.3 ppm (small cage), which can be accurately integrated for exact quantity of methane and other gases (Kumar et al., 2008). However, the difference in the isotropic chemical shifts of CO_2 in large and small cage of CO_2 hydrate is very small and

^{13}C MAS NMR (Ratcliffe and Ripmeester, 1986; Ripmeester and Ratcliffe 1998; Udachin et al., 2001) cannot separate the signals. We attempted to obtain the relative occupancies by acquiring static powder patterns on a sample of hydrate synthesized with ^{13}C -enriched $\text{CO}_2/\text{H}_2/\text{D}_2\text{O}$. However, due to the broadness of the ^{13}C HPDEC (High-Power Proton Decoupling) pattern at -100°C , the CO_2 lines in the large and small cages could not be separated. The static pattern at -40°C was better resolved but as mentioned earlier, CO_2/H_2 hydrate is not stable at that temperature and hence the result was discarded (please refer appendix C for the plot, Figure C-6). In the cases studied for both binary and ternary hydrate, ^{13}C MAS spectra do not show peak separation sufficient for distinguishing CO_2 in small and large cages of the hydrate. In the absence of distinct signals for CO_2 in small and large cages the use of the statistical thermodynamics approach (Kumar et al., 2008) for absolute occupancy of CO_2 in small and large cavities could not be used. Nevertheless, with the help of known hydrate phase composition from gas chromatography and the information obtained by NMR; an estimate can be made about cage occupancy values for each gas in the hydrate cages.

For CO_2/H_2 hydrate which forms structure I, NMR results suggest that $2.74 \pm 0.35 \times 10^{21}$ CO_2 molecules are present in every gram of hydrate (~ 0.21 gram of CO_2 per gram of hydrate). Assuming that all of the large cages of hydrate have to be filled for a stable CO_2/H_2 hydrate it can be said that in binary CO_2/H_2 hydrate 100% of the large cages (within experimental error) are occupied by CO_2 . This result is somewhat similar to the result we obtain by infrared spectroscopy (chapter 6) where we see most of the CO_2 is present in the large cages. However, given the error of $\pm 0.35 \times 10^{21}$ CO_2 molecules in our NMR results it is possible that a very small percentage of the small cages of CO_2/H_2

hydrate are actually occupied by CO₂. In order to see the cage distribution of H₂ we need to look at the ¹H MAS spectra of CO₂/H₂ hydrate in D₂O. As discussed above (Figure 5-9) H₂ molecules occupy only the small cages, both with single and double occupancies. We assign the signal at 4.09 ppm to single and 4.26 ppm to doubly occupied cages (Alavi et al., 2005). The ratio of hydrogen present in a doubly occupied cavity shows a peak three times stronger than the peak from single hydrogen molecule in the hydrate structure. In addition to the NMR results, we know that hydrate phase composition from gas chromatography suggests that the binary hydrate consists of 92 mol% CO₂ and 8 mol% H₂ (Table 5-1). Using the information from gas chromatography as well as from NMR spectra for the cage occupancy calculation, CO₂ occupies 100% of the large cages, whereas 9.3% of the small cages are occupied by bimolecular H₂ and 6.2% by single H₂ molecules (please see appendix C for details of calculation).

The hydrate from the CO₂/H₂/C₃H₈ mixture at 3.8 MPa is structure II. Figure 5-9 shows the ¹³C spectrum of the CO₂/H₂/C₃H₈ hydrate. Two closely spaced signals at 17.25 and 16.8 ppm with the intensity ratio of 2:1 are from CH₃ and CH₂ groups of propane in the large cages. The integral intensity of the signals corresponds to 6.92×10^{20} C₃H₈ /g (0.05 gram C₃H₈ per gram of hydrate), which is about 43% of the large cages filled for this hydrate. The CO₂ molecules occupy the remaining 57% of the large cages. For the same hydrate, the total intensity of the CO₂ signal corresponds to 1.7×10^{21} CO₂/g (0.124 gram of CO₂ per gram of hydrate). Since close to 0.068 grams of CO₂ is present in the large cages the rest (0.056 gram of CO₂) occupies the small cages, which is equivalent to 34.0 % of the small cage occupancy (Details of the calculation are given in appendix C). Therefore, the NMR results suggest that the large cages are occupied with CO₂ and C₃H₈

and CO₂ also occupies 34% of the small cages. Qualitative information from Infrared spectroscopy also shows that CO₂ occupies a significant number of small cages in the ternary hydrate. For the H₂ distribution over the hydrate cages, as mentioned earlier, the amount of H₂ in the hydrate is ~12 mol % (~0.0003 g) of the total amount of propane (Figure 5-10) which is equivalent to 0.3% of the small cage occupancy. This does not match with the hydrate phase composition obtained by gas chromatography as shown in Table 5-1. It has been reported previously that H₂ can leak through the hydrate cages on storage (Alavi et al., 2007; Okuchi et al., 2007). Also, NMR only detects ortho-hydrogen in the hydrate cages which can result in an up to two-fold underestimation of the actual amount of H₂ in the hydrate cages (Ulivi et al., 2007; also in this thesis: Appendix C). Therefore, the cage occupancy of H₂ in the small cages is greater than 0.6%. The cage occupancy values are reported in Table 5-2 for CO₂/H₂ and CO₂/H₂/C₃H₈ hydrate along with the hydration number. The equation used to calculate the hydration number is given in chapter 6 (equation 6.2).

Table 5-2: Estimate of cage occupancy values obtained by combination of results from gas chromatography and NMR. θ_s represents hydrogen doublet in small cages

Description	Hydrate structure	H ₂		CO ₂		C ₃ H ₈	Hydration number
		θ_s	θ_s'	θ_s	θ_L	θ_L	n
CO ₂ /H ₂	sI	0.062	0.093	0.000	1.000	0.000	7.09
CO ₂ /H ₂ /C ₃ H ₈	sII	0.006	0.000	0.340	0.570	0.430	10.05

5.4. CONCLUSIONS

In this work, structural and compositional characterization was carried out on hydrate samples formed from CO₂/H₂ and CO₂/H₂/C₃H₈ gas mixtures using PXRD, ¹H MAS NMR (with rotor synchronized spin echoes), ¹³C MAS NMR, mass spectrometry, FTIR

(with attenuated total reflection) and Raman spectroscopy. The information obtained enabled the determination of hydrate composition and cage occupancy. Gas hydrates made from (40/60 mol %) CO_2/H_2 mixtures form structure I hydrate at 8MPa. It was found that the large cages are almost fully occupied by carbon dioxide and the small cages were mainly occupied by hydrogen. Furthermore, NMR results suggest that 9.3% of the small cages are occupied by bimolecular H_2 and 6.2% by single H_2 molecules. It was observed that CO_2/H_2 hydrate shows self-preservation on hydrate decomposition. In a CO_2/H_2 separation process via gas hydrate formation an additive like propane reduces the hydrate formation pressure without compromising the CO_2 recovery. It was found that by introducing 2.6% C_3H_8 in CO_2/H_2 gas mixtures the ternary mixture forms pure structure II hydrate at 3.8 MPa. In the resultant hydrate CO_2 (57 %) and C_3H_8 (43 %) share the large cages and a significant portion of small cages is occupied by CO_2 (34 %). Based on the results obtained from this work it can be said that hydrogen occupies the small cages of structure I as well as structure II hydrate.

5.5. REFERENCES

- Alavi, S., Ripmeester, J. A. 2007. Hydrogen-Gas Migration through Clathrate Hydrate cages *Angew. Chem. Int. Ed.* 46, 6102-6105
- Alavi, S., Ripmeester, J. A., Klug, D. D. 2005. NMR shielding constant for hydrogen guest molecules in structure II clathrates. *J. Chem. Phys.* 123, 051107
- Anderson, R., Chapoy, A., Tohidi, B. 2007. Phase Relations and Binary Clathrate Hydrate Formation in the System H_2 -THF- H_2O *Langmuir*, 23, 3440-3444
- Fleyfel, F., Devlin, J. P. 1991. Carbon Dioxide Clathrate Hydrate Epitaxial Growth: Spectroscopic Evidence for Formation of the Simple Type-II CO_2 Hydrate. *J. Phys. Chem.* 95, 3811-3815
- Florusse, L. J., Peters, C. J., Schoonman, J., Hester, K. C., Koh, C. A., Dec, S. F., Marsh, K. N., and Sloan, E. D., 2004. Stable low-pressure hydrogen clusters stored in a binary clathrate hydrate. *Science* 306(5695), 469-471
- Henning, R. W., Schultz, A. J., Thieu, V., Halpern, Y. 2000. Neutron Diffraction Studies of CO_2 Clathrate Hydrate: Formation from Deuterated Ice *J. Phys. Chem. A* 104, 5066-5071
- Hashimoto, S., Murayama, S., Sugahara, T., Ohgaki, K. 2006. Phase Equilibria for H_2 + CO_2 + Tetrahydrofuran + Water Mixtures Containing Gas Hydrates *Journal of Chemical and Engineering Data*, 51:1884-1886
- Hester, K. C., Strobel, T. A., Sloan, E. D., Koh, C. A., Huq, A., Schultz, A. J., 2006. Molecular Hydrogen Occupancy in Binary THF- H_2 Clathrate Hydrates by High Resolution Neutron Diffraction *J. Phys. Chem. B*, 110, 14024-14027
- Kim, D-Y., Lee, H. 2005. Spectroscopic Identification of the Mixed Hydrogen and Carbon Dioxide Clathrate Hydrate *J. Am. Chem. Soc.* 127, 9996-9997
- Kumar, R., Linga, P., Moudrakovski, I., Ripmeester, J. A., Englezos, P. 2008 Structure and kinetics of gas hydrates from methane/ethane/propane mixtures relevant to the design of natural gas hydrate storage and transport facilities *AIChE*, 54, 2132-2144
- Lee, H., Lee, J-W., Kim, D. Y., Park, J., Seo, Y-T., Zeng, H., Moudrakovski, I. L., Ratcliffe, C. I., Ripmeester, J. A. 2005. Tuning clathrate hydrates for hydrogen storage. *Nature*, 434, 743-746
- Lokshin, K. A., Zhao, Y., He, D., Mao, W. L., Mao, H., Hemley, R. J., Lobanov, M. V., Greenblatt, M. 2004. Structure and dynamics of hydrogen molecules in the novel

- clathrate hydrate by high pressure neutron diffraction. *Phys. Rev. Lett.* 93, 125503-1
- Mao, W. L., Mao, H-K., Goncharov, A.F., Struzhkin, V.V., Guo Q, Hu J, Shu J, Hemley RJ, Somayazulu M, Zhao Y. 2002. Hydrogen Clusters in Clathrate Hydrate. *Science*, 297, 2247-2249
- Mao, W. L., Mao, H. 2004. Hydrogen storage in molecular compounds. *Proc. Natl. Acad. Sci. U.S.A.*, 101, 708-710
- Moudrakovski, I. L., Ratcliffe, C. I., McLaurin, G. E., Simard, B., Ripmeester, J. A. 1999. Hydrate Layers on Ice Particles and Superheated Ice: a ^1H NMR Microimaging Study *J. Phys. Chem. A* 103, 4969-4972
- Moudrakovski, I., Luzi, M., Kumar, R., Lu, H., Ripmeester, J. 2008. Experimental Solid State NMR of Gas Hydrates: Problems and Solutions. 6th International Conference on Gas Hydrate, Vancouver, BC Canada; 6-10 July 2008.
- Murphy, P. J., Roberts, S. 1995. Laser Raman spectroscopy of differential partitioning in mixed-gas clathrates in $\text{H}_2\text{O}-\text{CO}_2-\text{N}_2-\text{CH}_4$ fluid inclusions: Implications for microthermometry *Geochim. Cosmochim. Acta.* 59, 4809-4824
- Okuchi, T., Moudrakovski, I. L., Ripmeester, J. A. 2007. Efficient storage of hydrogen fuel into leaky cages of clathrate hydrate. *Appl. Phys. Lett.* 91, 171903(1) – 171903 (3)
- Ratcliffe, C. I., Ripmeester, J. A. 1986. ^1H and ^{13}C NMR studies on carbon dioxide hydrate, *J. Phys. Chem.* 90, 1259-1263
- Ripmeester, J. A., Ratcliffe, C. I. 1998. The diverse nature of dodecahedral cages in clathrate hydrates as revealed by ^{129}Xe and ^{13}C NMR spectroscopy: CO_2 as a small-cage guest, *Energy & Fuels*, 12, 197-200
- Senadheera, L., Conradi, M. S. 2007. Rotation and Diffusion of H_2 in Hydrogen-Ice Clathrate by ^1H NMR *J. Phys. Chem. B*, 111, 12097-12102
- Strobel, T. A. 2008. ON SOME CLATHRATES OF HYDROGEN, PhD Thesis, Colorado school of mines, Golden, Colorado, USA.
- Strobel, T. A., Taylor, C. J., Hester, K. C., Dec, S. F., Koh, C. A., Miller, K. T., Sloan, E. D. 2006. Molecular Hydrogen Storage in Binary THF- H_2 Clathrate Hydrates. *J. Phys. Chem. B*, 110, 17121-17125
- Struzhkin, V. V., Militzer, B., Mao, W. L., Mao, H-K, Hemley, R. J. 2007. Hydrogen Storage in Molecular Clathrates *Chem. Rev.* 107, 4133-4151

- Sugahara, T., Murayama, S., Hashimoto, S., Ohgaki, K. 2005. Phase equilibria for $\text{H}_2 + \text{CO}_2 + \text{H}_2\text{O}$ system containing gas hydrates. *Fluid Phase Equilibria*, 233, 190-193
- Sugahara, T., Mori, H., Sakamoto, J., Hashimoto, S., Ogata, K., Ohgaki, K. 2008. Cage Occupancy of Hydrogen in Carbon Dioxide, Ethane, Cyclopropane, and Propane Hydrates, *The open Thermodynamics Journal*, 2, 1-6
- Susilo, R., Moudrakovski, I. L., Ripmeester, J. A., Englezos, P. 2006. Hydrate kinetics study in the presence of nonaqueous liquid by nuclear magnetic resonance spectroscopy and imaging. *Journal of Physical Chemistry B*. 110, 25803-25809
- Susilo, R., Ripmeester, J. A., Englezos, P. 2007. Methane conversion rate into structure H hydrate crystals from ice. *AIChE*. 53, 2451-2460
- Takeya, S., Ripmeester, J. A. 2008. Dissociation Behavior of Clathrate Hydrates to Ice and Dependence on Guest Molecules *Angew. Chem.* 120, 1296-1299
- Uchida, T., Ikeda, I.Y., Takeya, S., Kamata, Y., Ohmura, R., Nagao, J., Zatsepina, O.Y., Buffett, B.A., 2005. Kinetics and Stability of $\text{CH}_4\text{-CO}_2$ Mixed Gas Hydrates during Formation and Long-Term Storage. *ChemPhysChem: a European journal of chemical physics and physical chemistry*, 6, 646-654
- Udachin, K. A., Ratcliffe, C. I., Ripmeester, J. A. 2001. Structure, Composition, and Thermal Expansion of CO_2 Hydrate from Single Crystal X-ray Diffraction measurements *J. Phys. Chem. B*, 105, 4200-4204
- Ulivi, L., Celli, M., Giannasi, A., Ramirez-Cuesta, A. J., Bull, D. J., Zoppi, M. 2007. Quantum rattling of molecular hydrogen in clathrate hydrate nanocavities. *Phys. Rev. B*, 76, 161401
- Wang, X., Schultz, A. J., Halpern, Y. 2002. Kinetics of methane hydrate formation from polycrystalline deuterated ice. *J. Phys. Chem. A*. 106, 7304-7309

6. APPLICATION OF THE ATR-IR SPECTROSCOPIC TECHNIQUE TO THE CHARACTERIZATION OF HYDRATES FORMED BY CO₂, CO₂/H₂ AND CO₂/H₂/C₃H₈⁵

6.1. INTRODUCTION

CO₂ hydrate forms a type-I cubic structure (Pm3n). Its unit cell contains 46 water molecules in a framework of two dodecahedral (5¹²) and six tetrakaidecahedral cages (5¹²6²) (Davidson, 1973). If all of the cages are singly occupied, the hydrate composition is CO₂·5.75H₂O. A number of spectroscopic and diffraction studies have addressed the composition of the hydrate and it is agreed that CO₂ molecules occupy almost all of the large cages in structure I as well as a fraction of the small cages, thus giving a hydration number between 5.75 and 7.66 (Ratcliffe and Ripmeester, 1986; Ripmeester and Ratcliffe, 1998; Fleyfel and Devlin, 1991; Udachin et al., 2001). Spectroscopic measurements useful for distinguishing cage populations should preferably show resolved peaks for guests in the large and small guests of the hydrate lattice. Unfortunately, Raman spectroscopic measurements are not able to distinguish the large and small cage populations in CO₂ hydrate (Sum et al., 1997; Udachin et al., 2001) although recent single-crystal measurements with polarized radiation have shown some promise (Ikeda et al., 1998). In ¹³C NMR spectra, the spectral pattern for pure CO₂ hydrate in sI has overlapping signals from the large and small cages, with each site giving

⁵ “A version of this chapter has been published. Kumar, R., Lang, S., Englezos, P., Ripmeester, J.A. (2009) Application of the ATR-IR spectroscopic technique to the characterization of hydrates of carbon dioxide. *J. Phys. Chem. A*. 113, 6308-6313.”

a powder pattern that is partially averaged by the dynamics of the guest molecules, which are in turn influenced by the cage symmetry (Ripmeester and Ratcliffe, 1998). Cage populations can be distinguished, but it is not a trivial matter.

Infrared spectroscopy (IR) detects the vibrations characteristic of chemical bonds or functional groups in a molecule. When infrared light interacts with matter, molecular vibrations that give changes in the molecular dipole moment tend to absorb infrared radiation in a specific frequency range depending on specific bond lengths and angles and can be more or less independent of the structure of the rest of the molecule. Bertie and Devlin (1983) prepared ethylene oxide hydrate using a cryogenic thin-film vapor-deposition technique and established this approach as a viable option for the study of clathrate hydrates by obtaining transmission FTIR spectra. Later Fleyfel and Devlin (1991) used the same method to prepare CO₂ hydrate and identified two separate peaks for CO₂ in large and small cages in sI and sII hydrates. They concluded that infrared patterns for guest molecules are usually significantly different from those observed for the same molecule in other phases. Besides this, it was also suggested that lower temperatures often cause a pronounced shifting, narrowing, and peak intensity enhancement by limiting intra-cage rotational motion. However, they reported that it was difficult to grow thin films of the simple clathrate hydrates of small *nondipolar* polyatomic molecules such as carbon dioxide, and it was only possible to form mixed hydrates having a small amount of a polar help gas such as ethylene oxide.

Because of its ability to probe chemical bonds, infrared spectroscopy is a technique of choice for analyzing surface complexes. However, water strongly absorbs IR, and methods based on internal reflection spectroscopy have been developed to

analyze wet samples. Attenuated Total Reflection Infrared (ATR-IR) Spectroscopy is used for analysis of the surface of materials (Mirabella, 1993). For either the bulk material or for a film, special sample preparation is not required for ATR analysis. FTIR analysis on SO₂ clathrate made from aqueous supercooled solutions in an ATR cell has been reported previously (Zhang and Ewing, 2004). In ATR-IR spectroscopy, the infrared radiation is passed through an infrared-transparent crystal with a high refractive index, allowing the radiation to reflect within the ATR element several times (Figure 6-1).

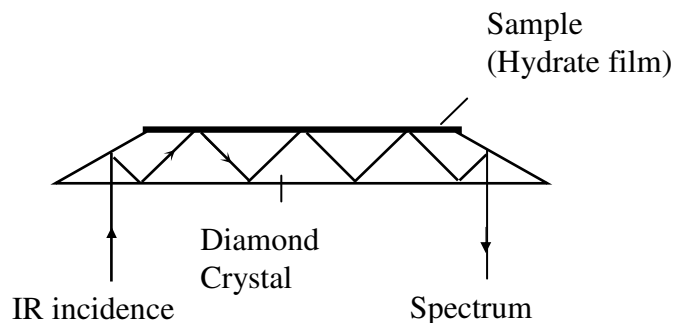


Figure 6-1: Schematic of ATR-IR Experiment

The surface to be sampled is either pressed into intimate optical contact with the top surface of the crystal, or, if possible, a thin film of sample is formed on the crystal for in-situ analysis (Hug, 1997). The IR radiation from the spectrometer enters the crystal at an angle chosen such that it will be totally reflected at the sample-crystal interface. There exists an evanescent wave, which means that even though the light is completely reflected, an oscillating electric field penetrates approximately one wavelength into the sample. Species with resonant transitions can absorb energy from this field. After a sufficient number of passes, the beam is directed out of the crystal and back into the normal beam path of the spectrometer.

In this paper, we use ATR FTIR spectroscopy to analyze a thin film of hydrate and show that this method, which is simple to use and obviates the need for helper molecules, corroborates results from the transmission approach used earlier by Fleyfel and Devlin (1991). In addition, the cage occupancies of CO₂, CO₂/H₂ and CO₂/H₂/C₃H₈ hydrates are determined based on peak area ratios of the CO₂ asymmetric stretch vibrations in the small and large cages obtained from the FTIR spectra and the hydrate phase composition obtained from gas chromatography.

6.2. MATERIALS AND EXPERIMENTAL SETUP

All of the gases used for the experiments were supplied by Praxair Canada inc., pure CO₂, pure H₂ and C₃H₈ (99.5% purity) were used to prepare the gas mixture. Apart from pure CO₂ hydrate, an 80/20 (mol%) CO₂/C₃H₈ mixture, a 40/60 (mol %) CO₂/H₂ mixture, and a 38.2/59.2/2.6 (mol %) CO₂/H₂/C₃H₈ were used for the hydrate formation. The supercritical fluid analyzer version of a Specac Golden GateTM Diamond ATR was slightly modified to synthesize and analyze the hydrates sample *in-situ*. The stainless steel sample chamber of this ATR cell is capable of withstanding pressures up to 40 MPa and when coupled with a temperature controller it can be operated over a range of temperatures. The system as purchased was designed to work from ambient to temperatures as high as 300°C. This setup was modified to run at sub-zero temperatures by making a provision to cool the cell by circulating nitrogen gas chilled by passing it through liquid nitrogen. The temperature controller maintained the desired operating temperature by heating the diamond top plate.

The stainless steel sample cell has a volume of 28μL; even less than 28μL of water is sufficient to form a thin layer of a hydrate film on the diamond surface. Hydrate

was allowed to form by pressurizing the cell with the appropriate gas for several hours at -20°C (*in-situ*). This hydrate was then decomposed by raising the temperature of the cell to room temperature and allowing the hydrate to form again by lowering the temperature slowly ($0.4^{\circ}\text{C}/\text{min}$) and waiting for two hours at -20°C . After two hours, the temperature is further reduced to -50°C , and the FTIR spectrum is obtained in the region of the CO_2 asymmetric stretch vibrations in the hydrate phase. Similarly, spectra for CO_2 in the gas phase and CO_2 dissolved in water were obtained at suitable temperatures and pressures. A Digilab Excalibur Series FTIR working at a nominal resolution of 1 cm^{-1} was used for this study, 50 scans were required to obtain good signal-to-noise ratios. A volume of two mL of water with CO_2/H_2 and $\text{CO}_2/\text{H}_2/\text{C}_3\text{H}_8$ gas mixtures was used to synthesize gas hydrate separately under similar conditions to the ATR experiment, in a 10 mL reactor and the hydrate phase composition was analyzed by gas chromatography, using an SRI 8610 C gas chromatograph (GC).

6.3. RESULTS AND DISCUSSION

As discussed in Chapter 5 the determination of the cage occupancies for the mixed hydrates of CO_2/H_2 and $\text{CO}_2/\text{H}_2/\text{C}_3\text{H}_8$ represents a considerable challenge. For determining CO_2 cage occupancies in the hydrate cage, ^{13}C NMR is not completely straightforward as one must use the anisotropic chemical shift patterns that give overlapping contributions for CO_2 in small and large cages (Ratcliffe and Ripmeester, 1986). Figure 6-2 shows ^{13}C MAS NMR spectra of CO_2 in the hydrate phase for CO_2/H_2 and $\text{CO}_2/\text{H}_2/\text{C}_3\text{H}_8$ hydrate. Only one signal (isotropic shift $\sim 125\text{ ppm}$) can be resolved in the spectrum for both CO_2/H_2 and $\text{CO}_2/\text{H}_2/\text{C}_3\text{H}_8$ hydrates.

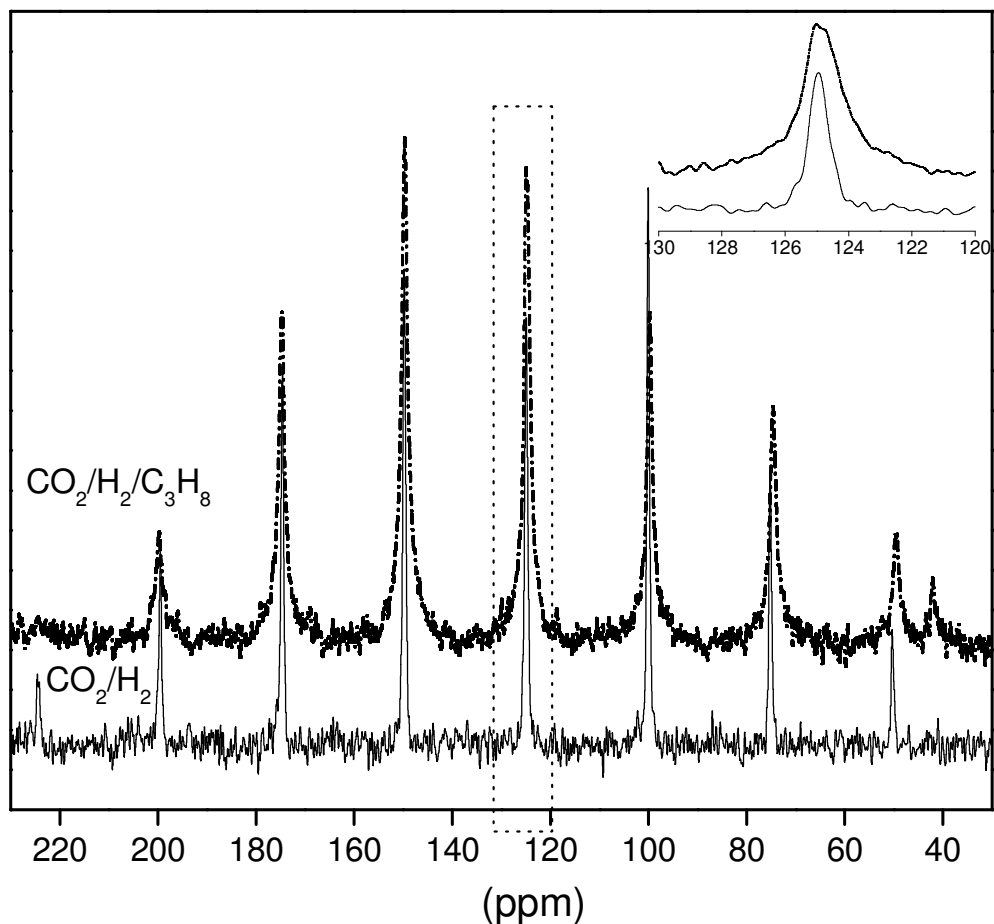


Figure 6-2: ^{13}C NMR spectra for CO_2/H_2 (sI) and $\text{CO}_2/\text{H}_2/\text{C}_3\text{H}_8$ (sII) hydrate obtained at atmospheric pressure and 173 K, spinning speed of 2500 Hz. Inset shows the close-up view of the peak at 125 ppm.

The observed spinning sideband pattern is characteristic of chemical shift anisotropy (CSA), as one may expect for pure CO_2 hydrate in sI (Ratcliffe and Ripmeester, 1986), where the spectrum reflects partial averaging of the CSA tensor for CO_2 due to dynamic processes in the anisotropic environment of the sI large cage in CO_2/H_2 hydrate, and from large as well as small cages in $\text{CO}_2/\text{H}_2/\text{C}_3\text{H}_8$ (sII) hydrate. It is important to note that the CO_2 resonances in sI and sII hydrates are at the same isotropic chemical shift (within experimental resolution). However, the peak width for CO_2 in sII

hydrate is greater than that of CO₂ in sI hydrate (insert in Figure 6-2). Depending upon the CO₂ and C₃H₈ concentration in the hydrate phase the peak width at half height varies.

As reported earlier in Chapter 5, for CO₂/H₂ hydrate, CO₂ only occupies the large cages of the resultant structure I hydrate and the small cages are occupied either by H₂ or remain nearly empty with a very small amount of CO₂ (<2%) in the small cages. However, for CO₂/H₂/C₃H₈ hydrate, CO₂ occupies the large cages as well as a significant portion of the small cages and it is possible that the presence of CO₂ in small as well as large cages in sII hydrate results in two resonances which however could not be resolved. A similar situation was observed for structure H hydrate of methane (Susilo et al., 2007).

In Chapter 5 Raman spectra for CO₂/H₂ and CO₂/H₂/C₃H₈ hydrate were obtained to determine the change in the vibrational frequency of the molecules when incorporated into the hydrate lattice. Figure 6-3 shows the two peaks which correspond to the Fermi diad of CO₂ in the hydrate cages, one at 1278 cm⁻¹ and the other 1382 cm⁻¹. We do not observe a splitting of the CO₂ bands for CO₂ in small and large cages. Also the peak positions for CO₂ in sI and in sII hydrate are almost the same, within the resolution of our Raman setup (± 1 cm⁻¹). However, again we see that the half-width of the CO₂ peak (~ 9.0 cm⁻¹) in the hydrate phase for sII hydrate is larger than that of CO₂ (~ 5.5 cm⁻¹) in the sI hydrate. As reported earlier in Chapter 5 for the sI hydrate of CO₂/H₂, CO₂ occupies all of the large cages and a very small number of CO₂ molecules (<2%) actually reside in the small cavities. However, in the sII hydrate formed by the CO₂/H₂/C₃H₈ mixture, CO₂ occupies the large as well as a significant portion of the small cages.

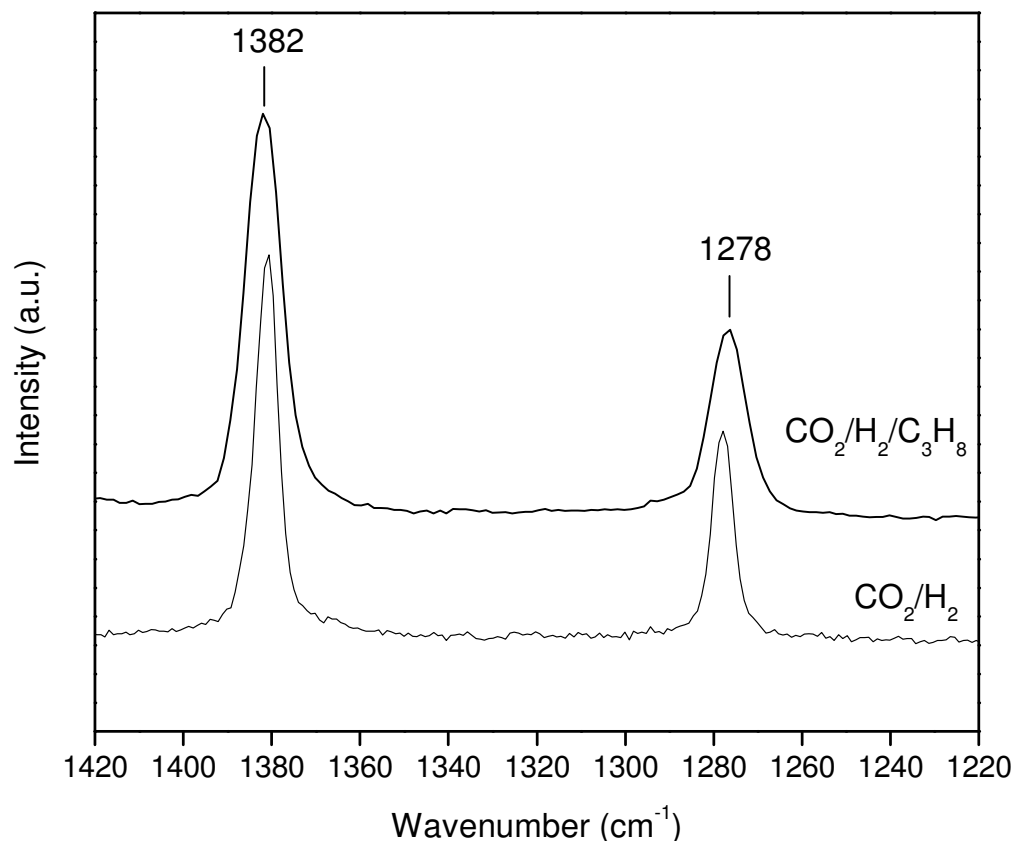


Figure 6-3: Raman Spectra showing Fermi diad of CO₂ in the hydrate phase for CO₂/H₂ (sI) and CO₂/H₂/C₃H₈ (sII) hydrate.

It is possible that CO₂ generates two peaks, one for small cages and one for large cages, however, the peak positions are too close to each other and hence result in a broader single peak (Sasaki et al., 2003; Susilo et al., 2007). This result is similar to what we observed for ¹³C NMR, i.e. the CO₂ peak in sII is broader as compared to that in sI hydrate. It is also possible that the influence of local environments (e.g. the presence of C₃H₈) for CO₂ in sII results in a broader peak. It is clear from Figures 6-2 and 6-3 that if CO₂ occupies a significant portion of the small and large cages in the hydrate phase it results in a broad signal for Raman spectroscopy as well for ¹³C NMR spectra as compared to a hydrate where CO₂ occupies only the large cages. Moreover, the

difference in peak position is not enough for a reliable deconvolution of the CO₂ peak in such a hydrate and hence quantitative determination of CO₂ hydrate is not straightforward.

To evaluate the feasibility of the technique, and the sensitivity of the CO₂ spectrum to the environment, the infrared spectrum of CO₂ in the anti-symmetric stretching region was recorded for CO₂ in different phases. The results shown in Figure 6-4 demonstrate that the vibrational frequency for CO₂ in different phases varies considerably, as does the bandwidth. Solid CO₂ was not observed, as the temperature of analysis did not go below -50°C . Since the spectra for CO₂ in the different phases give unique peak positions, infrared spectra recorded by the ATR technique can be used to good advantage for CO₂ hydrate characterization work.

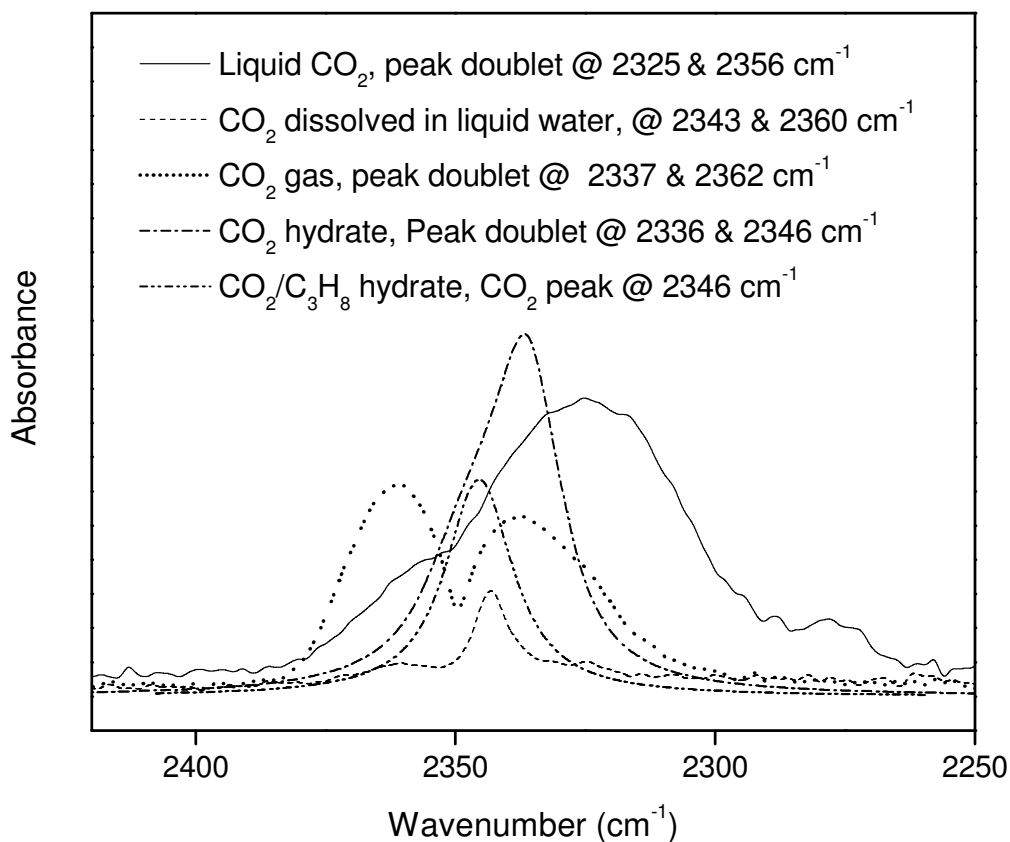


Figure 6-4: ATR-IR spectra of CO₂ showing unique peaks under different conditions

Figure 6-5a shows the FT-IR spectra of CO₂ hydrate synthesized in the ATR cell at 3.2 MPa. The spectra shown were obtained at -50°C . Vibrational frequencies for CO₂ in small and large cages are better resolved at lower temperatures and, in this case, a temperature significantly lower than the hydrate formation temperature was required in order to obtain well-resolved peaks. A higher operating temperature (compared to an analysis temperature of -50°C) for hydrate formation was chosen for a better growth rate of the CO₂ hydrate (Kawamura et al., 2002).

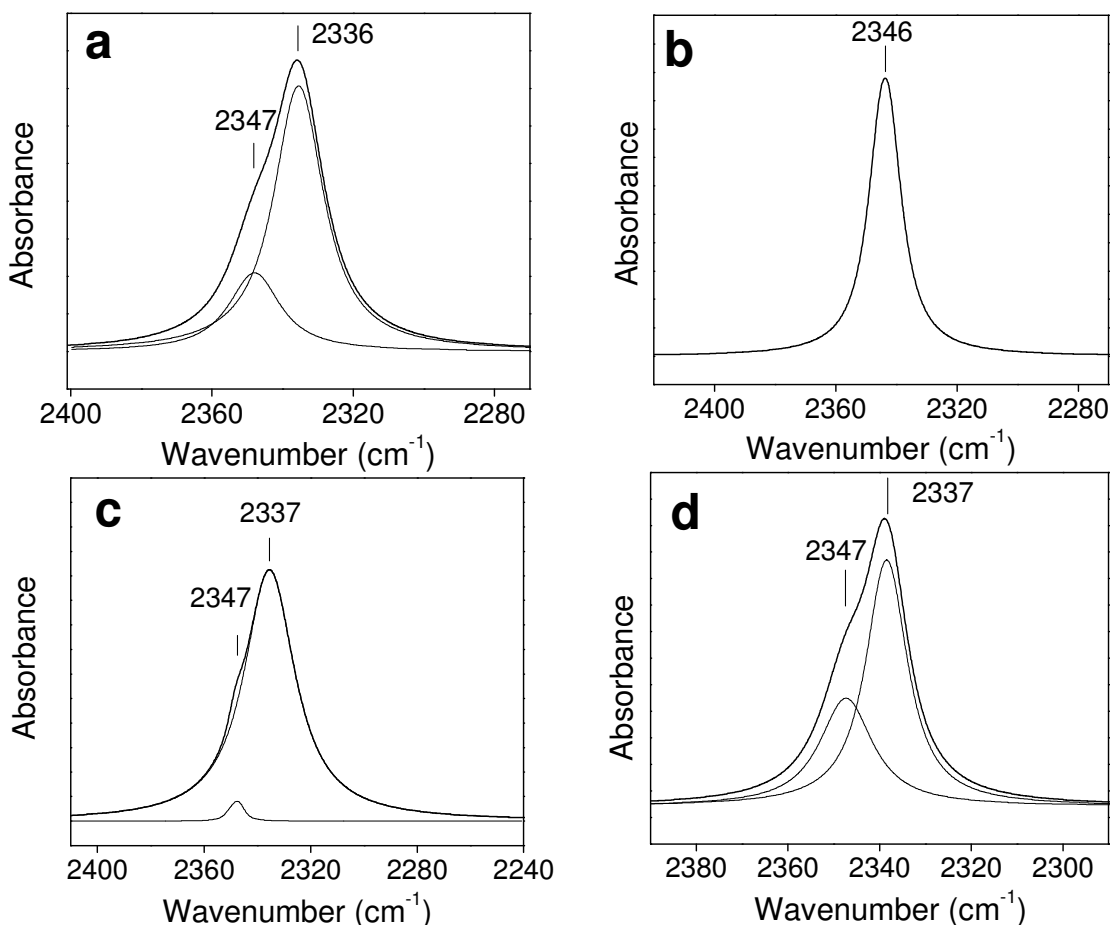


Figure 6-5: ATR-IR spectra showing CO₂ in the small and large cages of hydrate phase for (a) simple CO₂ hydrate (b) CO₂/C₃H₈ (sII), (c) CO₂/H₂ (sI) and (d) CO₂/H₂/C₃H₈ (sII) hydrate.

As shown in Figure 6-5a the infrared-active asymmetric stretch mode of CO₂ in pure CO₂ hydrate shows structure, and can be deconvolved into two peaks, one smaller peak at 2347 cm⁻¹ and a more intense peak at 2336 cm⁻¹. Based on the work of Fleyfel and Devlin we can assign the smaller peak to CO₂ in the small cages (5¹² cages) and the larger peak at 2336 cm⁻¹ can be assigned to CO₂ in the large (5¹²6²) cages of the resultant structure I hydrate.

Propane (C₃H₈) forms a stable simple structure II hydrate with all of the large cages occupied by C₃H₈, and all of the small cages empty (Handa, 1986). CO₂ has the ability to occupy small as well as large cages of structure I hydrate (Udachin et al., 2001). If a suitable CO₂/C₃H₈ gas mixture (where the C₃H₈ concentration is substantially above stoichiometric requirements for completely filled large cages) is allowed to form hydrate such that all of the large cages are occupied by C₃H₈, CO₂ can only occupy the small cages of the resultant structure II hydrate. This would allow us to check the peak position for CO₂ in small cages of structure II hydrate in the absence of any contribution from CO₂ in the large cages and would help to provide a cross reference to verify the peak positions for pure CO₂ hydrate. A gas mixture of 20% C₃H₈ with the remainder being CO₂ was used to form hydrate at 2 MPa (by following the same procedure as mentioned in the experimental section) such that all of the large 5¹²6⁴ cages were occupied by C₃H₈ molecules (this was verified by Figure 6-5b, where signals from CO₂ in the large cages are absent) and the smaller 5¹² cages of the resultant structure II hydrate by CO₂. As seen in Figure 6-5b, the FT-IR spectra of the hydrate product results in a single peak at 2346 cm⁻¹, which is the contribution of CO₂ present in the small cages of structure II CO₂/C₃H₈

hydrate. This also supports the assignment of the infrared peak at about 2347 cm^{-1} (± 1) at -50°C in Figure 6-5a to CO_2 occupying the small cages of sI.

FT-IR spectra of CO_2/H_2 (40/60 mol%) hydrate synthesized at 8 MPa were obtained at -50°C . The spectrum between $2250\text{--}2400\text{ cm}^{-1}$ is shown in Figure 6-5c. The peak with a shoulder shows the presence of CO_2 in the hydrate cages. The spectral traces are deconvolved, which results in two peaks, one larger peak at 2337 cm^{-1} indicating the presence of CO_2 in the large cages and a minor peak at 2347 cm^{-1} showing the presence of CO_2 in the small cages. Figure 6-5d shows the spectra recorded for $\text{CO}_2/\text{H}_2/\text{C}_3\text{H}_8$ (38.2/59.2/2.6 mol%) hydrate synthesized at 3.8 MPa. The spectra show two overlapped peaks, with an appearance similar to that for pure CO_2 hydrate. The spectrum in Figure 6-5d can be deconvolved into two peaks one smaller peak at 2347 cm^{-1} due to CO_2 in the small 5^{12} cages and a more intense peak at 2337 cm^{-1} resulting from the presence of CO_2 in the large $5^{12}6^4$ cages.

Looking at the integrated peak intensities for CO_2 for the binary and ternary hydrates, Figure 6-5c and Figure 6-5d respectively, the peak at 2347 cm^{-1} is much more prominent in Figure 6-5d than the peak at 2347 cm^{-1} in Figure 6-5c. It has been shown in the previous chapter that the ternary hydrate is a structure II hydrate, which has a 2:1 ratio of small to large cages. Thus there are more CO_2 molecules present in small cages as compared to the binary structure I hydrate, which has a 1:3 ratio of small to large cages. With just 2.6% C_3H_8 in the ternary gas mixture, which is not sufficient for 100 percent occupancy of all the large cages, the large cages in the resulting structure II hydrate are shared by C_3H_8 and CO_2 , and a significant amount of CO_2 occupies the smaller 5^{12} cages, along with H_2 . In the binary hydrate, CO_2 occupies all of the large cages and a very small

amount of CO₂ actually goes into the small cages, leaving almost all of the small cages for H₂.

6.3.1. Quantitative determination of the cage occupancy from FTIR results

It is generally accepted that Raman spectroscopy cannot be used to determine the relative concentration of different guests in the hydrates quantitatively without proper cross-calibration with another quantitative technique (Wilson et al., 2002). However, we have shown previously that with weakly polar guest molecules in hydrate cages a quantitative estimate of cage occupancies can be made with reasonable accuracy (Kumar et al., 2008). In the previous work Raman spectra were used along with the knowledge of the resultant structure from independent PXRD patterns and the hydrate phase composition from gas chromatography measurements. With the knowledge of the CO₂ ratio in the small and large cages (from FT-IR spectra) along with the knowledge of hydrate structure (from PXRD pattern) and hydrate composition (from gas chromatography) we will calculate the cage occupancies and compare these with cage occupancies obtained from NMR spectroscopy obtained in Chapter 5.

The powder XRD pattern obtained from the synthetic hydrate reveals that pure CO₂ hydrate synthesized at 3 MPa and binary CO₂/H₂ hydrate synthesized at 8 MPa is structure I hydrate, whereas ternary CO₂/H₂/C₃H₈ hydrate synthesized at 3.8 MPa forms structure II (details given in Chapter 5). Hydrates were synthesized in a 10 mL stainless steel reactor with 2 mL of water under similar conditions as for the *in-situ* ATR-IR setup for calculating the hydrate phase composition. All of the hydrate synthesized was decomposed and the gas evolved was analyzed by gas chromatography to obtain the water-free basis hydrate composition. The binary CO₂/H₂ hydrate is 93.0 ± 0.2 % CO₂

and $7.0 \pm 0.2\%$ H_2 , whereas ternary $CO_2/H_2/C_3H_8$ hydrate is $76.2 \pm 0.2\%$ CO_2 , $4.0 \pm 0.2\%$ H_2 , $19.8 \pm 0.2\%$ C_3H_8 . Several measurements of CO_2 hydrate were performed by FT-IR to obtain spectra with a good signal to noise ratio for obtaining occupancies and hydration numbers. All of the spectra collected were identical to that shown in Figure 6-5a. As CO_2 partitions between the small and large cavities of structure I, we were able to deconvolve the band shown in Figure 6-5a into two separate peaks. We take the area of the bands to represent the number of CO_2 molecules in each cavity. The ratio of the integrated intensities of the bands is 3.7, which we take to be the ratio of CO_2 molecules in large to small cages. After accounting for the fact that there are three times as many large as small cavities in sI, we obtained the cage occupancies.

In order to determine the absolute occupancy of CO_2 in the small and large cavities, we used the statistical thermodynamic expression Equation 6.1, for the chemical potential of water molecules in sI hydrate. The value for $\Delta\mu_w^o$ used in the calculation is 1297 J/mol (Sloan, 1998).

$$\begin{aligned}
 -\Delta\mu_w^o &= \frac{R \cdot T}{n_{H_2O}} \sum_i v_i \ln(1 - \theta_i) \\
 -\Delta\mu_w^o &= \frac{R \cdot T}{23} \left[3 \ln(1 - \theta_{l(CO_2)}) + 1 \ln(1 - \theta_{s(CO_2)}) \right]
 \end{aligned} \tag{6.1}$$

Equation 6.1 implies that unoccupied large cages represent a large energy penalty, and effectively constrains θ_l to be almost unity ($\theta_l=1$). Based on this and the information in the FTIR spectra ($\theta_l/\theta_s=3.7$) the occupancy of the small cavities by CO_2 (θ_s) was determined. The results are shown in Table 6-1. The column labeled n in Table 6-1 is the hydration number, calculated from Equation 6.2, where the sum is carried over all cages

and all guests. Equation 6.2 also demonstrates the hydration number calculation for CO₂ hydrate. θ_{L-C} and θ_{S-C} are the occupancies of CO₂ in the large and small cages of resultant sI hydrate which is multiplied by numbers of each type of cages in a unit cell, n_{H_2O} is the number of water molecule per unit cell. The value 6.04 for the hydration number obtained in the current study is in acceptable agreement with those obtained for CO₂ hydrate from single crystal x-ray structures, which range from 6.2 to 6.7 depending on hydrate synthesis pressure and temperature (Udachin et al., 2001).

$$n = \frac{n_{H_2O}}{\sum \theta_{cage, guest}} = \frac{n_{H_2O}}{2\theta_{S-C} + 6\theta_{L-C}} = \frac{46}{2 \times 0.81 + 6 \times 1} = 6.04 \quad (6.2)$$

Table 6-1: Estimate of cage occupancy values obtained by combination of results from Infrared spectroscopy and Gas chromatography.

Description	Hydrate structure	H ₂	CO ₂		C ₃ H ₈	Hydration number
		θ_S	θ_S	θ_L	θ_L	n
CO ₂	sI	-	0.81	1.0	-	6.04
CO ₂ /H ₂	sI	0.23	0.06	1.0	-	6.92
CO ₂ /H ₂ /C ₃ H ₈	sII	0.029	0.20	0.79	0.21	11.7

Figure 6-5c shows the FT-IR spectra of binary CO₂/H₂ hydrate. In order to obtain the hydrate guest composition, integration of the areas of the CO₂ bands was done and the occupancies were calculated. From the fitted curves of Figure 6-5c, the ratio of the integrated intensities of CO₂ in large cages to CO₂ in the small cages is 49.8 (Equation 6.3). Equation 6.4 expresses the H₂/CO₂ ratio obtained from gas chromatography, along with the assumptions that the large cages must be 100% occupied by CO₂ for stability of

the hydrate, and that at these modest pressures multiple cage occupancy of H₂ can be neglected a (small amount of multiple cage occupancy of H₂ in the small cages as found in previous chapter does not affect the calculation significantly).

$$\frac{3\theta_{L-C}}{\theta_{S-C}} = 49.8 \Rightarrow \frac{3 \times 1}{\theta_{S-C}} = 49.8 \Rightarrow \theta_{S-C} = 0.06 \quad (6.3)$$

$$\frac{\theta_{S-H}}{3\theta_{L-C} + \theta_{S-C} + \theta_{S-H}} = 0.07 \Rightarrow \frac{\theta_{S-H}}{3 \times 1 + 0.06 + \theta_{S-H}} = 0.07 \quad (6.4)$$

θ_{L-C} and θ_{S-C} are the occupancies of CO₂ in the large and small cages of resultant sI hydrate and θ_{S-H} is the occupancy of the small cages by hydrogen. H₂ is not expected to occupy the large cages of this hydrate especially considering the fact that the hydrate was synthesized at 8 MPa. Also, calculations done in previous Chapters based on proton NMR suggest that this assumption holds. As shown in Equation 6.3 the small cage occupancy of CO₂ in CO₂/H₂ hydrate is 6% ($\theta_{S-C} = 0.06$). Equation 6.4 then implies 23% of the small cages are occupied by hydrogen ($\theta_{S-H} = 0.23$). The cage occupancy values along with hydration number are also reported in Table 6-1.

Figure 6-5d shows the FT-IR spectra of the ternary CO₂/H₂/C₃H₈ hydrate, and again the deconvolved areas of the peaks are used to determine that the occupancy ratio of CO₂ in large to small cages is 1.8. In structure II hydrate there are twice as many small cages as large ones, hence the intensity ratio takes the form given in Equation 6.5. It can safely be assumed that C₃H₈ only occupies the large cages and H₂ only the small cages. Also for a stable hydrate, the combined occupancy of C₃H₈ and CO₂ in the large cages should be close to unity. These assumptions and the gas chromatography results are expressed in Equations 6.6 and 6.7. Solving Equation 6.5, 6.6 and 6.7 gives the cage

occupancy values and hydration number, shown in Table 6-1. Note that Equation 6.2 for hydration number calculation must be modified (to equation 6.8), as there are 16 small cages, 8 large cages and 136 water molecules in the unit cell of sII hydrate.

$$\frac{\theta_{L-C}}{2\theta_{S-C}} = 1.8 \quad (6.5)$$

$$\theta_{L-C} + \theta_{L-P} = 1 \quad (6.6)$$

$$\frac{\theta_{L-P}}{\theta_{L-P} + \theta_{L-C} + 2\theta_{S-C} + 2\theta_{S-H}} = 0.198 \quad (6.7a)$$

$$\frac{\theta_{L-C} + 2\theta_{S-C}}{\theta_{L-P} + \theta_{L-C} + 2\theta_{S-C} + 2\theta_{S-H}} = 0.762 \quad (6.7b)$$

$$\frac{2\theta_{S-H}}{\theta_{L-P} + \theta_{L-C} + 2\theta_{S-C} + 2\theta_{S-H}} = 0.04 \quad (6.7c)$$

$$n = \frac{n_{H_2O}}{\sum \theta_{cage, guest}} = \frac{136}{16\theta_{S-C} + 8\theta_{L-C} + 16\theta_{S-H} + 8\theta_{L-P}} \quad (6.8)$$

The cage occupancy values obtained here are in good agreement with the quantitative results, which we obtained by ^{13}C NMR studies performed on binary CO_2/H_2 hydrate. However, the cage occupancy values obtained for ternary $\text{CO}_2/\text{H}_2/\text{C}_3\text{H}_8$ hydrate analyzed by FT-IR shows significant variation from the ^{13}C NMR results. It must be noted that in this study hydrates were synthesized in two hours instead of approximately two days for the experiment reported in the previous chapter. This change in cage occupancy values can be attributed to dependency of cage dynamics on kinetics of hydrate formation. Also, leaking of H_2 molecules out of the hydrate crystal during NMR measurement was observed. Finally, the technique presented in this work can be used to evaluate

occupancies in CO₂ containing systems that demonstrate structure changes as a function of pressure (Servio et al., 1999a,b; Uchida et al., 2006)

6.4. CONCLUSIONS

This work demonstrates that ATR-Infrared spectroscopy is a straightforward and valuable analytical tool for investigating the properties of the CO₂ clathrate hydrate phases under in-situ temperature and pressure conditions. Unlike the Raman-active vibrational modes, the infrared active stretching mode of CO₂ in the hydrate cages provides a signature for CO₂ in small and large cages. Although the data must be supplemented with information from other techniques, ATR-IR is useful for the qualitative and quantitative determination of occupancy ratios and hydration numbers for simple and mixed hydrates of CO₂. For pure CO₂ hydrate, the large cages are almost fully occupied and the small cages were about 81% occupied. Similarly, it was observed that in the presence of excess C₃H₈, CO₂ only occupies the small cages of the resultant sII hydrate. The experimental values obtained for the hydrate cage occupancies are in good agreement with the values reported in the literature. Hydration numbers were indirectly determined from the occupancy of CO₂ in the small and large cavities of sI and sII hydrate. In addition, we have shown that ATR-Infrared spectroscopy combined with hydrate phase composition results obtained by gas chromatography can give similar information to that obtained from the more difficult NMR spectroscopic analysis, often considered the technique of choice in the quantitative analysis of hydrates.

6.5. REFERENCES

- Bertie, J. E., Devlin, J. P. 1983. Infrared spectroscopic proof of the formation of the structure I hydrate of oxirane from annealed low-temperature condensate *J. Chem. Phys.*, 78, 6340-6341
- Davidson, D. W., 1973. Gas Hydrates. In *Water: A Comprehensive Treatise*, Plenum Press; New York.
- Fleyfel F, Devlin JP. 1991. Carbon Dioxide Clathrate Hydrate Epitaxial Growth: Spectroscopic Evidence for Formation of the Simple Type-II CO₂ Hydrate. *J. Phys. Chem.* 95, 3811-3815
- Handa Y.P., 1986. Compositions, enthalpies of dissociation, and heat capacities in the range 85 to 270 K for clathrate hydrates of methane, ethane, and propane, and enthalpy of dissociation of isobutane hydrate, as determined by a heat-flow calorimeter *J. Chem. Thermodynamics* 18, 915-921
- Hug S. J. 1997. In Situ Fourier Transform Infrared Measurements of Sulfate Adsorption on Hematite in Aqueous Solutions *Journal of colloid and interface science* 188, 415-422
- Ikeda, T.; Mae, S.; Uchida, T. 1998. Effect of guest–host interaction on Raman spectrum of a CO₂ clathrate hydrate single crystal *J. Chem. Phys.*, 108, 1352-1359
- Kawamura, T., Komaib, T., Yamamoto, Y., Nagashima, K., Ohgaki, K., Higuchi, K. 2002 Growth kinetics of CO₂ hydrate just below melting point of ice *Journal of Crystal Growth* 234, 220–226
- Kumar, R., Linga, P., Moudrakovski, I., Ripmeester, J. A., Englezos, P. 2008 Structure and kinetics of gas hydrates from methane/ethane/propane mixtures relevant to the design of natural gas hydrate storage and transport facilities *AIChE*, 54, 2132-2144
- Mirabella, F. M. 1993, in F. M. Mirabella (Ed.), *Internal Reflexion Spectroscopy*, Dekker, New York.
- Ratcliffe, C. I., Ripmeester, J. A. 1986. ¹H and ¹³C NMR studies on carbon dioxide hydrate *J. Phys. Chem.* 90, 1259-1263
- Ripmeester, J. A., Ratcliffe, C. I. 1998. The diverse nature of dodecahedral cages in clathrate hydrates as revealed by ¹²⁹Xe and ¹³C NMR spectroscopy: CO₂ as a small-cage guest, *Energy & Fuels*, 12, 197-200

- Sasaki, S., Hori, S., Kume, T., Shimizu, H., 2003. Microscopic observation and in situ Raman scattering studies on high-pressure phase transformations of a synthetic nitrogen hydrate *J. Chem. Phys.*, 118, 7892-7897
- Servio, P., Lagers, F., Peters, C., Englezos, P. 1999a Gas hydrate phase equilibrium in the system methane-carbon dioxide-neohexane and water *Fluid Phase Equilibria*, 158-160, 795-800
- Servio, P., Mazza, J., Englezos, P. 1999b Incipient Equilibrium Gas Hydrate Formation Conditions for the $\text{CO}_2\text{-CH}_4\text{-Neohexane-NaCl-H}_2\text{O}$ and the $\text{CH}_4\text{-Polypropylene Glycol-NaCl-H}_2\text{O}$ *Int. J. of The Soc. of Mat. Eng. for Resources*, 7, 24-28.
- Sloan, E. D., Jr., 1998. *Clathrate Hydrates of Natural Gases*, Second Edition, Revised and Expanded, Marcel Dekker, NY.
- Sum, A. K., Burruss, R. C., Sloan, E. D. Jr. 1997. Measurement of Clathrate Hydrates via Raman Spectroscopy *J. Phys. Chem. B*, 101, 7371-7377
- Susilo, R., Ripmeester, J. A., Englezos, P. 2007. Characterization of gas hydrates with PXRD, DSC, NMR, and Raman spectroscopy *Chemical Engineering Science* 62, 3930-3939
- Uchida, T., Ohmura, R., Ikeda, I. Y., Nagao, J., Takeya, S., Hori, A., 2006 Phase Equilibrium Measurements and Crystallographic Analyses on Structure-H Type Gas Hydrate Formed from the $\text{CH}_4\text{-CO}_2\text{-Neohexane-Water}$ System. *J Phys Chem B*, 110, 4583.
- Udachin, K. A., Ratcliffe, C. I., Ripmeester, J. A. 2001. Structure, Composition, and Thermal Expansion of CO_2 Hydrate from Single Crystal X-ray Diffraction measurements *J. Phys. Chem. B*, 105, 4200-4204
- Wilson, L. D., Tulk, C. A., Ripmeester, J. A. 2002. Instrumental Techniques for the Investigation of Methane Hydrates: Cross-calibrating NMR and Raman Spectroscopic Data. Paper presented at: 4th Int. Conf. Gas Hydrates, Yokohama Japan, May 19-23, 2002.
- Zhang, Z., Ewing, G. E. 2004. Infrared Studies of the SO_2 Clathrate Hydrate *J. Phys. Chem. A* 108, 1681-1686

7. SUMMARY OF CONCLUSIONS, CONTRIBUTION TO KNOWLEDGE, AND RECOMMENDATIONS FOR FUTURE WORK

This thesis explores the feasibility of using gas hydrates for CO₂ and H₂ separation from a fuel gas mixture coming out of an IGCC power station. The thesis provided relevant thermodynamic (Kumar et al., 2006), kinetic (Linga et al., 2007a, Kumar et al., 2009b), structural and cage occupancy data (Kumar et al., 2009a, 2009c) which enabled the creation of a conceptual flowsheet (Linga et al., 2007b). The efficiency of the proposed separation process was also assessed (Kumar et al., 2009b)

7.1. SUMMARY OF CONCLUSIONS

Incipient equilibrium hydrate formation conditions from CO₂/H₂ and CO₂/H₂/C₃H₈ mixtures were determined. The results demonstrated that the hydrate formation pressures are substantially lower than those of pure H₂. Moreover, the addition of a 3.2 mol% C₃H₈ into a CO₂/H₂ mixture reduces the hydrate formation pressure by 50% (Kumar et al., 2006). An analysis of the equilibrium data, based on the Clausius–Clapeyron equation indicated that the CO₂/H₂ mixtures formed structure I hydrate, whereas the ternary mixture formed structure II (Kumar et al., 2006).

Gas hydrate formation experiments were carried out in a laboratory-size crystallizer operating in a semi-batch mode with a fixed amount of water (140 mL) and a continuous supply of gas to maintain constant pressure. Hydrates from CO₂/H₂ gas mixtures were formed at 273.7 K. Gas uptake measurements coupled with compositional analysis of the gas phase revealed that CO₂ is preferentially incorporated into the hydrate

phase offering the possibility for separation from the binary CO₂/H₂ mixtures (Linga et al., 2007a). A conceptual process flowsheet for a hybrid hydrate-membrane process was developed. Two metrics, CO₂ recovery and separation factor were proposed in order to assess the separation efficiency of the CO₂ capture process. CO₂ recovery of ~ 40% and separation factor ~100 were obtained in one stage operating at ~8 MPa and 273.7K. However, the high operating pressure in the first stage of hydrate formation makes this process uneconomical (Linga et al., 2007b).

To reduce the hydrate formation pressure in the first stage of hydrate based separation process, the fuel gas mixture of CO₂ & H₂ is mixed with propane to achieve 2.5 mol % propane content which is then subjected to gas hydrate crystallization at 273.7K and 3.8 MPa. The resulting CO₂-rich stream is directed to a second hydrate crystallization stage operating at 3.5 MPa and the same temperature whereas the CO₂-lean stream is fed to a membrane separation unit. The two stages together with the membrane enable the recovery of nearly pure CO₂ and H₂ streams (Kumar et al., 2009b). It is surprising to find that the addition of small amount of propane does not compromise the separation efficiency, thus a CO₂ recovery of around 40% in one stage was maintained (Kumar et al., 2009b). The only drawback is the fact that the rate of hydrate growth was slower compared to CO₂/H₂ hydrate formation.

The high separation efficiency in presence of propane was understood by structural and compositional characterization studies which were carried out by Powder X-ray Diffraction (PXRD), ¹H Magic Angle Spinning (MAS) NMR (with rotor synchronized spin echoes), ¹³C MAS NMR, mass spectrometry, Fourier Transform Infrared Spectroscopy (FT-IR) (with attenuated total reflection) and Raman spectroscopy.

The information obtained enabled the determination of hydrate composition and cage occupancy. Gas hydrates made from (40/60 mol %) CO₂/H₂ mixtures form structure I hydrate at 8 MPa (Kumar et al., 2009c). It was found that the large cages are almost fully occupied by carbon dioxide and the small cages were mainly occupied by hydrogen. Furthermore, NMR results suggest that 9.3% of the small cages are occupied by bimolecular H₂ and 6.2% by single H₂ molecules. It was observed that CO₂/H₂ hydrate shows self-preservation upon hydrate decomposition. By introducing 2.6% C₃H₈ in CO₂/H₂ gas mixtures the ternary mixture forms pure structure II hydrate at 3.8 MPa, however this hydrate does not show self-preservation like the CO₂/H₂ hydrate (Kumar et al., 2009c). In the resultant hydrate CO₂ (57 %) and C₃H₈ (43 %) share the large cages and a significant portion of small cages is occupied by CO₂ (34 %). Based on the results obtained from this work it can be said that hydrogen occupies the small cages of structure I as well as structure II hydrate.

In our molecular level work done on binary and ternary hydrate, FTIR was found to be a very important tool to suggest the occupancy ratio of CO₂ in the small and large cages which otherwise is a very difficult to obtain parameter by Raman / NMR spectroscopy. Unlike Raman spectroscopy the active vibrational modes in infrared spectroscopy provide a signature for CO₂ in small and large cages. Although the data must be supplemented with information from other techniques, ATR-IR is useful for the qualitative and quantitative determination of occupancy ratios and hydration numbers for simple and binary hydrates of CO₂. For pure CO₂ hydrate, the large cages are almost fully occupied and the small cages were about 81% occupied (Kumar et al., 2009a). Similarly it was observed that in the presence of excess C₃H₈, CO₂ only occupies small cages of the

resultant sII hydrate (at modest pressure of 2 MPa). The experimental values obtained for the hydrate cage occupancies of CO₂ are in good agreement with the values reported in the literature. Hydration numbers of CO₂/H₂ and CO₂/H₂/C₃H₈ were indirectly determined from the occupancy of CO₂ in the small and large cavities of sI and sII hydrate.

7.2. CONTRIBUTION TO THE KNOWLEDGE

This thesis makes the following contributions:

1. It validated through relevant equilibrium, kinetic and compositional measurements the applicability of hydrate formation to separate CO₂ from fuel gas mixtures.
2. It proposed a two stage hydrate-membrane hybrid process for pre-combustion capture of carbon dioxide resulting in ~99.0% CO₂ and ~99.0% H₂ streams.
3. It proposed two metrics, the CO₂ recovery and the separation factor to assess the efficiency of the separation process.
4. It identified propane the addition of which (2.5 mol %) could significantly reduce the operating pressure without compromising the separation efficiency. This reduction significantly lowers the compression costs in the first stage of the process.
5. It was found that the reduction in operating pressure in presence of propane comes from the fact that, CO₂/H₂/C₃H₈ mixture forms a different crystal structure (sII). The separation efficiency of the process is not compromised because in this new structure CO₂ occupies the small as well as the large cages whereas CO₂/H₂ forms structure I and CO₂ only occupies the large cages.

6. It was shown that in hydrates from CO_2/H_2 and $\text{CO}_2/\text{H}_2/\text{C}_3\text{H}_8$ mixtures H_2 indeed occupies a significant portion of small cages in both the structures. This removed a controversy that existed in the literature.
7. The ortho and para content of H_2 in the hydrate cages were identified (through Raman spectroscopy) and it was shown that, upon storage in liquid nitrogen ortho H_2 converts to para hydrogen.
8. It was shown through NMR spectroscopy that, in CO_2/H_2 hydrate two H_2 molecules occupy a significant number of small cages whereas the other small cages are occupied by only one H_2 molecule.

7.3. RECOMMENDATIONS FOR FUTURE WORK

The following recommendations are proposed for future work.

1. Our experiments showed that the hydrate process could definitely be operated in a semi-batch manner on a lab scale. The next technological challenge would be to demonstrate the hydrate based separation process at a pilot plant scale in a continuous operating mode.
2. The current gas uptake measurement were based on a stirred tank reactor where the liquid water and gas were brought in contact by a stirrer; for a scaled up design circulating the liquid contents or spraying through nozzles can be considered in order to enhance the heat and mass transfer rate for a better and more efficient process. An alternative approach like using a packed bed column (packed with silica gel to increase the contact area between gas and water) instead of a stirred reactor would help in reducing the operational cost by eliminating mixing requirements. A fluidized bed column (with ice powder operating at sub

- zero temperature) could help in increasing the hydrate formation rate. These alternate contact modes can be used to study the kinetics of hydrate formation and evaluated for better process efficiency.
3. Such a pilot plant study would enable the cost analysis of the hydrate based separation process for the separation of CO₂ from fuel gas mixture which can then be compared with more mature processes like the selexol based physical separation processes or zeolite-based pressure swing adsorption.
 4. The separation efficiency of the fuel gas mixture could be increased if the small cage occupancy of CO₂ can be increased. Molecular level work performed for this thesis suggests that while ~100 % of the large cages were occupied by CO₂ small cage occupancy of pure CO₂ hydrate is close to 80%. However, for CO₂/H₂ or CO₂/H₂/C₃H₈ hydrate the small cage occupancy of CO₂ reduces to a maximum of 30%. It has been found that just by increasing the hydrate formation pressure, the small cage occupancy can be increased therefore a different additive like THF or cyclopropane can be tried which can stabilize the resultant hydrate at lower pressure thus allowing us to work at a higher driving force. Higher driving force will also result in better growth rate of the hydrate crystals which was one of the limitations observed in presence of propane (explained in Chapter 4).
 5. In-situ high-pressure X-ray diffraction studies can be done on CO₂/H₂/C₃H₈ hydrate to detect the structural transition conditions as reported in Chapter 5.
 6. From molecular level studies, it was found that CO₂ in small and large cages of sI and sII hydrate could be detected through FT-IR spectroscopy. However, similar

measurements would have to be made to see if CO₂ in two different cages of sH could be detected by FT-IR spectroscopy.

7.4. REFERENCES

- Kumar, R., Wu, H., Englezos, P., 2006. Incipient hydrate phase equilibrium for gas mixtures containing hydrogen, carbon dioxide and propane. *Fluid Phase Equilibria*, 244, 167–171
- Kumar, R., Lang, S., Englezos, P., Ripmeester, J.A. 2009a. Application of the ATR-IR spectroscopic technique to the characterization of hydrates of carbon dioxide. *J. Phys. Chem. A*. 113, 6308-6313.
- Kumar, R., Linga, P., Ripmeester, J. A., Englezos, P. 2009b. A two-stage clathrate hydrate/membrane process for pre-combustion capture of carbon dioxide and hydrogen. *J. Envir. Engrg.* 135, 411-417.
- Kumar, R., Moudrakovski, I., Ripmeester, J. A., Englezos, P. 2009c. Structure and composition of CO_2/H_2 and $\text{CO}_2/\text{H}_2/\text{C}_3\text{H}_8$ hydrate in relation to simultaneous CO_2 capture and H_2 production. *AIChE J.* 55, 1584-1594.
- Linga, P., Kumar, R., and Englezos, P., 2007a. Gas hydrate formation from hydrogen/carbon dioxide and nitrogen/carbon dioxide gas mixtures. *Chemical Engineering Science* 62(16), 4268-4276.
- Linga, P., Kumar, R., and Englezos, P., 2007b. The clathrate hydrate process for post and pre-combustion capture of carbon dioxide. *Journal of Hazardous Materials* 149(3), 625-629.

8. APPENDIX A

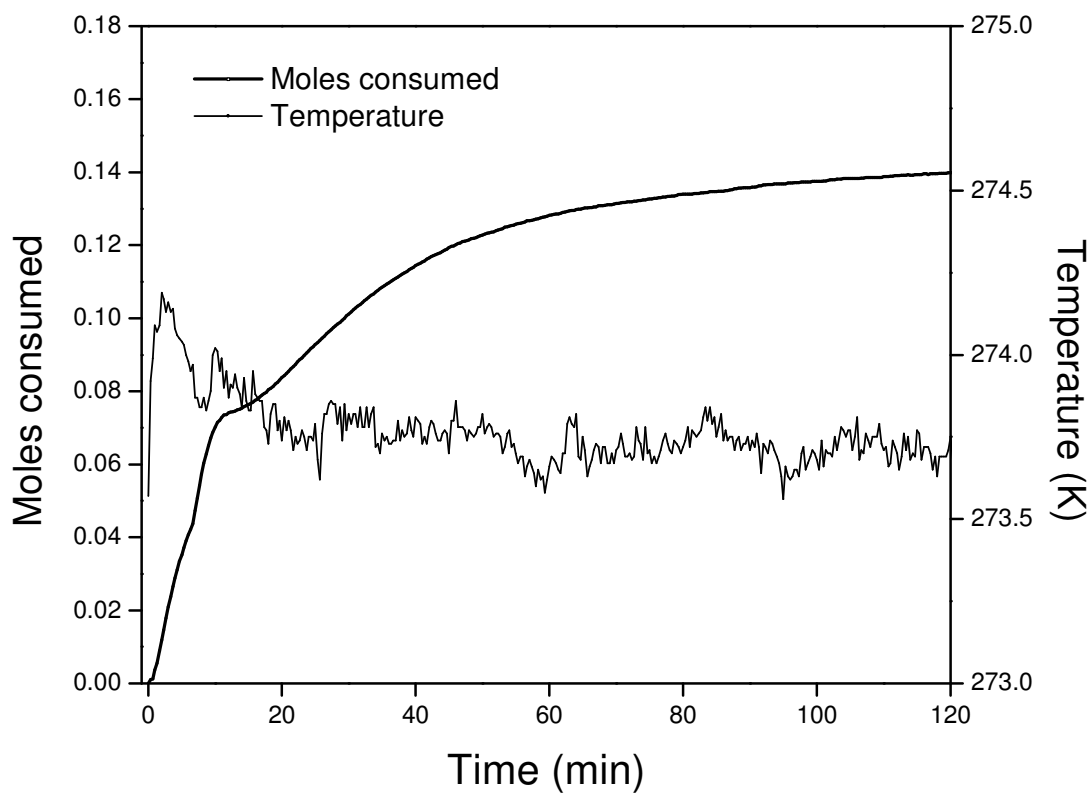


Figure A-1: Gas uptake measurement curve with temperature profile (Experiment 2, table 3-1)

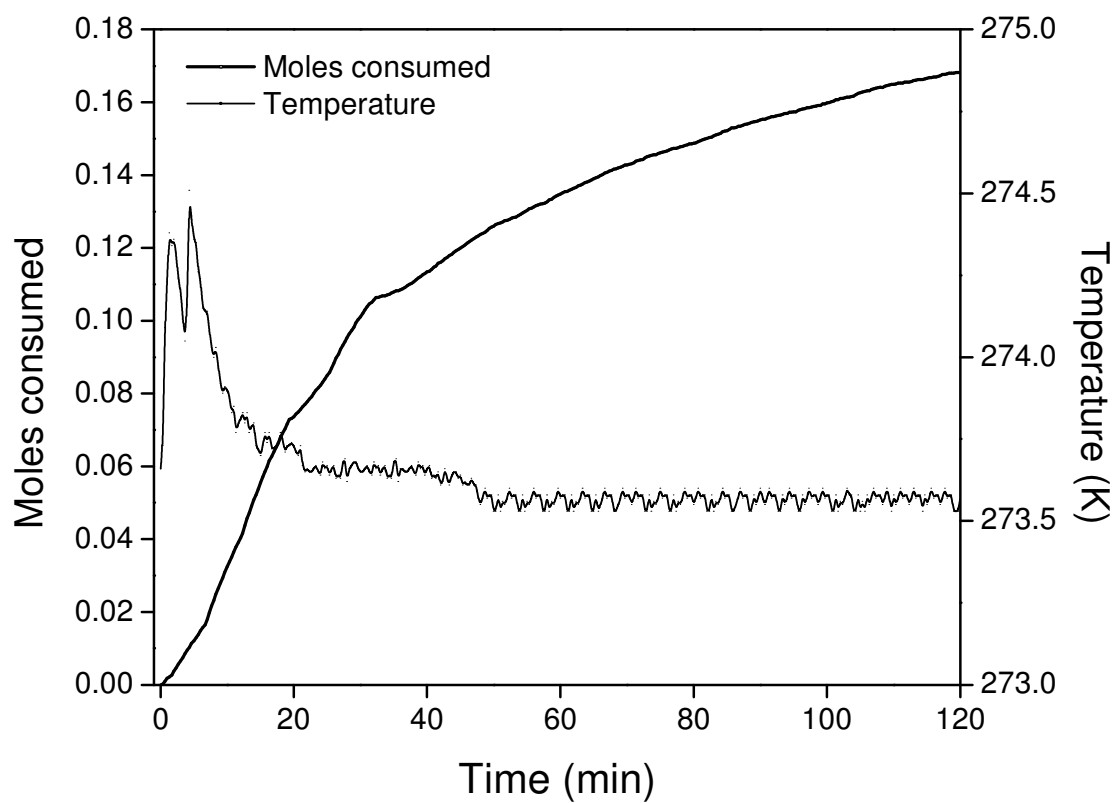


Figure A-2: Gas uptake measurement curve with temperature profile (Experiment 5, table 3-1)

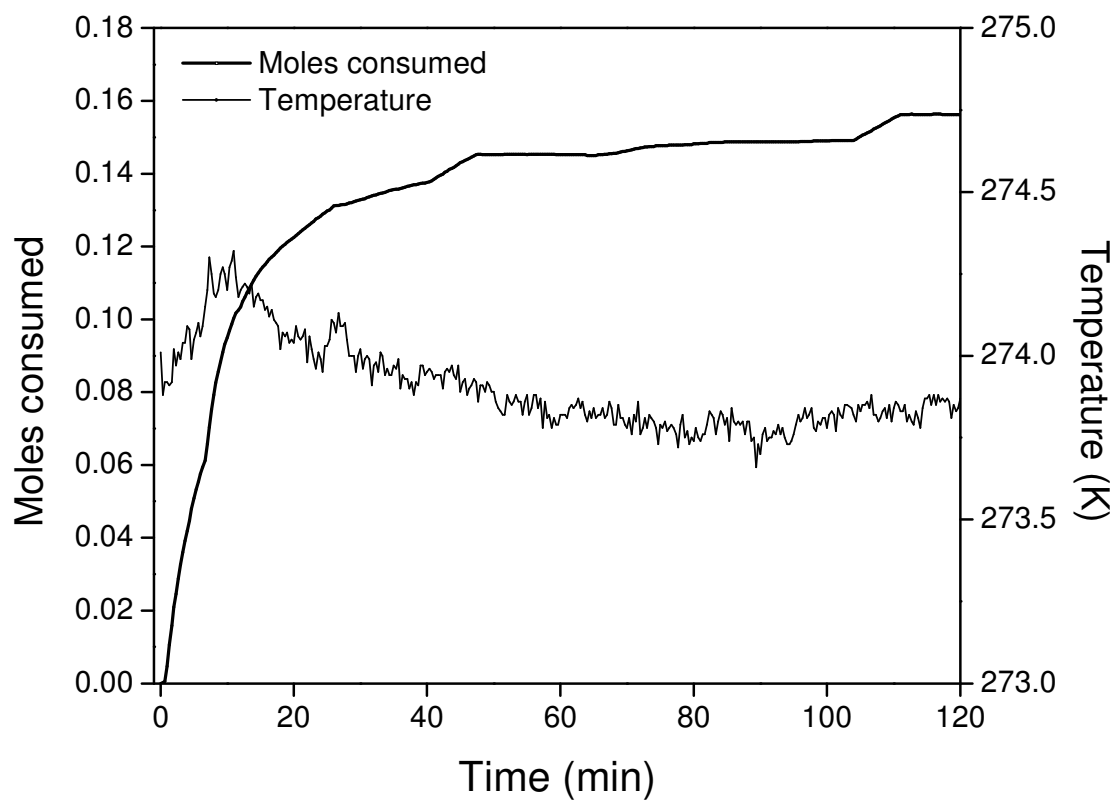


Figure A-3: Gas uptake measurement curve with temperature profile (Experiment 6, table 3-1)

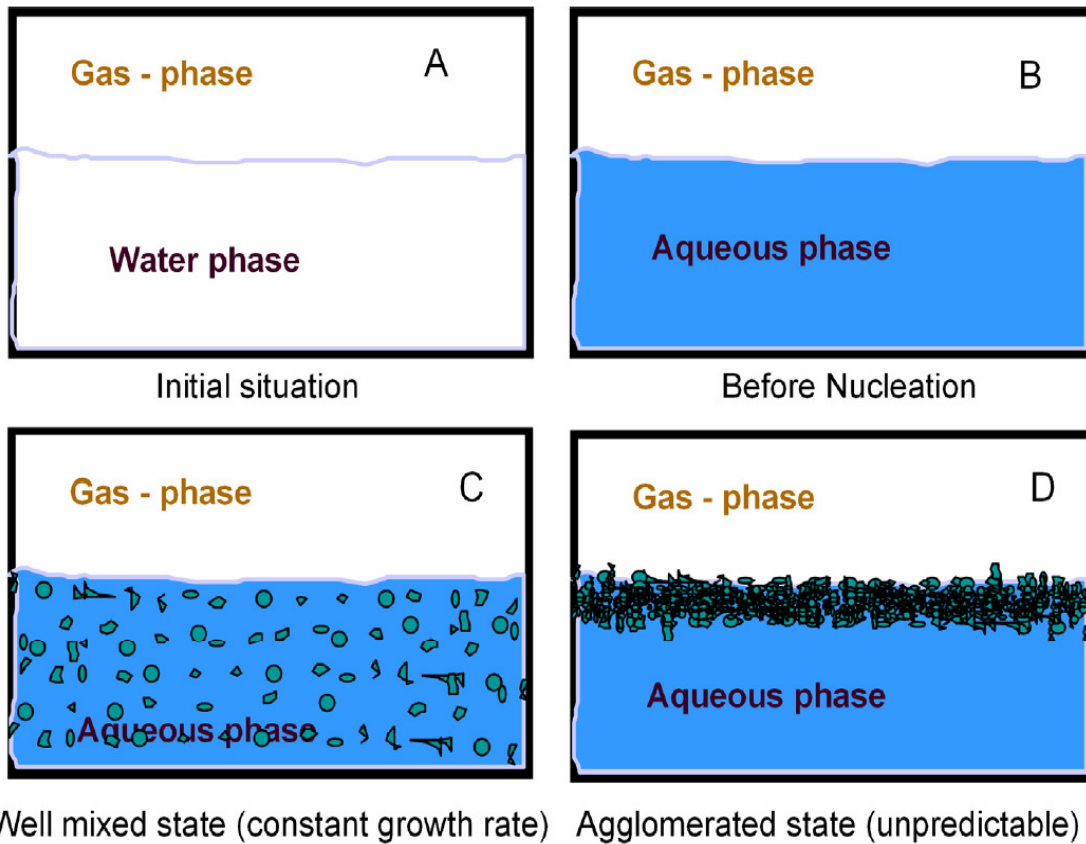


Figure A-4: Schematic of the mass transfer resistance encountered in the lab scale apparatus described in Chapter 3. (adapted from Linga, 2009^{*})

^{*} Linga, P. 2009. Separation of Carbon Dioxide from Flue Gas (Post-Combustion Capture) via Hydrate Crystallization, PhD Thesis, University of British Columbia, Vancouver BC Canada

9. APPENDIX B

GAS COMPRESSION CALCULATIONS FOR THE SEPARATION OF CO₂ FROM FUEL GAS MIXTURE FROM A POWER PLANT

The mass flow rates used for the calculations were obtained from the MIT report, “the future of coal” available at <http://web.mit.edu/coal/>. Details of the power plant emissions are shown in the figure below,

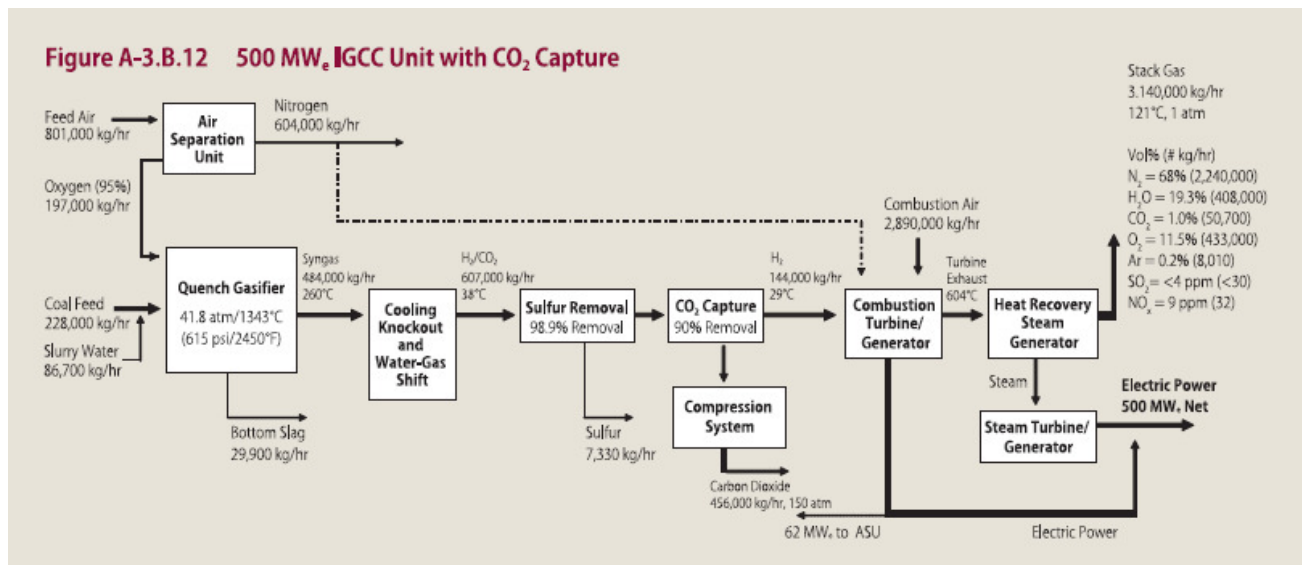


Figure B-1: A 500 MW_e IGCC unit with CO₂ capture (Source: MIT report on the Future of Coal)

Fuel gas mixture coming out of water-gas shift reactor is 607,000 kg/hr at 38°C. Neglecting presence of any impurity and assuming the molar ratio of this fuel gas mixture as 40:60 CO₂/H₂. The total fuel gas load for separation process is 31,915 kmol/hr, of which total amount of CO₂ is 12,766 kmol/hr and H₂ is 19,149 kmol/hr. It is assumed that the fuel gas mixture is obtained at 2.5 MPa (minimum pressure suggested in IPCC, 2005).

The operating pressure of the crystallizer is 3.8 MPa, $P_{out}/P_{in} = 3.8/2.5 = 1.52$, we need one compression stages, heuristic from Seider et al. (2004).

According to Biegler et al. (1997), the work required for compression is given by,

$$W = \mu \times N \times \left(\frac{\gamma}{\gamma - 1} \right) \times R \times T_0 \times \left[\left(\frac{P_N}{P_0} \right)^{\frac{\gamma - 1}{\gamma N}} - 1 \right] \quad (A1)$$

where,

μ = molar flow rate = 31,915 kmol/hr

$N = 1$ (Number of compression stages)

$P_N = 3.8$ MPa

$P_0 = 2.5$ MPa

$\gamma = C_p/C_v = 1.4$

$R = 8.314$ kJ/kmol K

$T_0 = 274.15$ K

The theoretical value of W was determined from equation A1 to be 8.98 MW. Assuming a compressor efficiency of 0.8 and motor efficiency of 0.9, the W_{real} was determined to be 12.48 MW.

REFERENCES

- Biegler, L. T., Grossmann, I. E., and Westerberg, A. W., 1997. Systematic Methods of Chemical Process Design, Prentice Hall PTR, New Jersey.
- IPCC. (2005). "Carbon dioxide capture and storage, IPCC Special report." Intergovernmental Panel on Climate Change.
- Seider, W. D., Seader, J. D., and Lewin, D. R., 2004. Product and Process Design Principles: Synthesis, Analysis, and Evaluation, Wiley.
- MIT. (2007). "The Future of Coal." Available from: <http://web.mit.edu/coal/>.

10. APPENDIX C

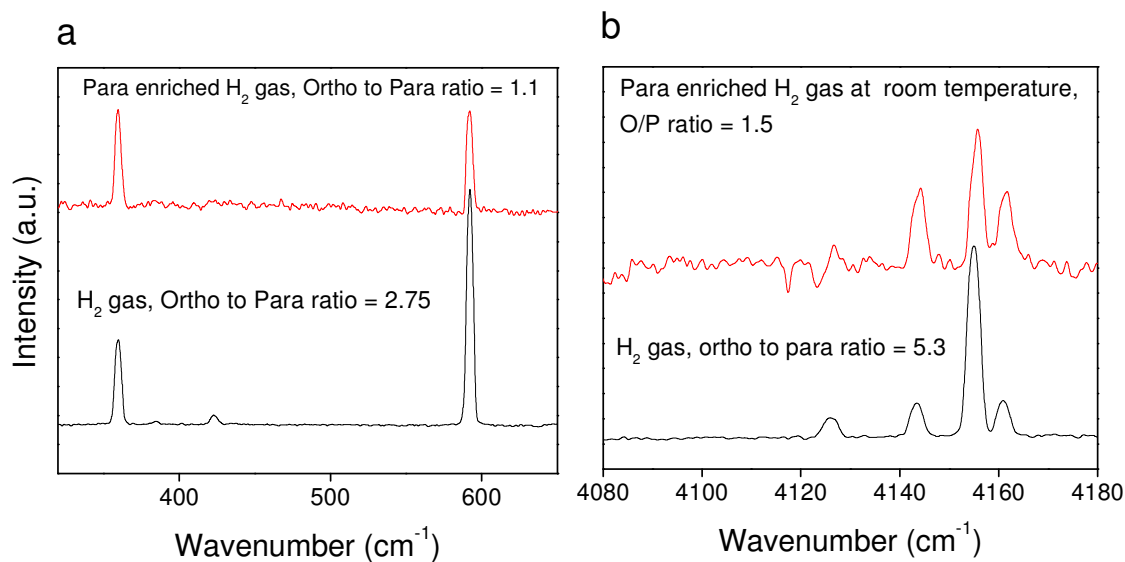


Figure C-1: Raman spectra of H₂ gas measured at room temperature and dry ice temperature showing H₂ rotational band (320 cm⁻¹ to 650 cm⁻¹) and vibrational band (4100 cm⁻¹ to 4200 cm⁻¹). Para enriched gas was obtained at liquid nitrogen temperature, however Raman measurement was done at dry ice temperature.

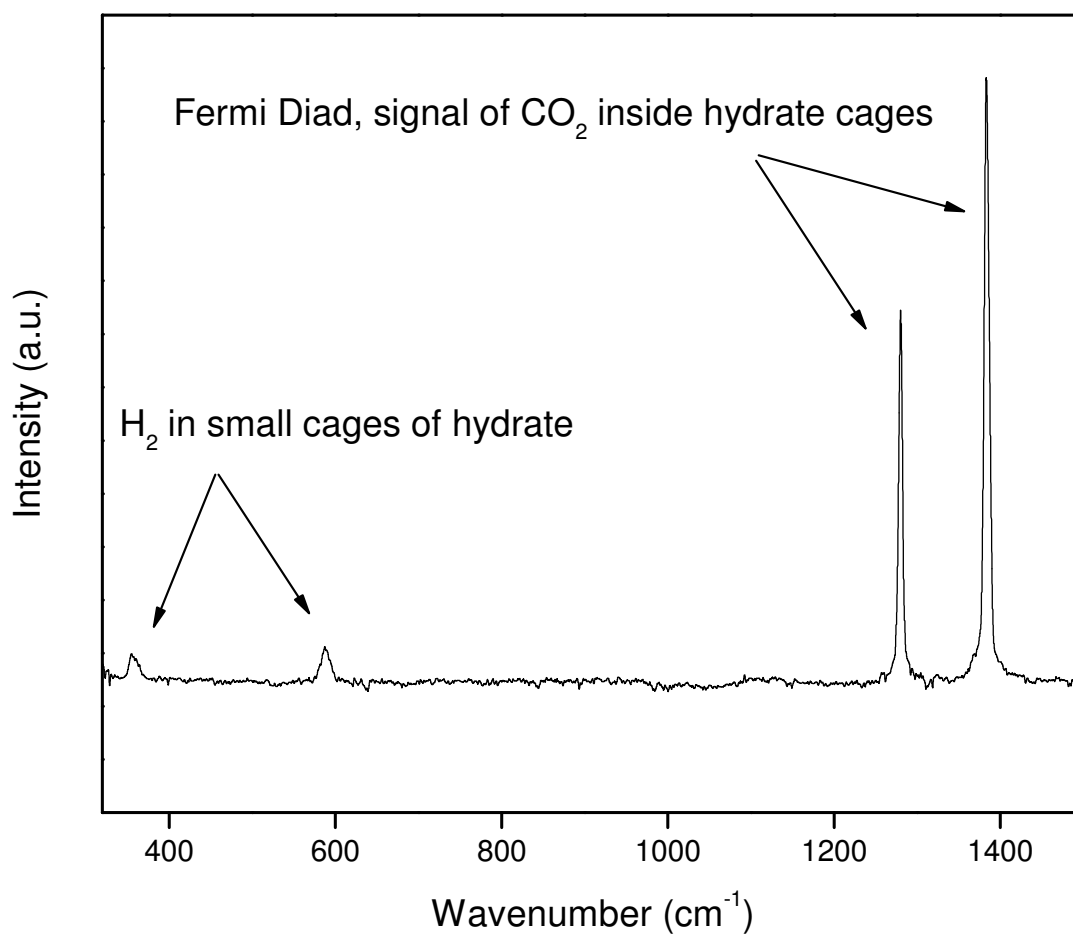


Figure C-2: Raman spectrum for the Fermi diad of CO₂ incorporated into hydrate phase from the CO₂/H₂ gas mixture. Note the two rotational modes for H₂ occupying the hydrate cages one each from ortho and para hydrogen.

ADDITIONAL INFORMATION ON FIGURE 5-7

The Raman spectra obtained in Figure 5-7 does not allow us to state whether the hydrates from the binary or ternary mixtures show multiple cage occupancies in the small cage. Generally, a peak doublet in spectra of the guests in hydrate phases arises from guest occupancy in small and large cages respectively, as in the case of methane hydrate (Kumar et al., 2008) and nitrogen hydrate (Ohno and Hondoh, 2006). However, for this binary hydrate all the large cages are occupied by CO₂ therefore it is not possible that one of the peaks in the doublet shown in Figure 5-7 is from H₂ in the small cages and the other from H₂ in the large cages. However, it is possible that one of the peaks in the doublet is due to partial occupancy of small cages occupied by bimolecular H₂. In order to investigate this more detailed study was carried out, with H₂/THF hydrate.

Figure C-3 shows the H₂/THF hydrate, where THF occupies all the large cages of resultant sII hydrate. The peak doublet obtained for H-H stretching mode can be deconvolved in two separate spectra one at 4120 cm⁻¹ and other at 4126 cm⁻¹. If one of the peaks is due to bimolecular H₂ in the hydrate phase the peak ratio should change with a set pattern upon changing the hydrate formation pressure. However as shown in Figure C-3 hydrates were synthesized at varying pressure ranging from 7MPa to 16 MPa, there was no significant change in the peak ratio at different pressure and always a peak ratio of ~1:1 was obtained within experimental variation. Similar trends can be seen for the rotational peaks where there is no visual change in the intensity of each peak. These results indicate that peak doublet obtained for H-H stretch mode from the H₂ gas inside small cages is not because of singly and doubly occupied small cages.

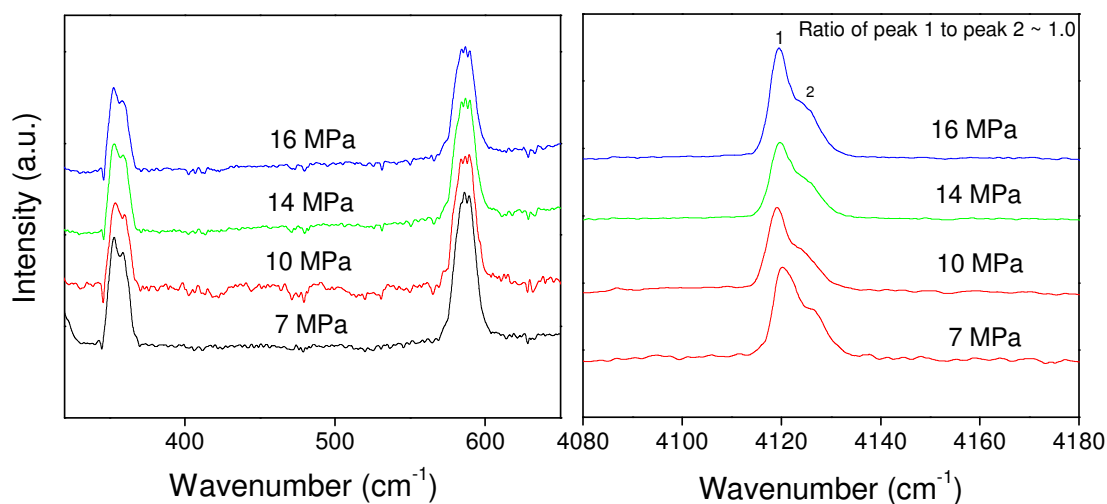


Figure C-3: Raman spectra of H_2 /THF/ H_2O hydrate phase measured at liquid nitrogen temperature and atmospheric pressure, showing H_2 rotational band and vibrational band inside the hydrate cages. Hydrate was synthesized at -13°C with 5.7% THF hydrate. No significant difference in the peak ratio (peak 1 : peak 2) is observed by changing the hydrate synthesis pressure.

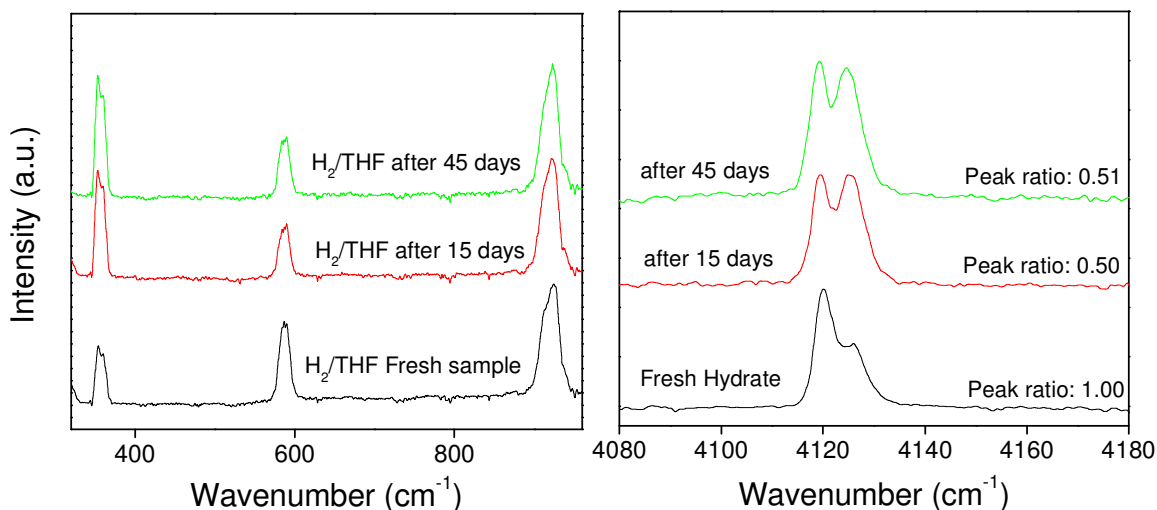


Figure C-4: Raman spectra of H_2 /THF/ H_2O hydrate phase measured at liquid nitrogen temperature and atmospheric pressure, showing H_2 rotational band and vibrational band inside the hydrate cages. Hydrate was synthesized at -13°C with 5.7% THF hydrate. H_2 Peak doublet in the vibrational mode as well rotational mode changes with time, even though no significant change in THF peak (950 cm^{-1}) is observed.

Figure C-4 shows the rotational and stretching mode of H_2 inside the hydrate cages when stored under liquid nitrogen. As evident from the spectra, the peak doublet

changes with time pointing towards either H₂ leaking from the hydrate cages and thus changing the peak ratio or hydrogen inside the hydrate cages gets converted from ortho hydrogen to para hydrogen thus resulting in a bigger para peak compared to ortho peak. The change in intensity of two rotational bands and area under each spectrum compared to THF peak at 950 cm⁻¹ suggests that, H₂/THF hydrate is quite stable at liquid nitrogen temperature. However, ortho H₂ converts to para H₂ upon storage in liquid nitrogen. The conversion of ortho to para is catalyzed by some O₂ impurity in the hydrate structure as well as some O₂ impurity in liquid nitrogen where hydrates are stored. Being paramagnetic molecule O₂ catalyses the conversion of ortho hydrogen to para hydrogen. To verify the ortho to para conversion inside the hydrate cages few extra experiments was done where H₂/THF hydrate were synthesized in presence of paramagnetic compounds. Two different paramagnetic gases were used in this study, for the first synthesis an O₂/H₂ gas mixture were used to form hydrate with fully occupied THF hydrate and for the second synthesis a mixture of H₂/CF₃NO (trifluoro-nitroso-methane)/C₃H₈ was used to form sII hydrate. O₂ as well as CF₃NO occupies the hydrate phase, O₂ shares the small cages of resultant sII hydrate with H₂, where as CF₃NO shares the large cages of resultant sII hydrate with C₃H₈. As shown in Figure C-5, H₂ in the hydrate cages in presence of paramagnetic molecules (O₂ and CF₃NO) shows a bigger para peak compared to H₂/THF hydrate. Similar trends are observed for rotational as well for stretching mode of H₂.

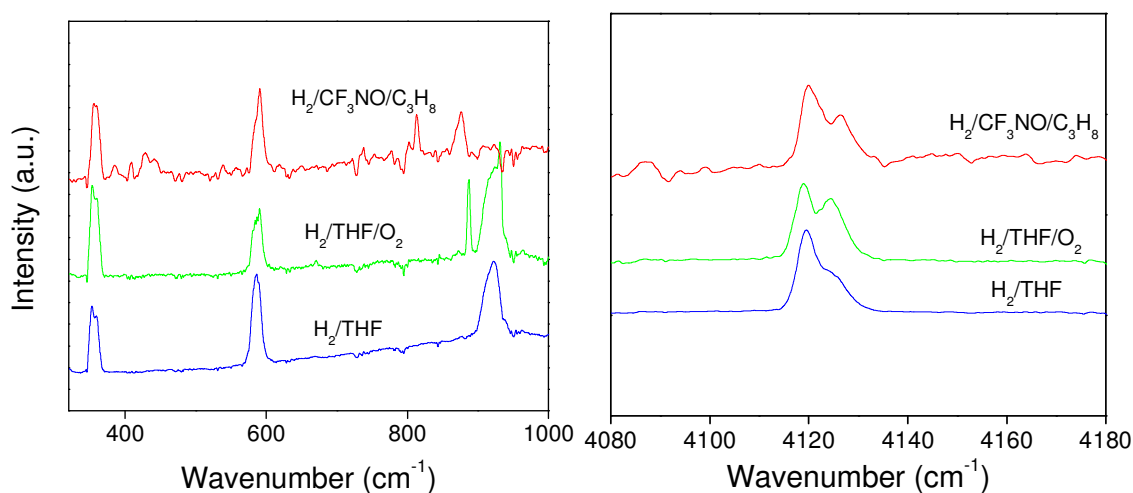


Figure C-5: Raman spectra for mixed hydrate of H_2 measured at liquid nitrogen temperature and atmospheric pressure, showing H_2 rotational band and vibrational band. Hydrate was synthesized at -13°C with paramagnetic compounds which occupy the hydrate cages. H_2 Peak doublet in the vibrational mode as well rotational mode shows different peak ratio in presence of paramagnetic compounds.

These results make it quite clear that the peak doublet in the stretching band actually results from H_2 in the small cages of hydrate. Also, Raman spectra was not able to detect any doubly occupied small cages or a possibility of H_2 going into large cages from hydrate synthesized at moderate pressure and recovered at liquid nitrogen temperature and atmospheric pressure.

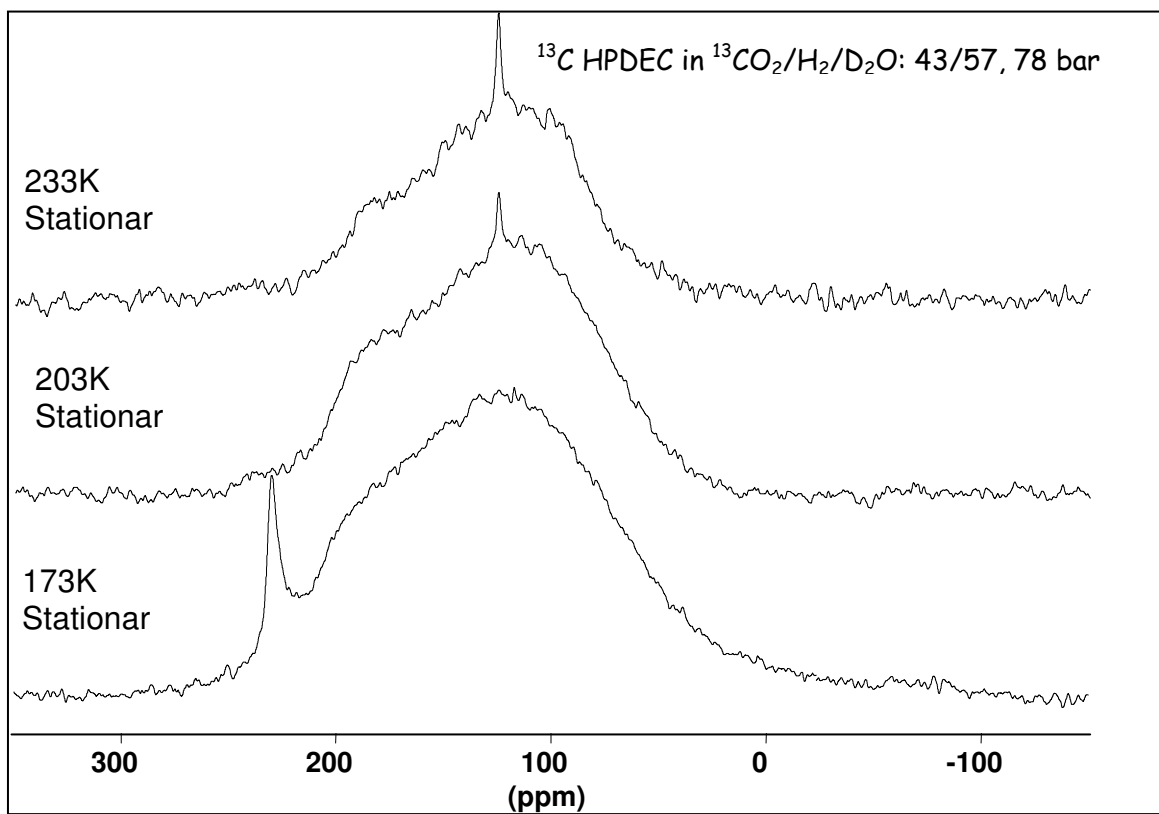


Figure C-6: ^{13}C NMR spectroscopy (static powder pattern) does not show peak splitting of CO_2 in the hydrate cages at 173K and atmospheric pressure. At higher temperature hydrate begins to decompose.

CAGE OCCUPANCY CALCULATION

Calculation of cage occupancy values are based on the fact that in a unit cell of structure I hydrate there are 6 large cages, 2 small cages and 46 water molecules. For CO₂ hydrate with all the large cages occupied by CO₂ and all the small cages being empty, NMR result should show ~0.24 grams of CO₂ /per gram of hydrate. Mass % of H₂ in the hydrate synthesized for this study is very small (0.4 mass %) and for practical calculations can be ignored.

Mass from 6 CO₂ molecules in the large cages (6x44) = 264 units

Mass from 0 CO₂ molecule in the small cages (0x44) = 0 units

Mass from 46 water molecule (46x18) = 828 units

Therefore CO₂ mass fraction of this hydrate = 264/(264+828) = 0.241

Since, NMR results suggest that the synthesized hydrate has 0.21 (±0.02) grams of CO₂ per gram of hydrate, all the CO₂ in the hydrate phase has to be in the large cages (for a stable hydrate, 100% of the large cages are assumed to be filled).

From gas chromatography results we know that for every 100 moles of gas coming out of hydrate after decomposition there is 92 moles of CO₂ and 8 moles of H₂. In structure I for 100% occupied large cages (by CO₂) and 100% occupied small cages (by H₂) the ratio should have been 92 moles (of CO₂) and 31 moles (of H₂) (as large cage to small cage ratio in structure I is equal to 3:1). Instead we see just 8 moles of H₂, which suggests that only 25% of the small cages are occupied by H₂. Also from NMR we see that integral peak intensity for doubly occupied small cage is 3 times as big as singly occupied small cages and given the fact that doubly occupied cage (due to two hydrogen molecules) would give twice the area of singly occupied cage, the effective ratio of

doubly occupied cages to singly occupied cages are 3:2. Hence these two equations can be solved for H₂ occupancy values in small cages.

$$2x + y = 25$$

$$x / y = 3/2$$

x = % of bi molecular hydrogen in the small cages

y = % of single hydrogen in the small cages

$$x = 9.3 \text{ \& } y = 6.2$$

Similarly, in structure II hydrate there are 8 large cages, 16 small cages and 136 water molecule. Fortunately molecular mass of C₃H₈ and CO₂ are same, hence the calculation of cage occupancy becomes easier.

Mass from 8 C₃H₈/CO₂ molecules in the large cages (8x44) = 352 units

Mass from 16 CO₂ molecules in the small cages (16x44) = 704 units

Mass from 136 water molecules (136x18) = 2448 units

Mass fraction of 100% occupied large cages = $352/(704+352+2448) = 0.100$

NMR results suggest 0.05 grams of C₃H₈ per grams of hydrate in the hydrate phase. Therefore, for first approximation 50% of the large cages are occupied by C₃H₈ and rest by CO₂ (0.05 grams of CO₂). Mass fraction of the 100% occupied small cages is equal to 0.200, therefore 0.075 grams of remaining CO₂ (which does not occupy the large cages) should give 37.5% occupancy of small cages. Regressing the calculation (for the second time using 37.5% occupied small cages for calculating the overall mass of the hydrate) we converge for these numbers for cage occupancy (shown in Table 5-2). Again the mass fraction of H₂ has been ignored from the calculation.

REFERENCES

- Kumar, R., Linga, P., Moudrakovski, I., Ripmeester, J. A., Englezos, P. 2008 Structure and kinetics of gas hydrates from methane/ethane/propane mixtures relevant to the design of natural gas hydrate storage and transport facilities AIChE, 54, 2132-2144
- Ohno H and Hondoh T. Micro-Raman Study of Air Clathrate Hydrates in Polar Ice from Dome Fuji, Antarctica. *Physics and Chemistry of ice: Proceedings of the 11th international conference on the physics and chemistry of ice*, Bremerhaven, Germany on 23-28 July, 2006. edited by Werner F. Kuhs, published by the Royal Society of Chemistry, Cambridge, UK, 2007